Final Report

MM5 Simulations for TexAQS 2000 Episode

Prepared for:

Houston Advanced Research Center
Texas Environmental Research Consortium (TERC)
4800 Research Forest Dr
The Woodlands, TX 77381

and:

Texas Commission on Environmental Quality
12118 Park 35 Circle
Austin, Texas 78753

Prepared by:

ATMET, LLC
PO Box 19195
Boulder, Colorado 80308-2195

14 August 2003

Table of Contents

List of Figures

1 Introduction

The August-September TexAQS 2000 Houston-Galveston Ozone episode has been studied and modeled by several groups using the Penn State/NCAR MM5 model, including John Nielson-Gammon from the Department of Atmospheric Sciences at Texas A&M University (TAMU) and a group at the MCNC. Several deficiencies have been noted in the results of these simulations. The purpose of the current project is to attempt to correct some of these deficiencies by investigating the sensitivity of MM5 to various changes in model configuration and parameterizations. We have also focused a portion of our discussion on the rapid ozone formation events (ROFE) of 25 August and 30 August.

ATMET produced an Interim Report for this project in January 2003 detailing a number of idealized tests of the MM5 basic numerics, along with a large number of short-term (2-3 day) sensitivity runs. We will not include the majority of the Interim Report here, but we have included a summary in Section 2. These sensitivity runs verified that our recommendations of the "best" MM5 configuration (based on a previous project of the 1993 H/G episode) would still hold for the 2000 episode. A few new features, however, in later versions of MM5, such as a new land-surface model (LSM), warranted testing and consideration for inclusion.

A large number of graphical products are located on the web site we maintained for this project: http://bridge.atmet.org/tceq/forecast.shtml. Also, full statistical plots are available at http://bridge.atmet.org/tceq/stats.shtml. For the sake of brevity, we will not attempt to reproduce the full set of information here.

This report is organized as follows.

- Section 2 – the Interim Report is summarized.
- Section 3 – the weather and ozone characteristics for the episode period are summarized. We have repeated this section from previous reports, but have added the additional days from the TCEQ "extended" episode.
- Section 4 – the MM5 model, the data sets used for the model input files and verification, and the configurations used in these simulations are described.
- Section 5 – the simulation results are described and discussed.
- Section 6 – the study results are summarized briefly along with suggestions for future work.

2 Summary of Interim Report

There were two main aspects of the Interim Report (ATMET 2003), the idealized tests of the non-hydrostatic dynamics of MM5 and further sensitivities focusing on a three-day period of the TexAQS 2000 episode. A summary of these topics follows.

2.1 Idealized Non-hydrostatic Tests

The non-hydrostatic dynamics of MM5 seemed to perform adequately for the idealized tests we attempted: the moist bubble and the stationary mountain waves. While MM5 had various difficulties with the trapped lee wave simulations, it was unclear whether the causes were from the non-hydrostatic dynamics or from other aspects of the numerical formulation, such as top and lateral boundary conditions. Our conclusion was that the MM5 non-hydrostatic dynamics are functioning adequately.

2.2 Sensitivity Tests

A series of sensitivity tests was performed on the 29 August – 1 September 2000 TexAQS case. These tests all used 4 domains with grid spacings ranging from 108 km on grid 1 down to 4 km on grid 4. A few tests also looked at an additional domain 5 of 1.33 km grid spacing. MM5 Version 3.5 was used. From these tests, the following conclusions were made:

- The MRF PBL performed better than the ETA, GS, and BT PBL schemes, on grids down to a 4 km resolution. PBL tests were not performed at a finer resolution, but based on past experience (ATMET 2002a) we expect that this conclusion will also hold at 1 or 1.33 km grid spacings.
- The RRTM radiation scheme significantly improved the performance of the MRF PBL scheme, especially at night. It should not, however, be used at the same time as the Land Surface Model (LSM) scheme, as a cold nighttime temperature bias resulted.
- The LSM, without the RRTM, also significantly improved the performance of the MRF PBL scheme. The results with the LSM showed increased sensitivity to the vegetation characteristics, as would be expected. Subjectively, this increased sensitivity is deemed an improvement. The use of the LSM is thus recommended, although a choice between it or the RRTM scheme must be made.
- 2-way interactive grid nesting is recommended for all grids. Although the sensitivity tests showed a minimal impact of 2-way

nesting over high time-frequency 1-way nesting, we feel that this result is likely due to the relatively quiet ambient synoptic flow. In general, it is more consistent numerically and meteorologically to use the 2-way interactive nesting. While there are times when it may seem more pragmatic to use a 1-way nest, it is difficult to predict when it will give undesirable results.

- When FDDA is used, the observation nudging appears to perform better than the grid nudging for the surface verifications, although the limited number of sensitivity tests performed made it difficult to draw a firm conclusion. The observation nudging was only performed for surface observations however, and the statistics were only calculated against those same surface observations. Grid nudging that included the surface analysis nudging led to potential model adjustment problems likely related to problems in the small-scale analyses. Upper air grid nudging was less successful than the surface observation nudging.

While we recommended not using the RRTM longwave radiation scheme in conjunction with the OSU LSM, these results were based on MM5 v3.5. In the meantime, v3.6 became available which did not show this undesirable behavior using RRTM with the NOAH LSM, the follow-on to the OSU LSM. Therefore, the actual runs described in subsequent sections did use the RRTM in conjunction with the LSM.

3 Weather Discussion

The period of interest extends from 16 August to 7 September 2000 during which ozone measurements exceeded standards during several days.

3.1 Ozone exceedances

Table 1 summarizes ozone measurements in the Houston-Galveston area as reported by the Texas Natural Resource Conservation Commission (TNRCC) for the period of interest.

Table 1. Transient High Ozone Events observed during the Texas Air Quality Study (TexAQS). Table from TNRCC Report: Accelerated Science Evaluation of Ozone Formation in Houston-Galveston Area, September 13, 2001.

Date (2000)	Number of stations exceeding 124 ppb (hourly ave)	Highest hourly average ozone (ppb)	Greatest observed hourly rise (ppb)	Greatest observed hourly fall (ppb)	Number of stations with hourly rise or fall >40 ppb
17 Aug	1	150	39	37	0
18 Aug	1	130	17	43	0
19 Aug	1	146	48	38	0
21 Aug	9	153	86	71	3
23 Aug	0	101			
24 Aug	0	111			
25 Aug	12	194	91	69	8
26 Aug	1	140	39	42	0
27 Aug	0	87			
28 Aug	0	122			
29 Aug	3	146	41	55	0
30 Aug	7	199	49	96	4
31 Aug	10	168	47	71	2
1 Sept	2	163	48	52	1
2 Sept	1	125	24	48	0
3 Sept	1	127	27	39	0
4 Sept	2	145	69	68	1
5 Sept	3	185	55	41	1
6 Sept	1	156	30	23	0

Two high ozone events are of particular interest:

- 24-26 August 2000: A ROFE event occurred on 25 August. The meteorological conditions for this case were relatively stagnant with light easterlies. A very distinct sea breeze penetrated inland to the Houston area and was instrumental in the meteorological

interactions. ATMET (2002b) studied this case in detail in our previous RAMS TexAQS study.

- 29-31 August 2000: A ROFE event occurred on 30 August. This case is especially interesting (and in contrast to 25 August) because a meteorological "regime shift" occurred on 30 August with a wind change from light southeasterly to strong westerly. With the strong westerly flow, very warm surface temperatures developed. Much higher PBL depths also occurred for this case, as discussed in ATMET (2002b).

3.2 16 August – 6 September weather description

A day-by-day textual weather summary in the Houston area is included directly from Nielson-Gammon's 5 February TNRCC report (Nielson-Gammon 2002a) for the period 23 August through 1 September. We have added further discussion based on synoptic charts for the extended early and late periods of this investigation. The daily 1800 UTC GOES 8 visible images were acquired by ATMET from NCDC and are included as a visual aid to the description.

3.2.1 *August 16*

A ridge of high pressure covered much of the central U.S. at 500 mb. Mean sea-level and 850 mb analyses indicate anticyclonic circulation over the western Gulf of Mexico putting the Houston area in southerly synoptic flow. Radar-derived precipitation suggests minimal convective activity occurred in the Houston/Galveston area with some offshore activity noted to the southwest. Surface observations indicated that the sea-breeze front traveled well past Houston, which was likely enhanced by the southerly synoptic flow.

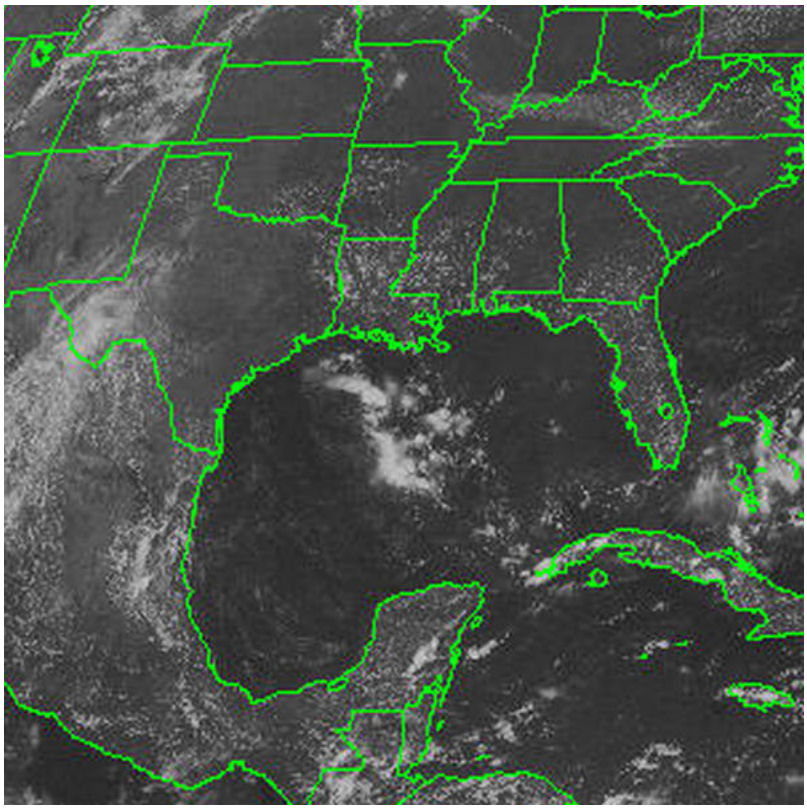

Figure 1: GOES 8 Visible image at 1800 UTC 16 August 2000.

3.2.2 *August 17*

Mid-level (500 mb) high pressure had weakened somewhat with more zonal flow indicated across the northern tier of states. Surface and 850 mb analyses showed the anticyclonic circulation to have broken down into a general east to southeast on-shore synoptic flow. Minimal convective activity was again suggested by satellite and radar data with only light cumulus noted northeast of the Houston area. The sea-breeze front easily passed through Houston that was, again, likely aided by the on-shore synoptic flow.

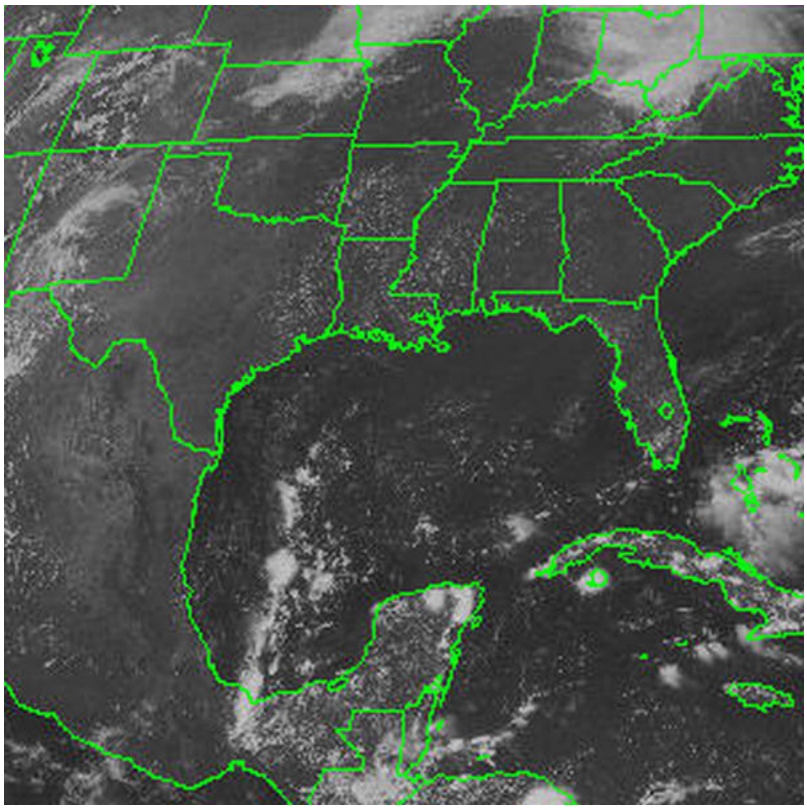

Figure 2: GOES 8 Visible image at 1800 UTC 17 August 2000.

3.2.3 *August 18*

Little change was noted from the previous day with continued weak mid-level high pressure, and general southeasterly, on-shore surface synoptic flow. The 850 mb analysis indicated very dry air along and over the Texas coast that contributed to another day of minimal convective activity. Another well-developed sea-breeze front traveled well past the Houston area.

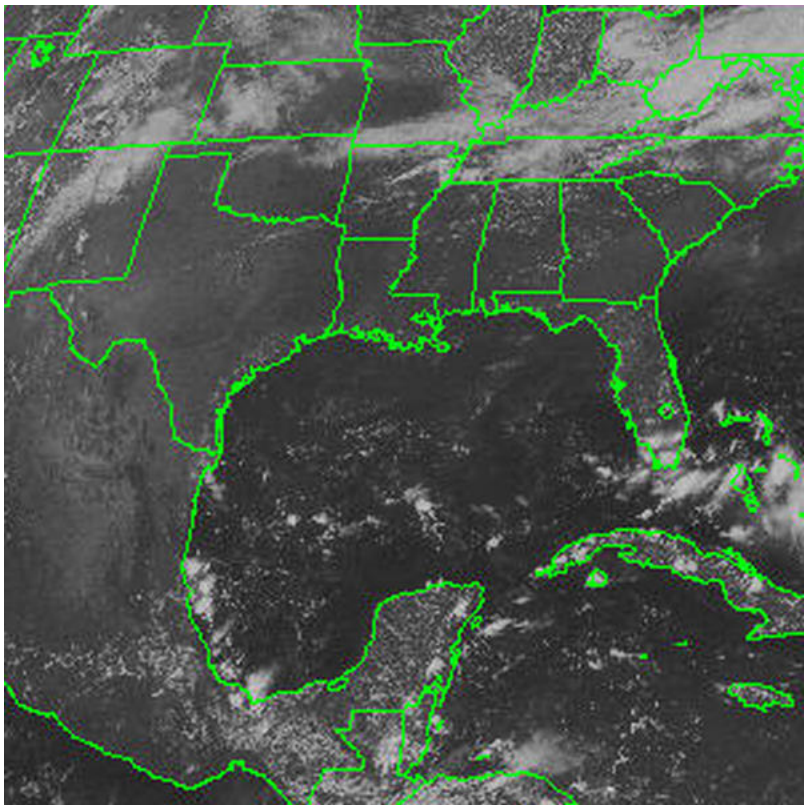

Figure 3: GOES 8 Visible image at 1800 UTC 18 August 2000.

3.2.4 *August 19*

19 August was another day with minimal convective activity. Weak mid-level high pressure continued along with general southeasterly, on-shore synoptic flow. A large area of surface high pressure located over the Great Lakes had allowed northerly flow to reach the Gulf Coast from Mississippi to the Florida Panhandle. More significant convective activity was noted along the weak frontal boundary with the development of a more organized complex positioned south of the Florida Panhandle. Once again, the sea-breeze front easily pushed through the Houston area.

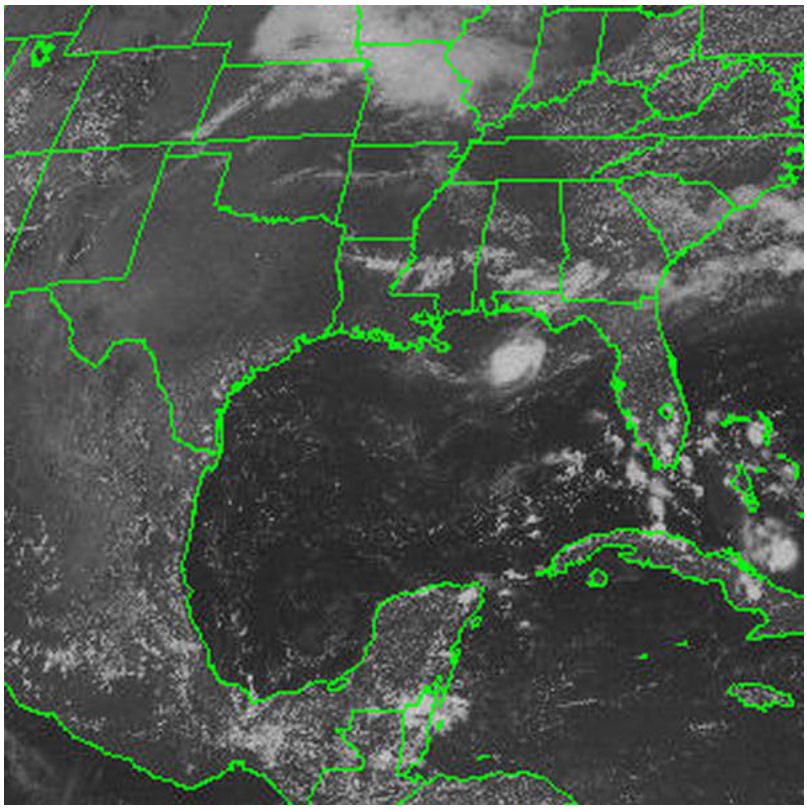

Figure 4: GOES 8 Visible image at 1800 UTC 19 August 2000.

3.2.5 *August 20*

Convective activity continued to remain minimal with similar synoptic conditions at both the low and mid-levels. The weak frontal boundary remained along the Mississippi through Florida Panhandle coastal region. The sea-breeze front again easily made it through the Houston area. (Visible satellite imagery was missing for 20 August at NCDC.)

3.2.6 *August 21*

Little change was noted at the mid-levels. The Great Lakes surface high has progressed slowly east and has helped to strengthen the easterly flow over the Gulf. The stronger on-shore flow appeared to have increased the low-level moisture along the Texas coast creating more abundant convective activity, although radar derived precipitation suggested little rainfall in the Houston-Galveston area. Another well-developed sea-breeze front traveled well past metro Houston.

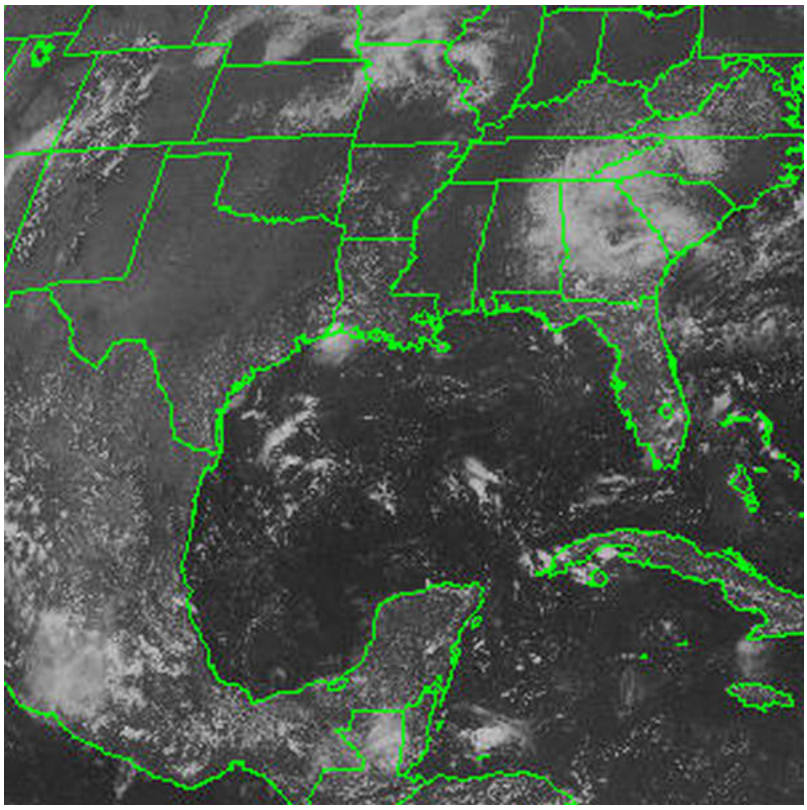

Figure 5: GOES 8 Visible image at 1800 UTC 21 August 2000.

3.2.7 *August 22*

Much more abundant convective activity was present with continued on-shore synoptic flow carrying moisture into the Texas coast. Radar-derived precipitation indicated rainfall along the entire Texas coast with embedded amounts from showers up to an inch. Surface observations suggested that the sea-breeze front traveled through the Houston area.

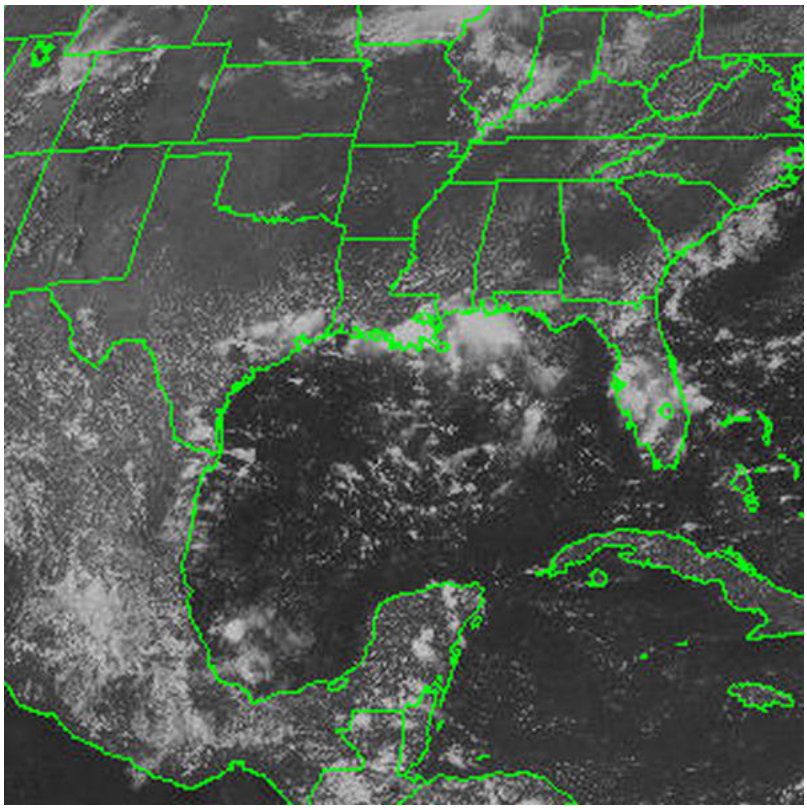

Figure 6: GOES 8 Visible image at 1800 UTC 22 August 2000.

3.2.8 *August 23*

Convective showers were present just offshore and in East Texas at 1200 UTC, with a particularly intense cluster of showers in Brazoria County. By 1500 UTC, showers had also developed at the common convective initiation points around Houston: in Galveston and Chambers counties to the northeast and southwest of where Galveston Bay meets the Gulf of Mexico, and in extreme eastern Harris County just inland of the head of Galveston Bay. By 1800 UTC, the original showers had dissipated, and other showers had come and gone too. Remaining showers were mostly at least 50 mi from downtown Houston. Shower activity steadily decreased the rest of the day, with most of the lingering activity offshore or near the coast well to the east or southwest of Houston. The morning shower activity left a blanket of middle to high-level cloud over Houston. Temperatures at most locations did not reach 90 F, a consequence of the reduced insolation and the presence of cool convective outflows. Winds were light for most of the day, gradually veering from the northeast in the morning to easterly at 2200 UTC before strengthening from the southeast during the following few hours. (from Nielson-Gammon 2002a)

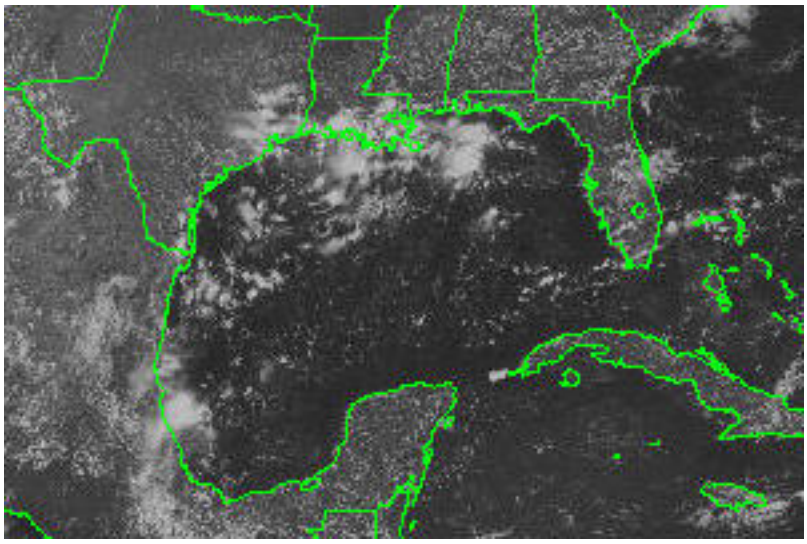

Figure 7: GOES 8 Visible image at 1800 UTC 23 August 2000.

3.2.9 *August 24*

Beginning around 0700 UTC, isolated showers began moving onshore from the Gulf of Mexico. These showers would make it a few miles inland before dissipating. A transition took place around 1500 UTC, as the offshore showers dissipated and showers began forming inland near the coast. One large area of showers moved into the Houston area from Beaumont, while another area formed west of Galveston Bay. By 1900 UTC, the two areas of showers had merged into an organized convective system. The gust front at the leading edge of this system progressed west-northwestward, from downtown Houston at 1900 UTC to the northwestern edge of Harris County at 2130. Intense showers followed the gust front, while widespread light rain persisted for several hours following the first line of showers. Rainfall ended throughout the area by 0200 UTC August 25. On this day, the squall line was the key phenomenon. The urban air and morning pollutants were replaced by rain-cooled air from the free troposphere in the afternoon. (from Nielson-Gammon 2002a)

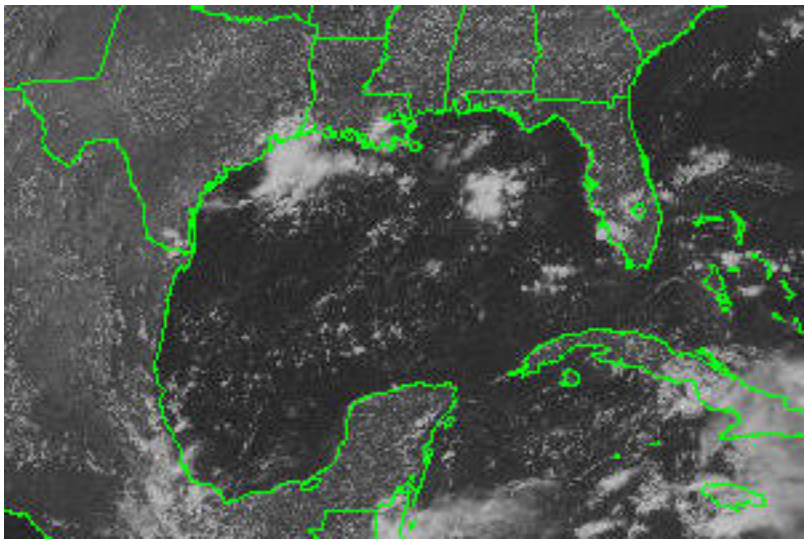

Figure 8: GOES 8 Visible image at 1800 UTC 24 August 2000.

3.2.10 *August 25*

Thunderstorms formed in the unstable air mass on this day as well, but by this time the area of instability had moved down the coast and the convective activity was centered on the Coastal Bend/Matagorda Bay area. At 2000 UTC a couple of showers formed near the center of Richmond County, probably along the outflow boundary of the Matagorda storms, and aircraft data suggest that the reinforced outflow boundary reached the western edge of Harris County late in the afternoon. This probably altered the late afternoon ozone pattern, since the highest ozone had moved west of the city by mid-afternoon. A few other isolated showers developed near Liberty in the late afternoon. Otherwise, skies in the Houston area were clear to partly cloudy all day. Scattered fair weather cumulus developed by 1500 UTC and persisted through 2300 UTC. Surface winds in the Houston area were light from the northeast in the morning, becoming particularly light and variable around 1600 UTC. Light easterly winds had become widespread by 1900 UTC, and the few hours of very light winds were probably instrumental in the very high levels of ozone that were observed later in the afternoon. From 1900 UTC onward, surface winds gradually strengthened and veered to southeasterly by 2100 UTC, remaining from the southeast at 10 knots through 0000 UTC. A localized air mass of high ozone followed a trajectory consistent with these winds, moving westward away from the ship channel and then northwestward out of the city. Highs in most areas were in the low to mid 90s. (from Nielson-Gammon 2002a)

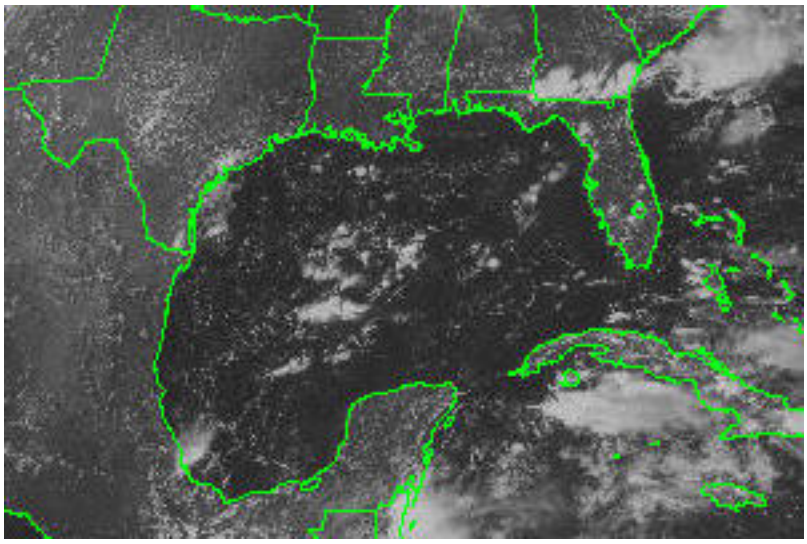

Figure 9: GOES 8 Visible image at 1800 UTC 25 August 2000.

3.2.11 *August 26*

Southeast Texas and its surroundings were free of rain showers on this day. Fair weather cumulus developed around 1500 UTC and had pretty much dissipated by 2200 UTC. Overnight lows were in the low 70s, warmer near the center of Houston. Winds veered overnight, being light from the south at 0400 UTC and light from the west at 1000 UTC. During the final few hours of the night, the winds became very light and variable, with a general northerly direction. Winds became more uniform as the daytime boundary layer deepened. At 1400 UTC, winds were from the northwest, at 1500 UTC from the west, and at 1600 from the south. The generally light winds were locally reinforced by a bay breeze. By 2000 UTC winds were from the southeast nearly everywhere, and they strengthened from the southeast during the remaining hours of the day. As a consequence of the bay breeze and afternoon onshore flow, temperatures were warmest inland. High temperatures ranged from the low 90s near Galveston bay to the upper 90s northwest of Houston. The highest ozone was observed by aircraft north of Galveston Bay around 1800 UTC, possibly originating near the ship channel in the morning. The polluted air mass was carried northwest by the afternoon breezes, resulting in an exceedance in Conroe. (from Nielson-Gammon 2002a)

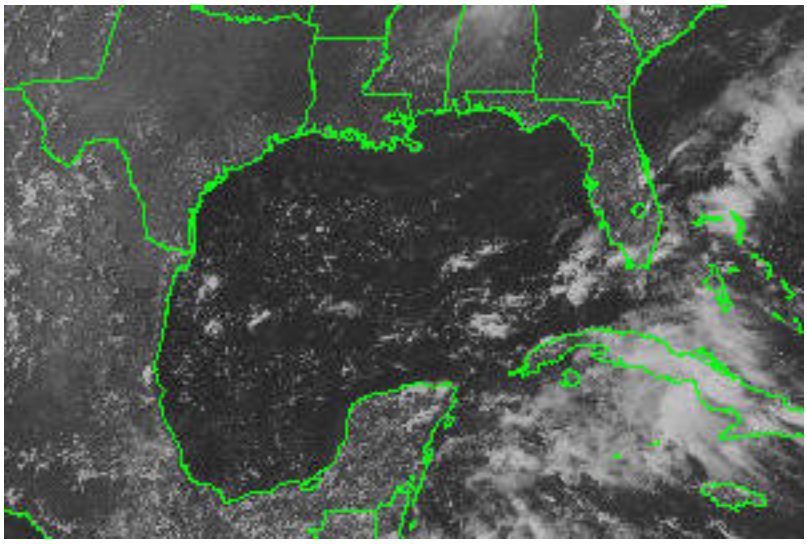

Figure 10: GOES 8 Visible image at 1800 UTC 26 August 2000.

3.2.12 *August 27*

Overnight winds closely resembled those of the previous night, except that a steady westerly flow was present across the ship channel around 1200 UTC. Low temperatures were near 70 in northern areas, upper 70s near the city center. Rain was completely absent overnight; during the morning, a few isolated showers were present to the south of the metropolitan area, but they did not have an impact on the air mass over Houston. During mid to late afternoon, a few very small showers formed in the Houston area. Convective clouds were a bit more widespread than on August 26, being present in some areas as early as 1400 UTC and not dissipating until 2300 UTC, earlier at coastal locations where the onshore flow suppressed convective development. During the morning, especially around 1400 UTC and 1500 UTC, winds were light, with surface observations suggesting a convergence zone in the ship channel area. Beginning around 1600 UTC, the northerly winds north of the ship channel became southerly, then southeasterly, increasing in velocity through the day with several observations of 15 knots by 2200 UTC and 2300 UTC. High temperatures followed the same pattern as the previous day too. (from Nielson-Gammon 2002a)

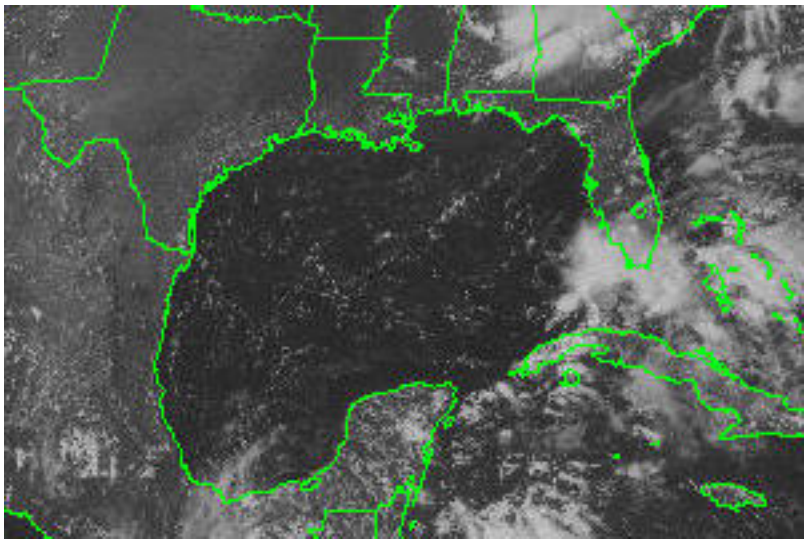

Figure 11: GOES 8 Visible image at 1800 UTC 27 August 2000.

3.2.13 *August 28*

The stronger winds continued overnight, and the winds were slower to veer than on the previous two days. Winds didn't become southerly until 0600 UTC, and at 1000 UTC they were from the southwest rather than from the west. Winds were light and variable the next two hours, and predominantly from the northeast at 1300 UTC. By 1600 UTC they had reversed direction again, becoming south-southwesterly before backing to southeasterly by 1900 UTC. Following the familiar pattern, winds continued to strengthen from the southeast for the remainder of the afternoon. By evening, winds were not quite as strong from the southeast as on the previous day. With no showers in the area, clouds followed the familiar evolution, developing at the top of the boundary layer in midmorning and dissipating from the coast inland in late afternoon. (from Nielson-Gammon 2002a)

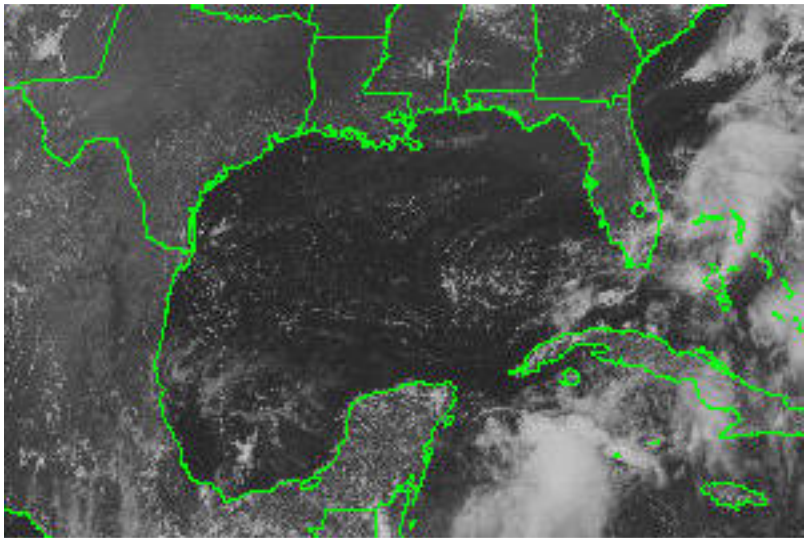

Figure 12: GOES 8 Visible image at 1800 UTC 28 August 2000.

3.2.14 *August 29*

The overnight and morning hours of August 29 were almost identical to August 26. The primary difference was the daytime cloud development, which was confined mostly to points south and west of downtown Houston. Temperatures were a couple of degrees warmer as well. By midday, more substantial differences had become apparent. Winds were still predominantly westerly across the Houston metropolitan area at 1800 UTC, except for the Galveston Bay breeze, not becoming southerly until 2000 UTC and southeasterly at 2100 UTC. This wind pattern made for ozone that was also similar to the ozone on August 26. The highest values were observed near and northeast of the ship channel in early afternoon, with stations north of Houston reporting high ozone later in the afternoon and evening. The day was essentially cloud-free, with the exception of a few isolated showers that developed along the Louisiana border during late afternoon. (from Nielson-Gammon 2002a)

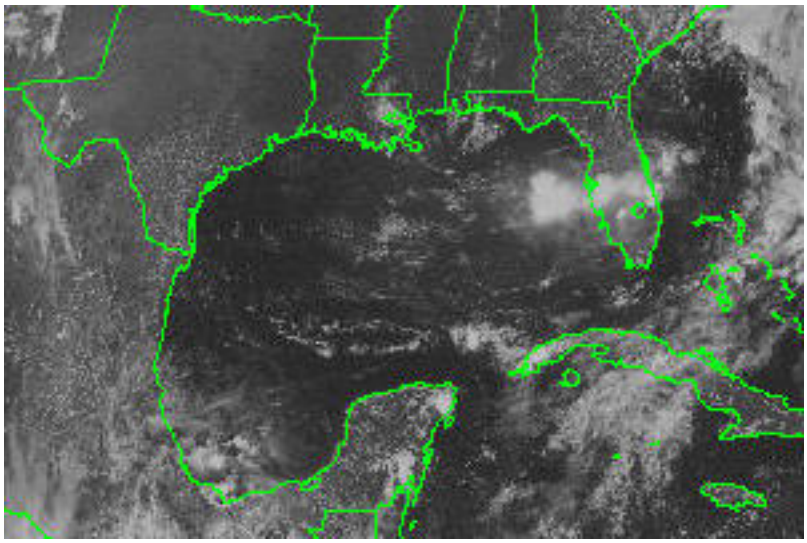

Figure 13: GOES 8 Visible image at 1800 UTC 29 August 2000.

3.2.15 *August 30*

Based on examination of profiler and surface observations, August 30 marks a regime shift from predominantly southeasterly flow to predominantly westerly flow. The westerly component developed overnight. Already by 0200 UTC the winds were from the south. They were from the west-southwest at 0600 UTC and from the west at 1000 UTC. Unlike previous nights, in which the wind became light and variable around sunrise, flow persisted from the west and winds continued to veer. At 1300 UTC they were from the west-northwest and remained from that direction, gradually strengthening, through 1700 UTC. Finally, around 1800 UTC, winds became lighter. Some variation was observed

across the Houston metropolitan area, with winds being from the west in western areas and from the north in eastern areas. During the following few hours, most winds were light and variable. Meanwhile, along the coasts, bay and gulf breeze fronts developed and winds behind the fronts became onshore. Finally, by 2300 UTC, a generally light south-southeasterly flow had developed over the entire area, even ahead of the bay and gulf breeze fronts, which appear to have not reached downtown Houston by this time. Consistent with the reduced clouds were lower dew points, in the upper 50s in the afternoon except behind the sea breeze front where they were much higher. Consistent with the reduced clouds and offshore winds, temperatures were higher as well. Most locations had high temperatures in the low to mid 100s. Consistent with the light afternoon winds, very high ozone was observed in the ship channel area, with the highest ozone found behind the bay breeze front. (from Nielson-Gammon 2002a)

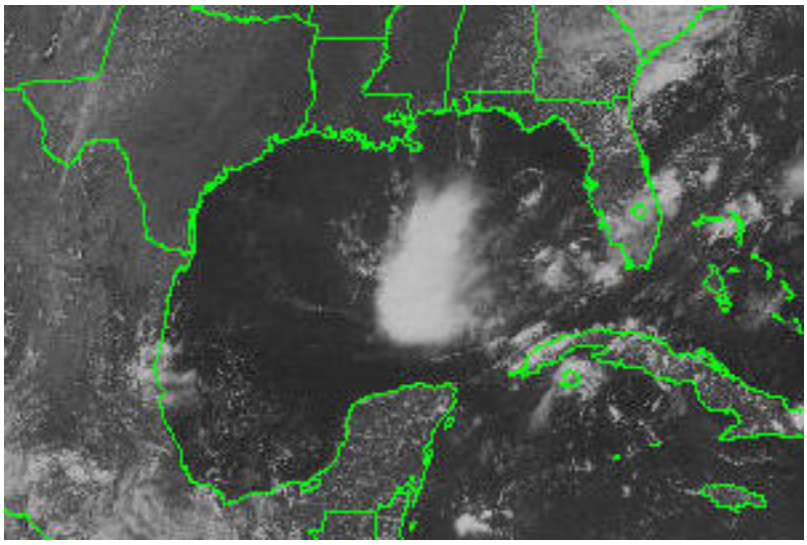

Figure 14: GOES 8 Visible image at 1800 UTC 30 August 2000.

3.2.16 *August 31*

Again at 0200 UTC winds were mostly southerly. By 0700 UTC winds were from the west everywhere, and remained from the west through 1200 UTC. Wind speeds at 1200 UTC (3-7 knots) are consistent with downward extrapolation of the La Porte lidar data. From 1300 UTC to 1700 UTC the winds increased in speed from the west-northwest and then decreased again. Following a few hours of light and variable winds, southerly winds had developed by 2300 UTC. Temperatures were even higher than the previous day, reaching the mid 100s in most locations. Skies were clear in the morning. Over the Piney Woods, north and northeast of Houston, convection began to develop after 1800 UTC, producing some showers in mid-afternoon in the Beaumont area and a shower near Liberty around 0000 UTC. As on the previous day, high ozone was associated with the light winds in the afternoon. (from Nielson-Gammon 2002a)

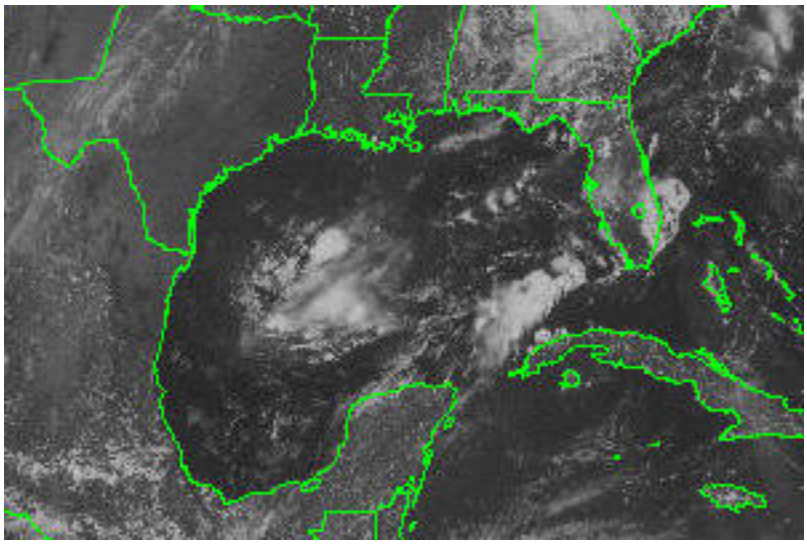

Figure 15: GOES 8 Visible image at 1800 UTC 31 August 2000.

3.2.17 *September 1*

Overnight, winds never developed an easterly component. Winds were from the south-southwest at 0200 UTC and gradually veered overnight. By sunrise winds were light and west-southwesterly, again consistent with the La Porte lidar data. As the morning developed the winds increased in speed while maintaining a west-southwesterly direction, reaching 15 knots in places by 1500 UTC. While winds became lighter by the afternoon, they never truly became light and variable. Nevertheless, some high ozone was observed over and downstream of the Houston ship channel. By 2100 UTC winds were from the southwest and had begun intensifying again. Afternoon dewpoints were in the low 60s instead of the upper 50s, and partly cloudy skies were common throughout the day. As on August 31, convection developed over the Piney Woods, but this convection was much more widespread and produced an outflow boundary that moved southwestward into the center of Houston by 2300 UTC. Strong northeast winds were followed by light and variable winds, before the onset of widespread south-westerlies around 0500 UTC the next day. (from Nielson-Gammon 2002a)

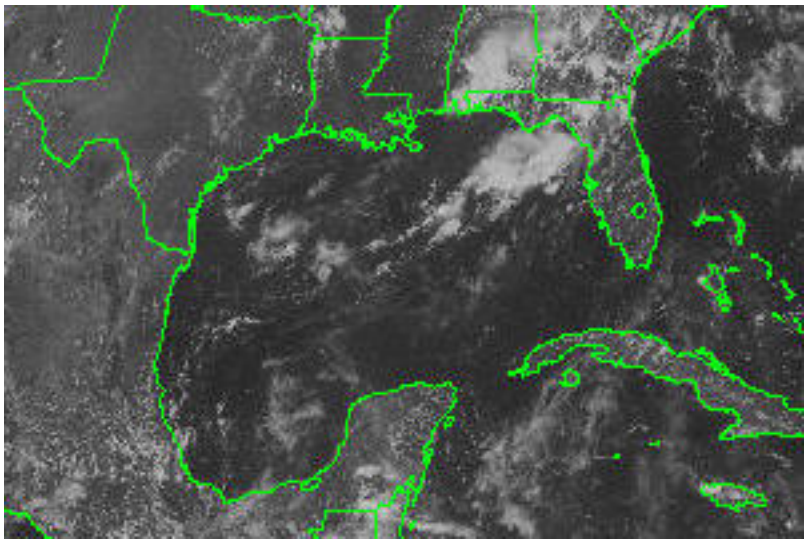

Figure 16: GOES 8 Visible image at 1800 UTC 1 September 2000.

3.2.18 *September 2*

Weak high pressure over Texas was noted at 500 mb with a weak trough positioned over the eastern U.S. and a stronger, long-wave trough over the western U.S. Low-level (850 mb) synoptic flow was generally south to southeast while, at the surface, anticyclonic flow was centered over the southwest Gulf of Mexico. Radar-derived precipitation indicates rainfall fell along a west-east area north of Houston with heavier showers northeast of Houston. Surface wind observations indicated more of a westerly component through the morning hours, and eventually winds backed to southwest and south late in the day near Houston in conjunction with the arrival of the sea-breeze front that did not penetrate further inland than the metro area.

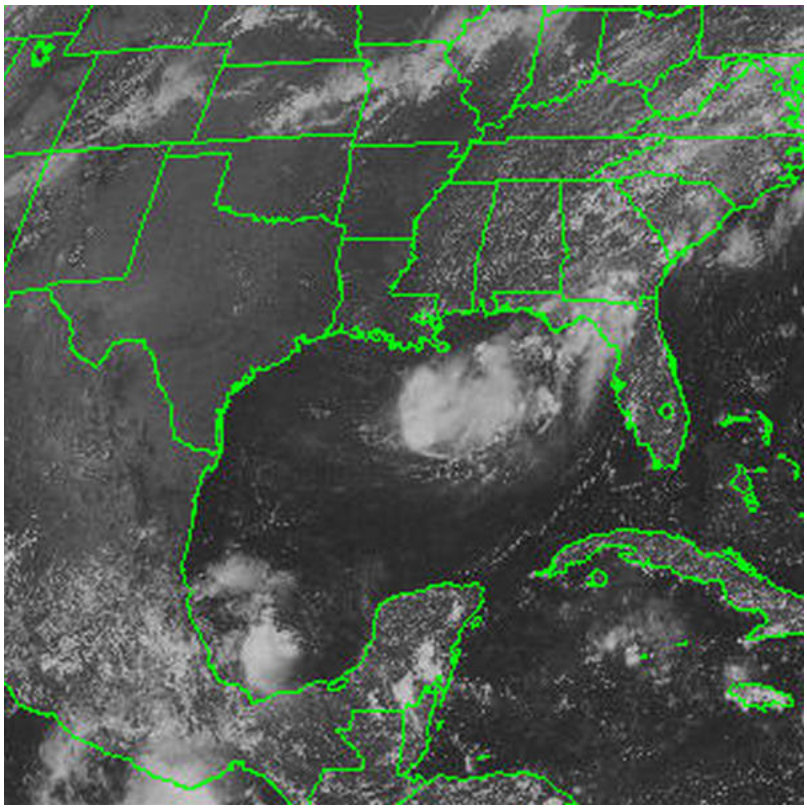

Figure 17: GOES 8 Visible image at 1800 UTC 2 September 2000.

3.2.19 *September 3*

Surface anticyclonic circulation continued over the southwest Gulf that created more of a westerly flow in the surface winds. Convective rainfall is noted northeast of Houston. Surface wind observations remained west to southwest through the daylight hours with no indication of the sea-breeze front reaching Houston.

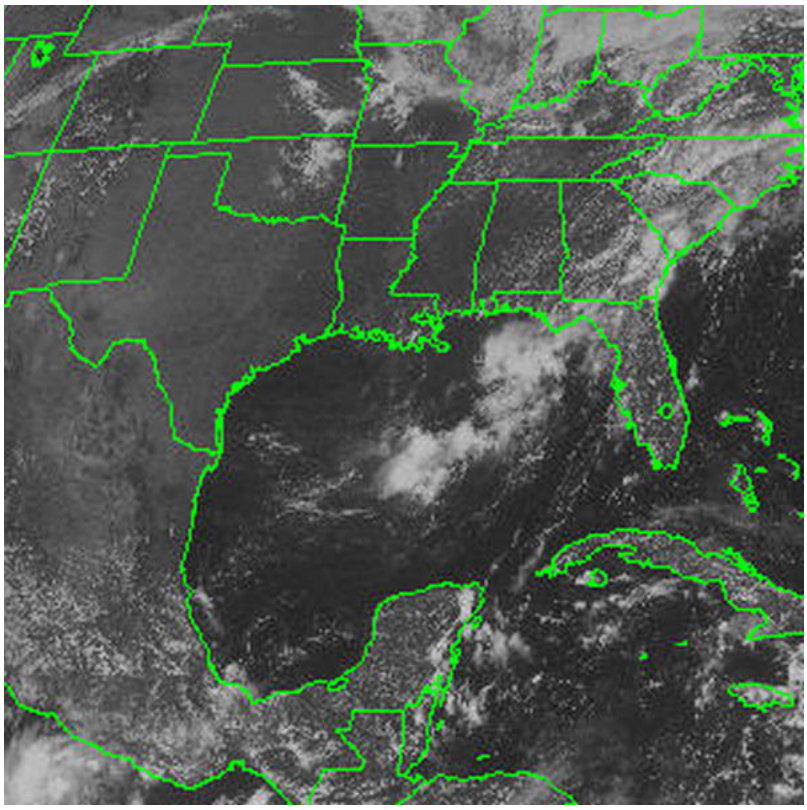

Figure 18: GOES 8 Visible image at 1800 UTC 3 September 2000.

3.2.20 *September 4*

The mid-level (500 mb) ridge centered over the Texas Panhandle tended to strengthen with time putting eastern Texas under the influence of north to northeast flow from 850 mb and above. Surface wind observations remained westerly through the morning, then tended to northeasterly before veering southerly as the sea-breeze front reached to about the metro area. Radar-derived precipitation was light, but widespread along the Texas coast.

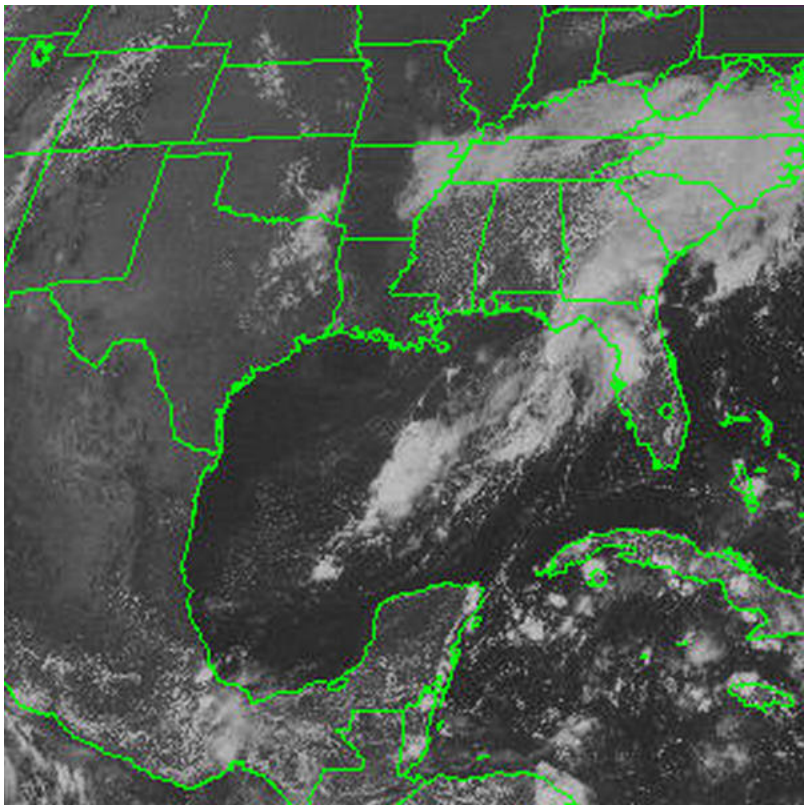

Figure 19: GOES 8 Visible image at 1800 UTC 4 September 2000.

3.2.21 *September 5*

The 500 mb ridge showed further strengthening over the Texas Panhandle which combined with a large surface high pressure over the northeastern U.S. to create synoptic flow from the northeast. Surface observations were light overnight and became northeasterly after sunrise. On-shore flow started around 2100 UTC and the sea-breeze managed to reach Houston metro by about 0000 UTC. Radar-derived precipitation was light and primarily confined to the southwest of Houston.

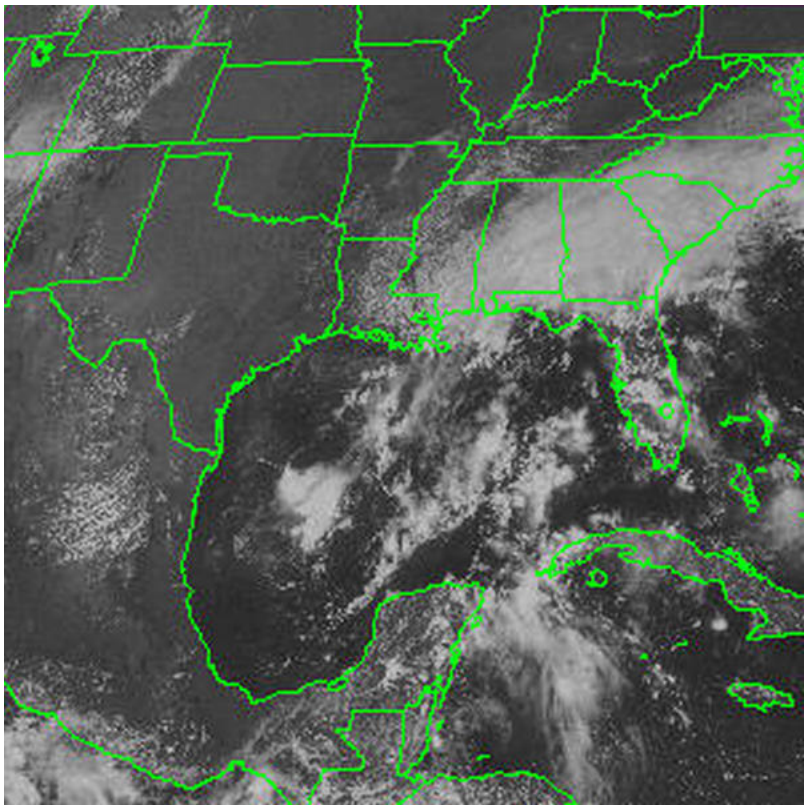

Figure 20: GOES 8 Visible image at 1800 UTC 5 September 2000.

3.2.22 *September 6*

The west coast trough at 500 mb started to lift and shear-out while the Texas ridge began to elongate to the northeast. This strengthened the northeast synoptic flow near the surface. Surface observations indicated light northeasterly flow overnight that continued and strengthened during the morning hours. Similar to the previous day, on-shore flow started around 2100 UTC and a sea-breeze front penetrated to about the metro area by 0000 UTC. Radar-derived precipitation was light and confined to off-shore areas.

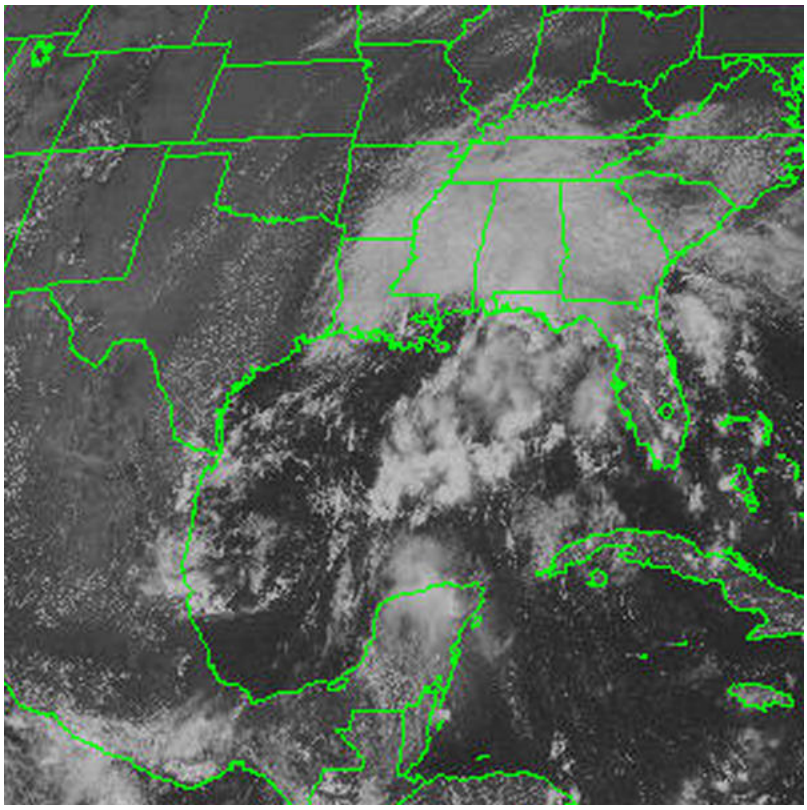

Figure 21: GOES 8 Visible image at 1800 UTC 6 September 2000.

3.3 Precipitation analyses

The 24-hr NCEP 4 km precipitation analyses were also acquired by ATMET and are included in Figure 22. This is a prototype, real-time, hourly, multi-sensor National Precipitation Analysis (NPA) that has been developed at the National Centers for Environmental Prediction (NCEP) in cooperation with the Office of Hydrology (OH). This analysis merges two data sources that are currently being collected in real-time by OH and NCEP. Approximately 3000 automated, hourly rain gauge observations are available over the contiguous 48 states via the GOES Data Collection Platform (DCP) and ASOS. In addition, hourly digital precipitation (HDP) radar estimates are obtained as compressed digital files via the AFOS network. The HDP estimates are created by the WSR-88D Radar Product Generator on a 131 x 131 4-km grid centered over each radar site. The data analysis routines, including a bias correction of the radar estimates using the gage data, have been adapted by NCEP on a national 4-km grid from algorithms developed by OH ("Stage II") and executed regionally at NWS River Forecast Centers (RFC). Hourly and 6-hourly analyses are also available, but the 24 hour analyses give a good summary of the differing weather (little precipitation) on the ozone episode days.

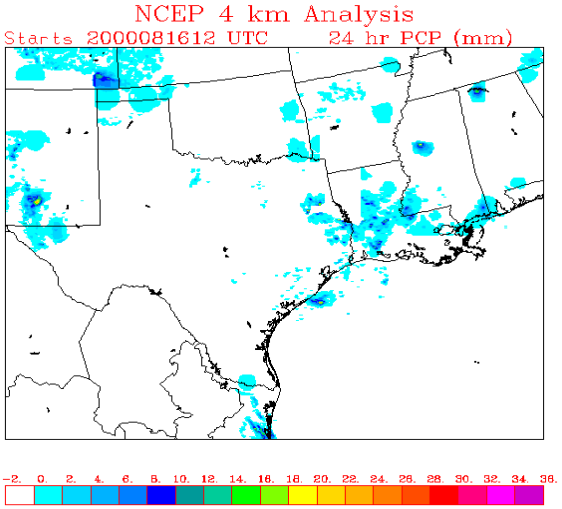

1200 UTC 17 August 2000

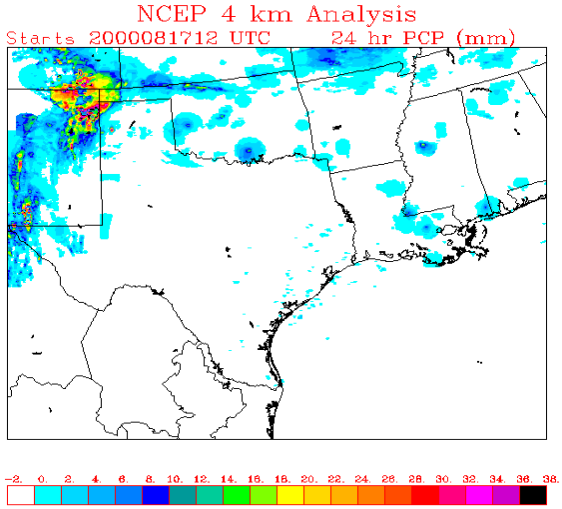

1200 UTC 18 August 2000

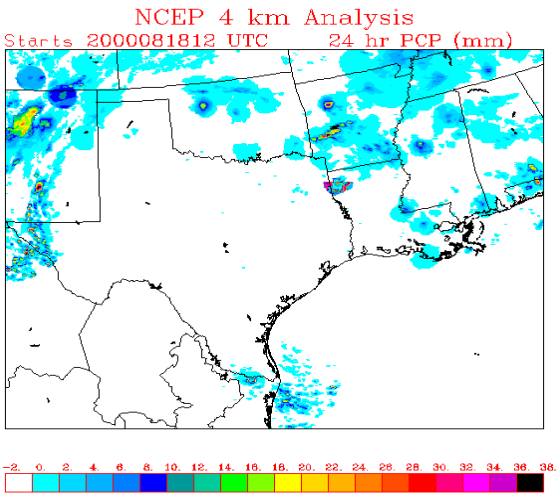

1200 UTC 19 August 2000

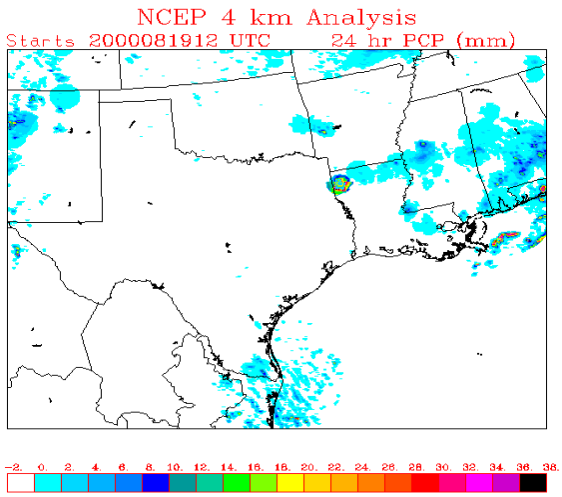

1200 UTC 20 August 2000

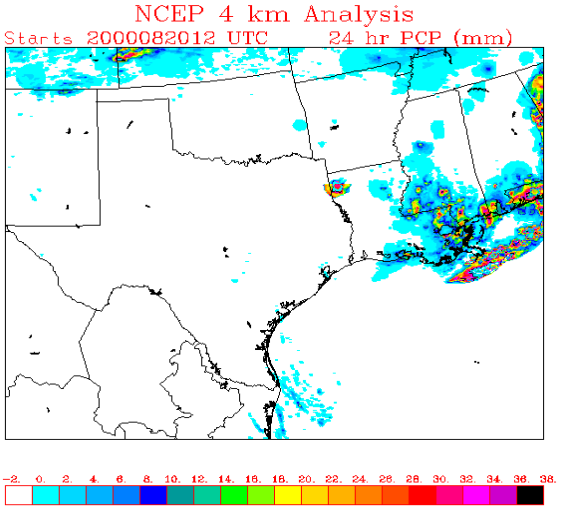

1200 UTC 21 August 2000

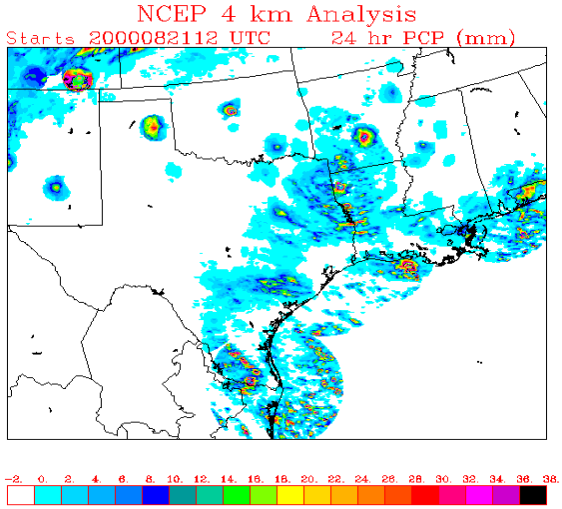

1200 UTC 22 August 2000

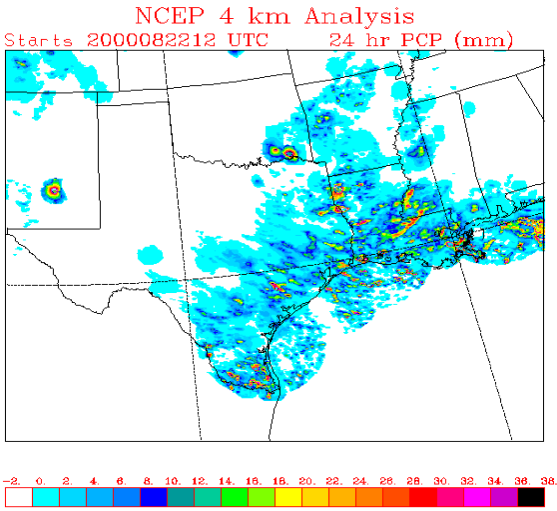

1200 UTC 23 August 2000

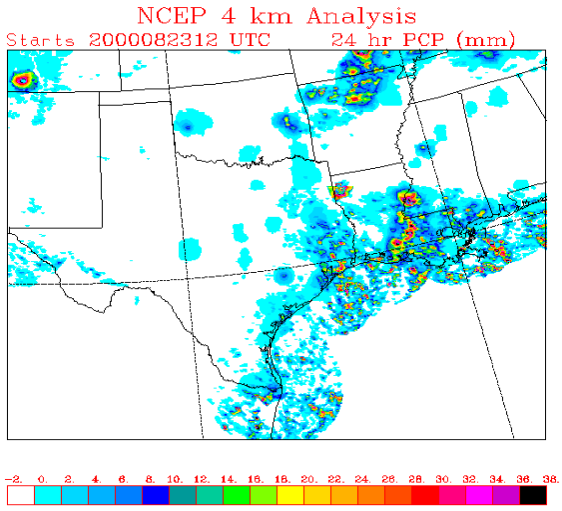

1200 UTC 24 August 2000

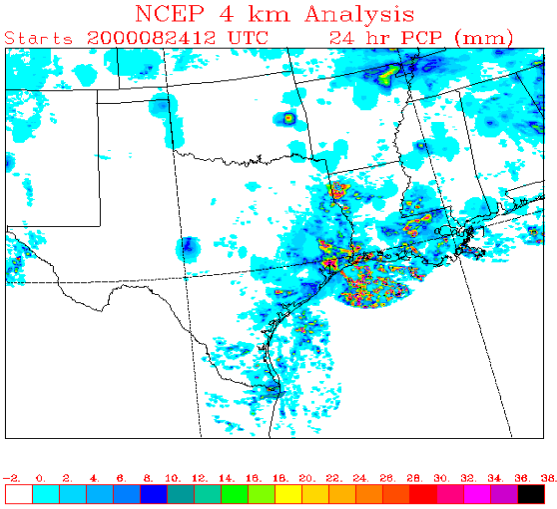

1200 UTC 25 August 2000

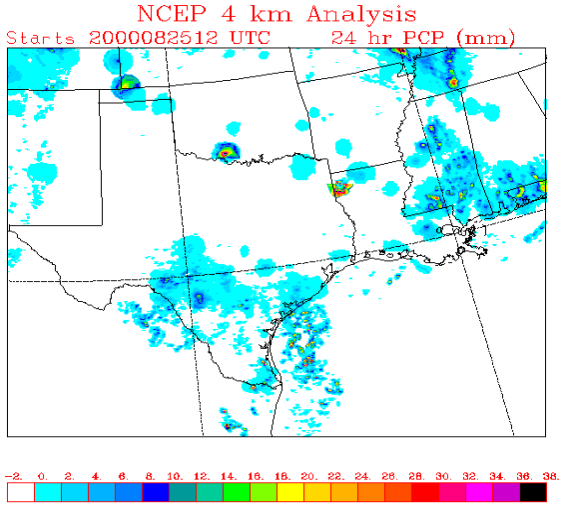

1200 UTC 26 August 2000

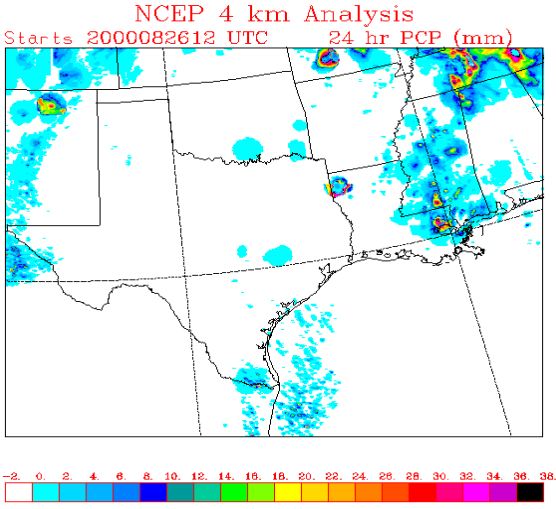

1200 UTC 27 August 2000

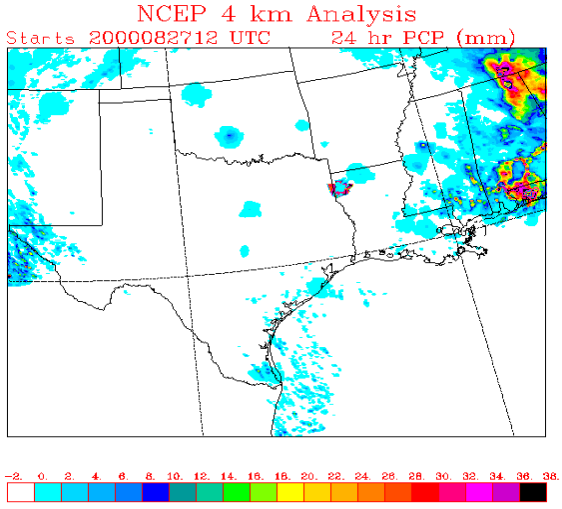

1200 UTC 28 August 2000

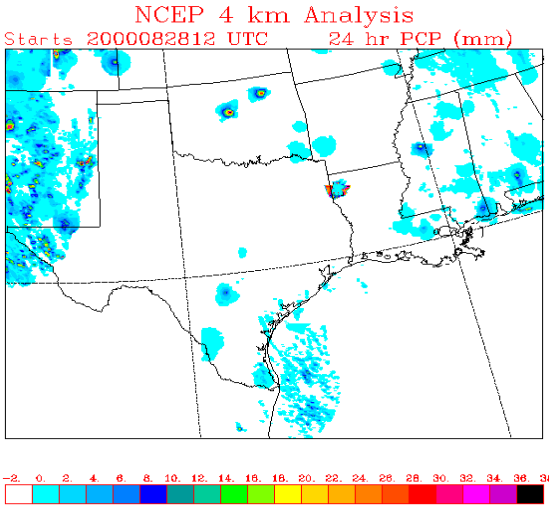

1200 UTC 29 August 2000

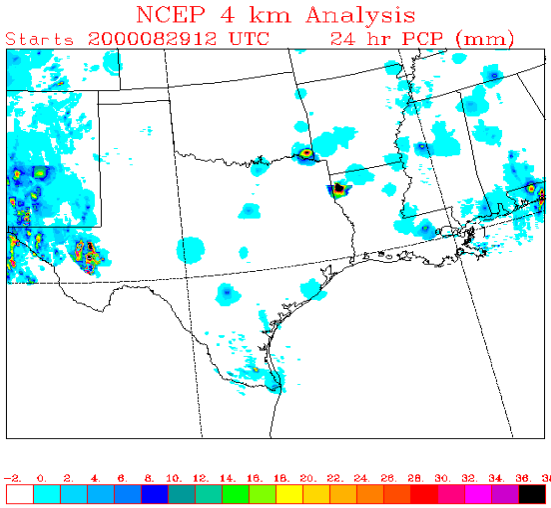

1200 UTC 30 August 2000

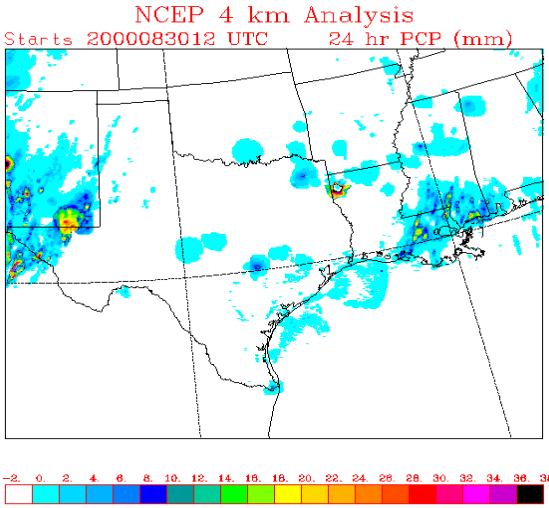

1200 UTC 31 August 2000

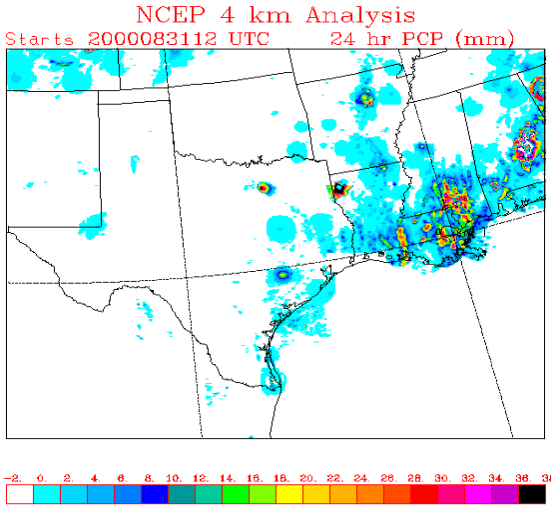

1200 UTC 1 September 2000

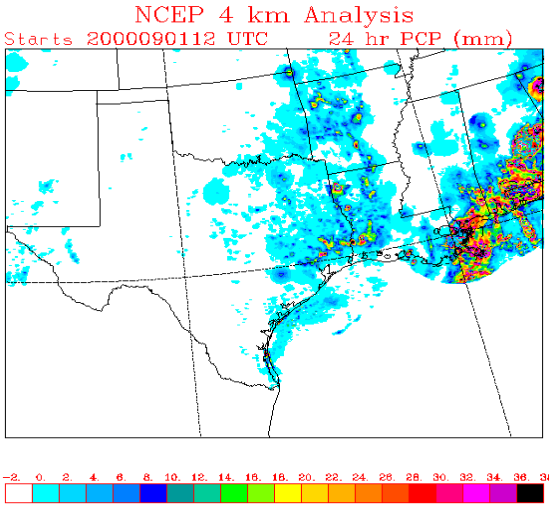

1200 UTC 2 September 2000

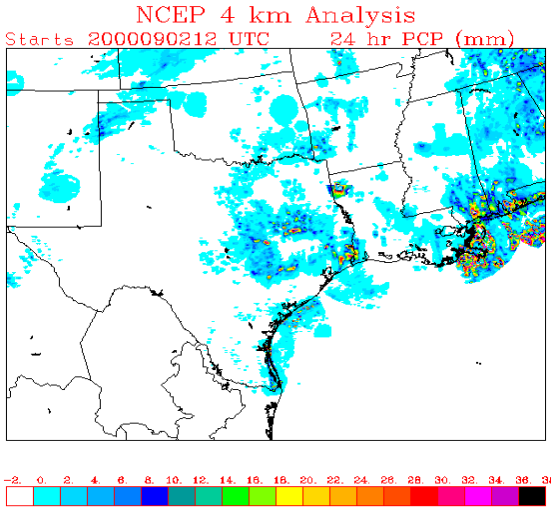

1200 UTC 3 September 2000

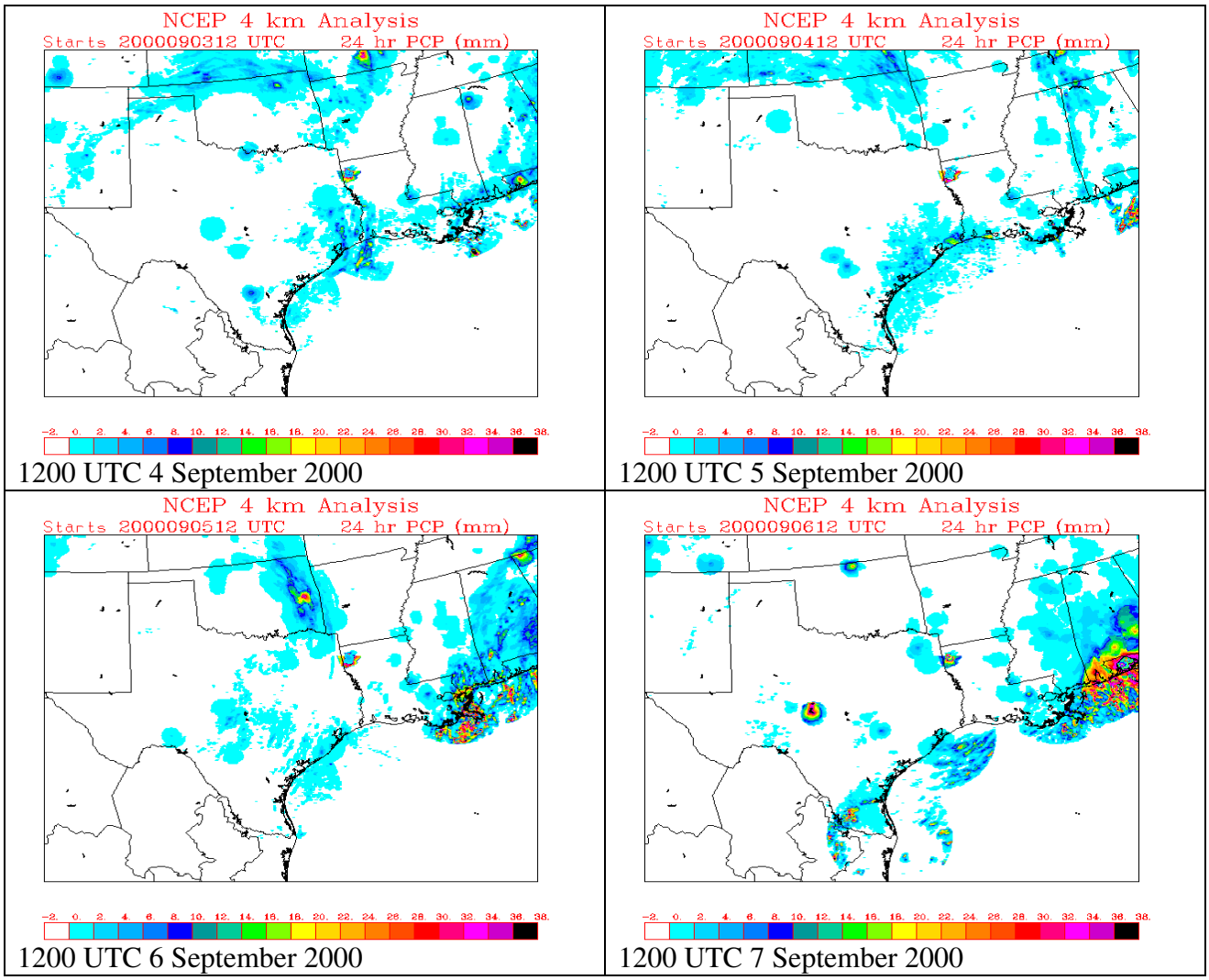

Figure 22: NCEP 4 km Stage 4 analyses of 24 hr total precipitation (mm) from 1200 UTC 17 August through 1200 UTC 7 September 2000.

4 Numerical model data preparation

4.1 Atmospheric data

The NCEP ETA Data Assimilation System (EDAS) gridded analyses, standard National Weather Service (NWS) observations, special TexAQS surface observations, and NOAA/ETL 915 MHz profiler observations were used to create gridded model analyses for all simulations. These data sets are described in more detail.

4.1.1 *Large scale gridded analyses*

The EDAS data set was used as the background/first-guess analysis. Only the 00-hour analyses were used (i.e. no ETA forecasts). The EDAS is the 3D-VAR analysis produced at NCEP every 3 hours and used as the initial analysis for ETA model forecasts. In August 2000 (the case studied in this project), the ETA /EDAS grid spacing was 32 km/45 levels. It is important to note, however, that the standard gridded data set that NCEP makes available to the public uses the ETA 212 grid, which has a 40 km horizontal grid spacing and 50 mb increment pressure surfaces. Thus, even though the EDAS analysis was performed on a 32 km grid, the data set input into the MM5 models was at 40 km grid spacing.

4.1.2 *Standard NWS observations*

The rawinsondes and surface observations reported by the NWS and other national meteorological centers are archived at NCAR. The rawinsondes are reported every 6 hours and the surface observations are archived every three hours. These data were accessed for the entire period.

4.1.3 *Special observations from TexAQS-2000 monitoring sites*

Special surface observations taken in August/September 2000 from the TexAQS-2000 monitoring sites were included in the data analyses. This dataset was compiled by Nielsen-Gammon at TAMU and provided by TCEQ. The data were processed into ATMET's RAMS format. The location of these observations is shown in Figure 23.

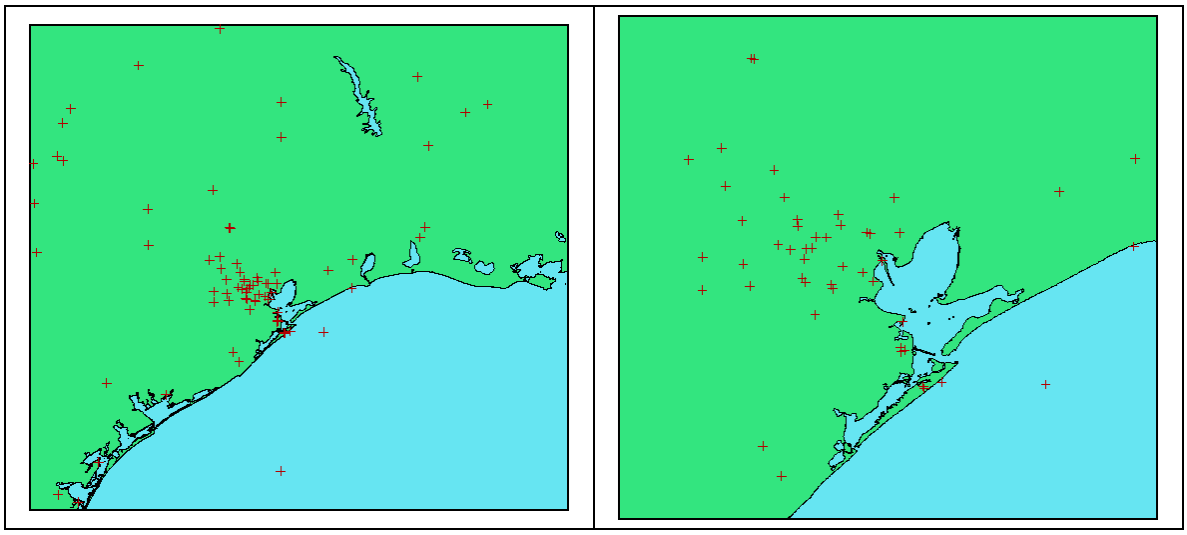

Figure 23: TexAQS surface observing site locations within a) MM5 domain 4, and b) a close-up over the Houston area.

4.1.4 *NOAA/ETL profiler data from the TexAQS-2000 experiment*

Six profilers were located in the Texas-Galveston area for this experiment: Houston Southwest Airport (HOU), UH Coastal Research Center at Lamarque (LAM), Ellington Field (ELL), Houston Downtown (HTN), Wharton Power Plant (TX2), and Liberty Municipal Airport (LMA). The locations are shown in Figure 24. The profilers at these sites were all 915 MHz instruments and the data has been processed and quality-controlled by NOAA/ETL. The final wind soundings are 60-minute averages. ETL quality-controlled the data for migrating bird contamination and gross errors. In addition, at ATMET, based on past experience with using profiler data, we added a gross error check for the horizontal wind and also a vertical wind component check. Even though we do not use the vertical wind component from the profiler, the magnitude of that component has been found to be a good gross error check on the horizontal wind quality. Out of 44,135 separate profiler observations (including each level as a separate observation) for the 6 profilers from 0000 UTC 22 August through 0000 UTC 3 September, 232 observations were flagged as potentially bad by using a gross error check of 1ms-1 on the vertical velocity component. Nielson-Gammon (2002c) also discussed some of the quality-control issues related to this profiler data set.

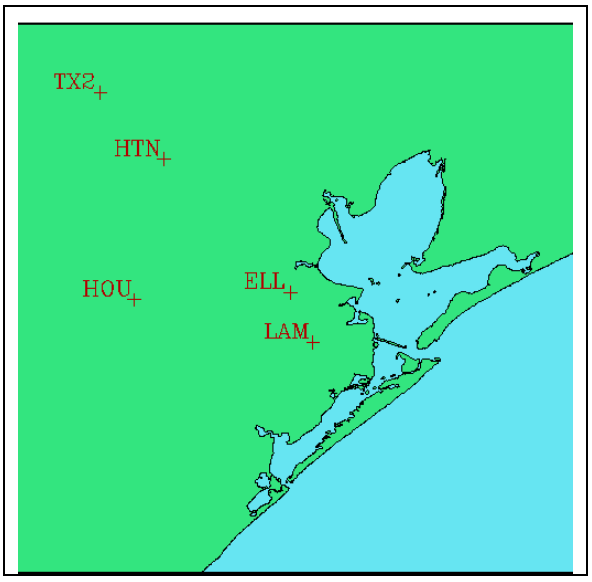

Figure 24: Locations of TEXAQS profilers.

4.2 Pre-processing and Analysis

4.2.1 *Domain configuration*

All full-episode simulations were performed using a four domain MM5 nested grid configuration. The grid spacings were set to 108, 36, 12, and 4 km respectively. 40 terrain-following sigma-p layers were used in the vertical with the lowest model level at approximately 10m AGL and the model top set to 50 mb. Table 2 and Table 3 provide grid dimension details and Figure 25 illustrates the nested grid system.

Table 2: MM5 domain dimensions.

Domain	East-West	North-South	Vertical
1	53	43	40
2	55	55	40
3	100	100	40
4	151	136	40

Table 3: MM5 vertical sigma levels.

1.000	0.998	0.995	0.990	0.985	0.980	0.975	0.965
0.955	0.940	0.925	0.910	0.895	0.875	0.855	0.835
0.810	0.785	0.755	0.725	0.695	0.660	0.625	0.590
0.540	0.485	0.425	0.360	0.300	0.250	0.200	0.160
0.125	0.100	0.075	0.050	0.035	0.025	0.015	0.010
0.000							

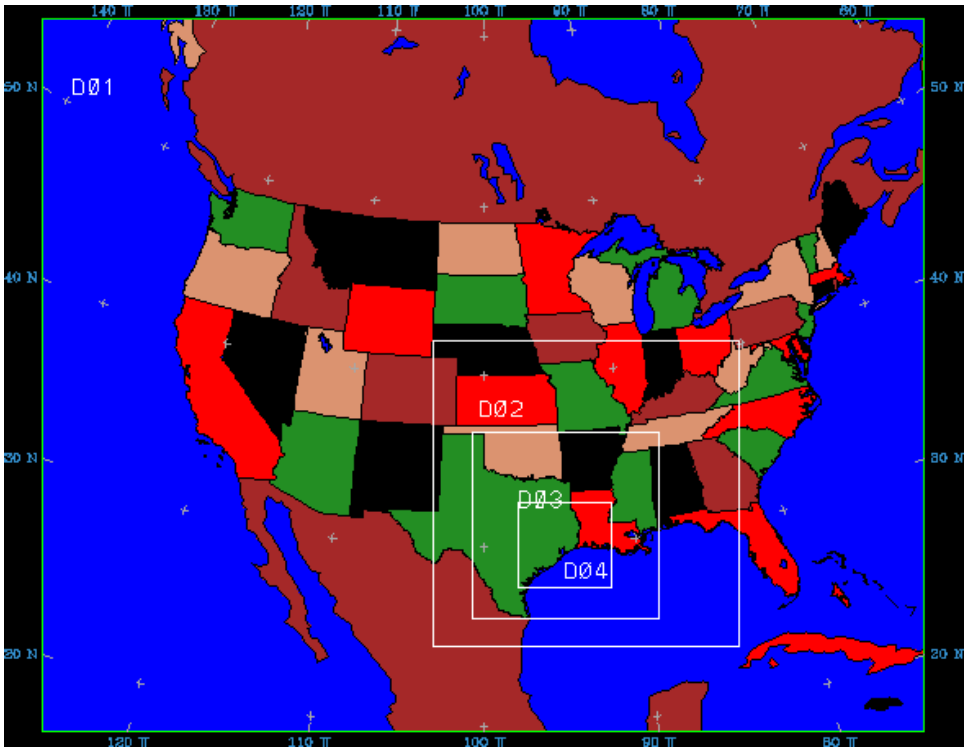

Figure 25: MM5 nested grid configuration.

Model terrain, soil type, vegetation category, and percent vegetation were all derived from 5-minute data sets that are provided with MM5. The primary source for this information is USGS. Grid 4 dominant land use category is shown is Figure 26.

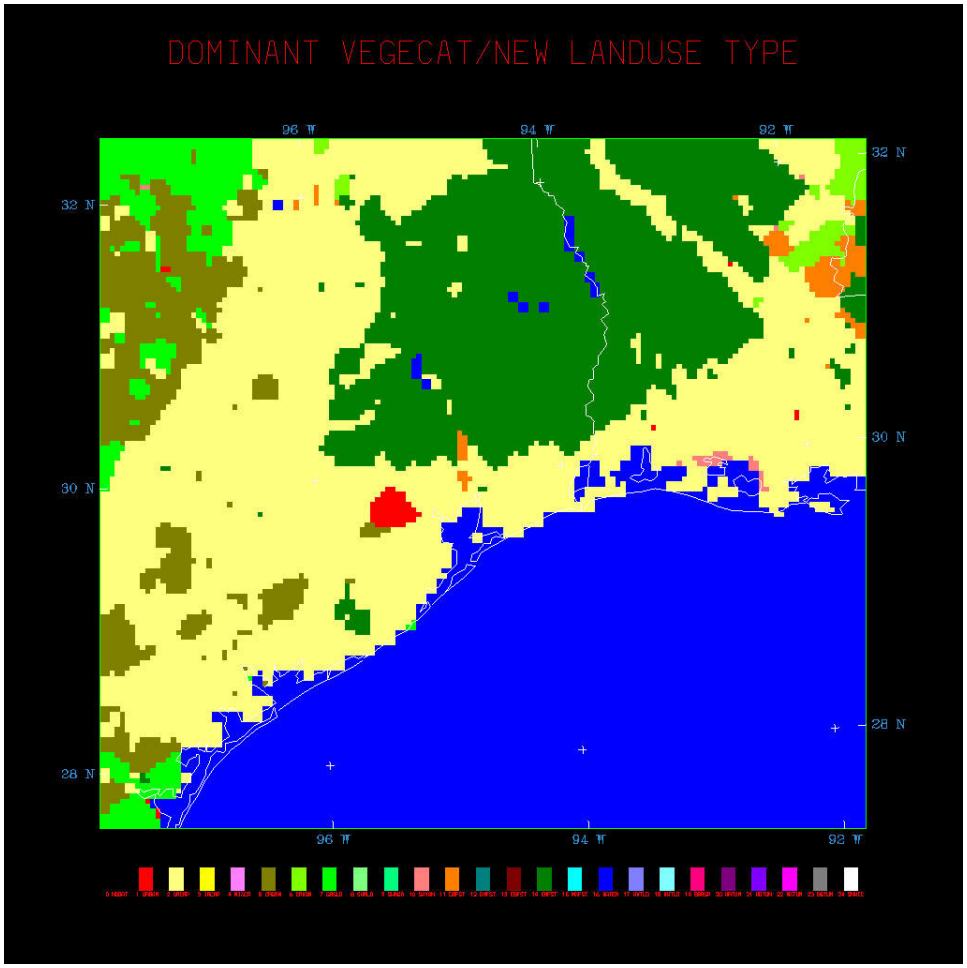

Figure 26: Grid 4 dominant land use category derived from 5-minute USGS data.

4.2.2 *Quality Control and Analysis*

The MM5 LITTLE_R program was used to generate the boundary condition files and the analyses used for the initialization and gridded FDDA tests. The LITTLE_R package was used instead of the RAWINS package because it is easier to modify for non-standard observation types. The TexAQS observations had previously been put into RAMS format for a RAMS study (ATMET 2002b) so code was developed to input the RAMS-format surface and upper air observations into LITTLE_R. The standard surface and upper air observations were also available in RAMS format from the ATMET (2002b) project.

The LITTLE_R package has most of the same options as the RAWINS package, including quality control (QC). The QC checks included "error max" checks against the first guess as well as "buddy checks" against nearby observations. Based on past experience, we chose the MQD analysis scheme, with an observation minimum of 50; if less than 50 observations are available then a Cressman analysis was used. We found

that this cutoff was necessary because the MQD analysis does not produce good results when very few observations are available.

4.3 Post-processing and statistical validation

Validation results were generated with a statistical evaluation package called METSTAT, which was provided to ATMET. The software package was written by Environ for TNRCC and is the same as that used by Nielsen-Gammon (2002c). Both hourly and daily statistics of bias, gross error, RMS error (total, systematic, and unsystematic), and index of agreement are generated for wind, temperature, and humidity. We also used the RAMS Evaluation and Visualization Utilities (REVU) statistics package for some graphics and the web site statistics.

The statistics presented in this report are generated from model domain 4 forecasts and only against two subsets of observations that were defined by TCEQ: 1) 30 stations in the Houston vicinity (Figure 27) and 2) ten stations in the Beaumont vicinity (Figure 28).

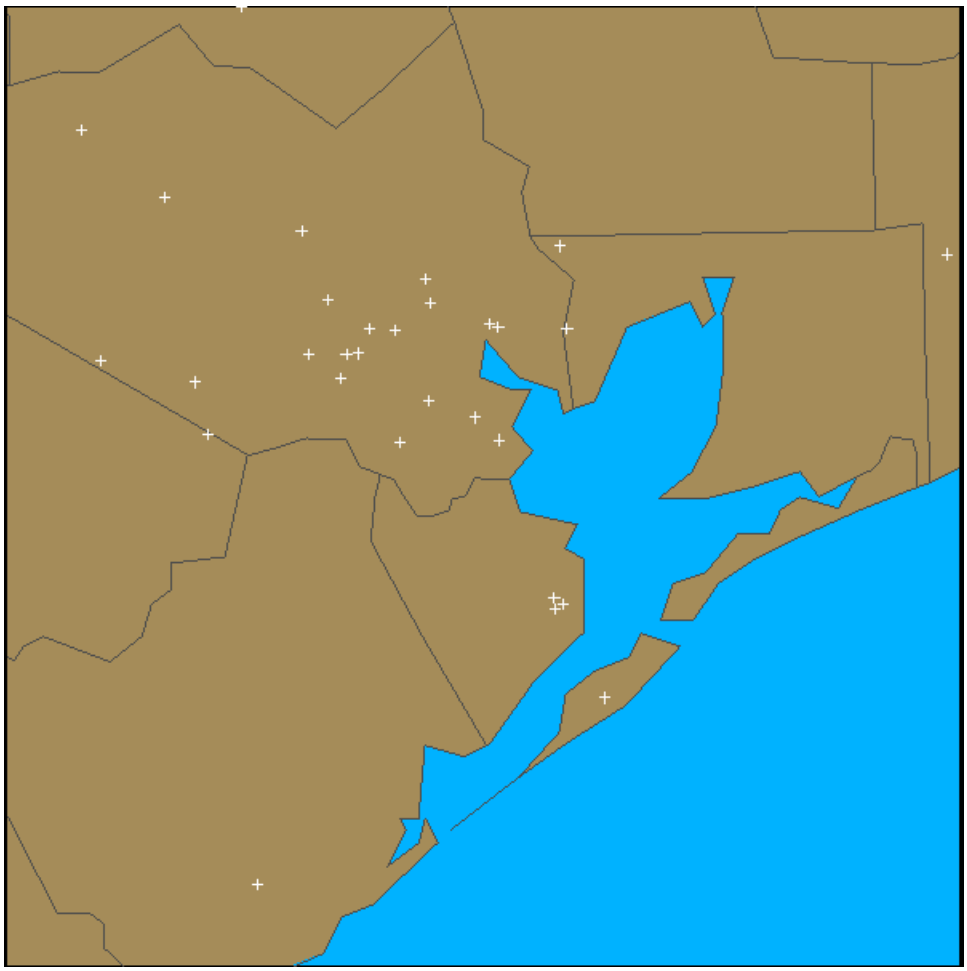

Figure 27: Station locations used in Houston area METSTAT statistical analysis.

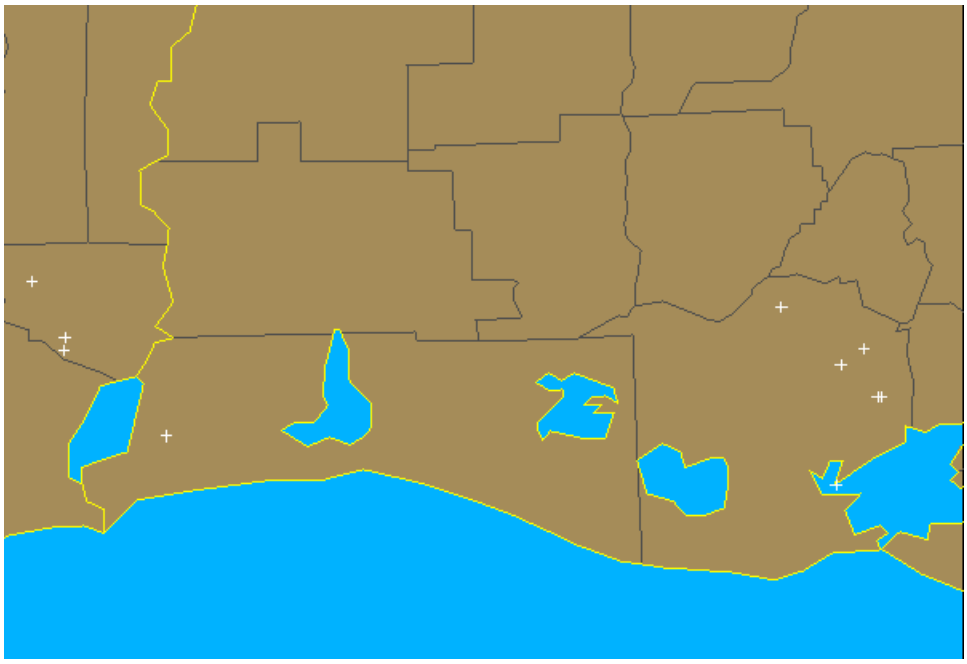

Figure 28: Station locations used in Beaumont area METSTAT statistical analysis.

Model forecasts were interpolated horizontally to station observation locations using bilinear interpolation. Vertical interpolation or reduction techniques were not deemed necessary or advantageous, since the lowest model level (~10m AGL) was sufficiently close to the observation shelter height that is typically 1.5m AGL for temperature and humidity and 10m AGL for wind. We discussed this issue in a technical note available on our web site: http://bridge.atmet.org/harc/reports/validate.pdf.

5 MM5 TexAQS sensitivity simulations

Three MM5 simulations were completed for the entire 22.5 day period of interest. Model physics were selected to be consistent with the Nielsen-Gammon simulations. The latest available version of MM5 (v3.6.0) was employed. The model physics configuration is summarized in Table 4. Grid nudging was applied using the MM5 four-dimensional analysis nudging technique applied above the PBL. The goal is to preserve model predictions that are close to reality while allowing the model to add mesoscale detail in the boundary layer. Analysis nudging strength is set to the MM5 default and is summarized in Table 5.

Table 4: Model Physics

Soil model	NOAH land-surface
Radiation	RTTM radiation scheme
Planetary boundary layer	MRF PBL scheme
Microphysics	Simple ice
Cumulus parameterization	Grell (grids 1-3) None (grid 4)
Nesting	Two-way interactive
Nudging	Four-dimensional grid analysis nudging applied above PBL

Table 5: Analysis nudging coefficients (s^{-1})

Grid	Temperature	Mixing ratio	Wind
1	2.5e-4	1.0e-5	2.5e-4
2	1.0e-4	1.0e-5	1.0e-4
3	1.0e-4	1.0e-5	1.0e-4
4	1.0e-4	1.0e-5	1.0e-4

There were three significant differences between the ATMET runs and the "final" Nielsen-Gammon simulation. The first was the use of two-way interactive nesting, rather than one-way as used by Nielsen-Gammon. The second was a slightly different vertical grid structure. We had used the same structure from our previous TCEQ project (ATMET, 2002a) where the first level was about 10 m above the ground. Nielsen-Gammon's first level was about 20 m above the ground. The third was the utilization of the NOAH land-surface model (Chen and Dudhia 2001a,b) that became available in MM5 version 3.6. Unlike the simple ground heat budget model available in earlier versions of MM5, the NOAH LSM uses four soil levels to explicitly predict soil temperature and moisture resulting in improved surface boundary conditions to the atmospheric model. The improved LSM now available in MM5 is an essential component that

complements the atmospheric model designed to function at grid spacings down to 1km (Chen and Dudhia 2001a).

The NOAH LSM requires the initialization of soil temperature and moisture. This is accomplished using data from EDAS and interpolation techniques similar to those employed for the atmospheric data initialization. These techniques are provided as part of the MM5 software package. Some corrections to the MM5 code, however, were necessary to properly incorporate the EDAS data. EDAS soil temperature and moisture analyses currently use a missing value flag of zero to indicate meaningless grid points over water. As described in section 4.1.1, EDAS analyses were horizontally interpolated from the native 32-km grid to a 40-km grid prior to public dissemination. The horizontal interpolation technique employed at NCEP does not recognize the missing value flag of zero over water. The result is coastline data points on the 40-km EDAS grid have been derived from a mixture of realistic over-land values and unrealistic over-water values of zero. This creates colder soil temperature and drier soil moisture values along the coasts. Since these values no longer conform to the missing flag standard, the MM5 analysis package recognizes these points as valid and incorporates them into the final analysis that is used for model initialization. We developed techniques to recognize these faulty coastline values and to replace them with "nearest-land-neighbor" values.

5.1 Experiment 1 – Control

5.1.1 *Results*

Experiment 1 statistical validation results for the Houston area are summarized in Figures 29-31. Temperature results (Figure 29) show a diurnal prediction bias with colder than observed morning temperatures and afternoon temperatures somewhat warmer than observed. The typical cold bias is around 3K and is fairly uniform through the forecast period. The warm afternoon biases are mostly small (~1K), with the exception of one period from 22-24 August showing larger warm biases of 4 to 6K. Significant convective activity occurred in the Houston area during this time and the model did not correctly capture the convection; hence, the warm bias.

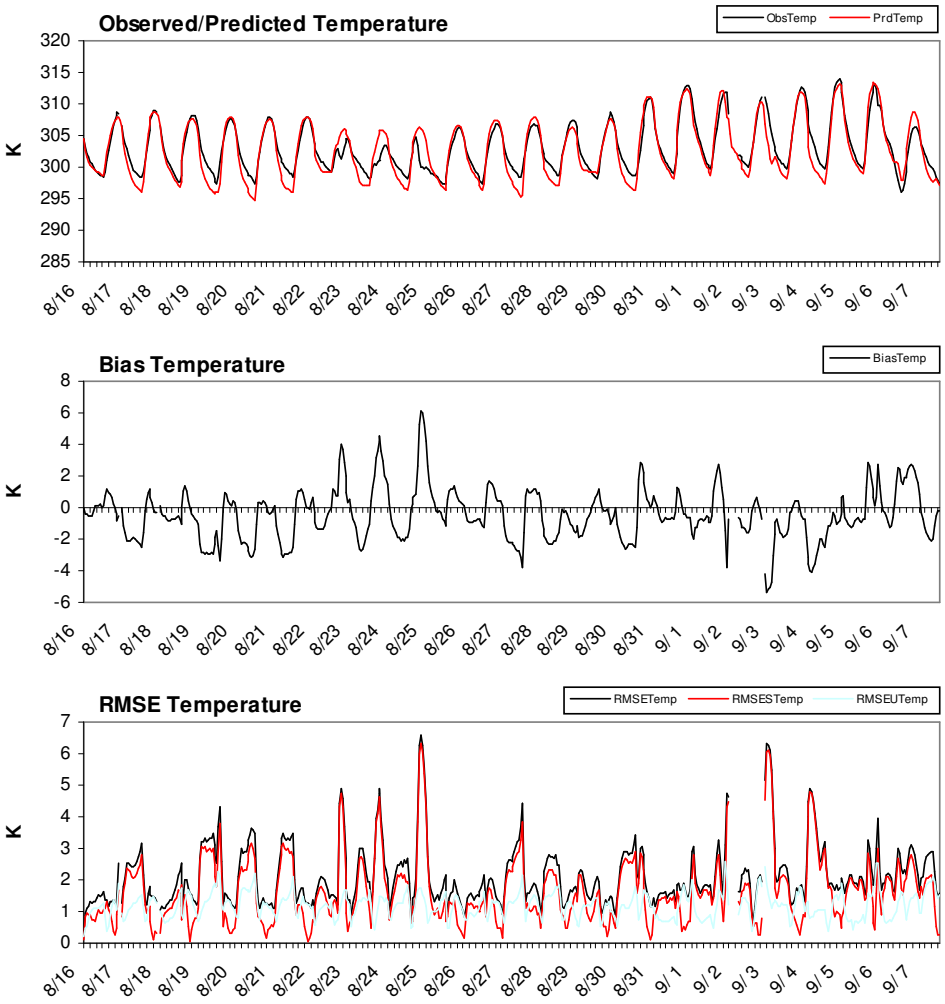

Figure 29: METSTAT hourly temperature (K) statistics for Experiment 1 using 30 Houston vicinity observations.

Of the 30 Houston area stations designated by TCEQ, only five sites routinely reported humidity data. ATMET also conducted a statistical evaluation using all available data within model domain 4, which included about 70 sites. These results are posted online at http://bridge.atmet.org/tceq/stats.shtml. Despite the limited data set presented here, the following results are representative of the larger domain 4 evaluation. Dew point results from the five stations (Figure 30) show a dry bias through almost the entire forecast period. Dry biases are mostly in the range of 2 to 6K with a tendency for higher dry biases during the afternoon. There are two periods of very significant dry bias, one during the afternoon of 20 August and the other during the afternoon of 30 August, where the dry bias exceeds 10K. A closer examination of 20 August is discussed in the next section.

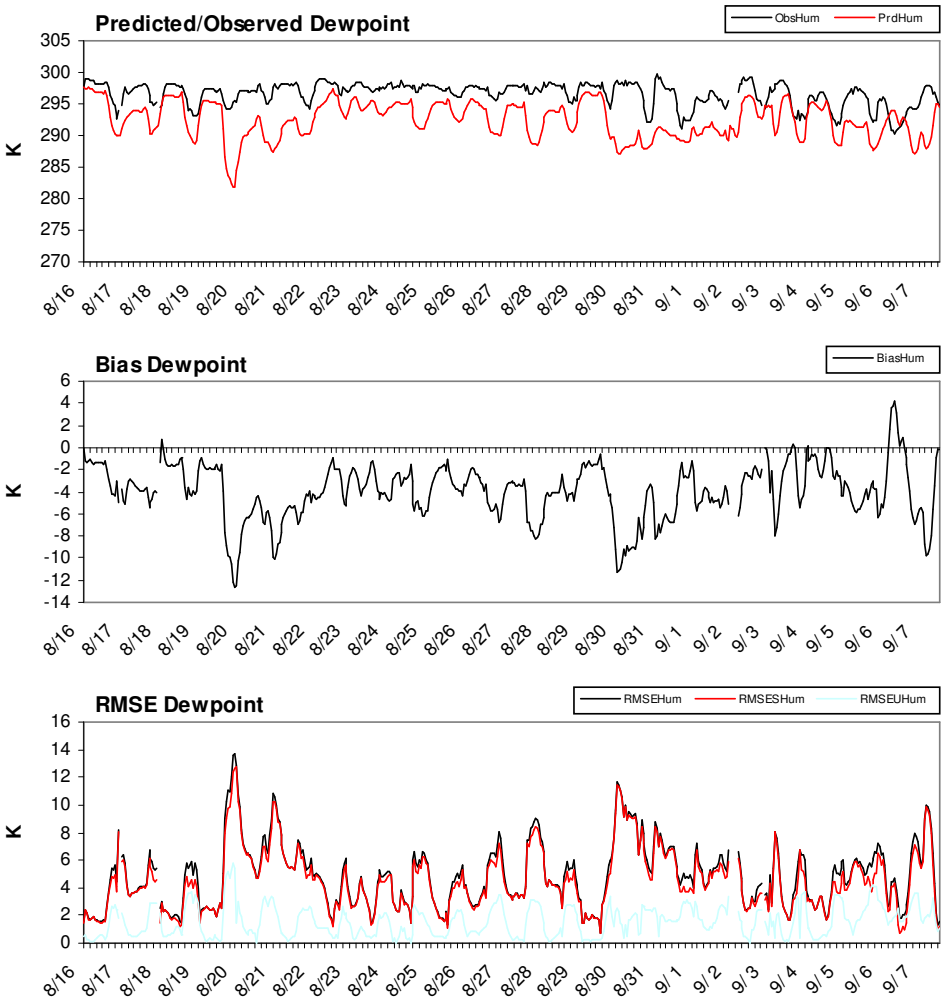

Figure 30: METSTAT hourly dew point (K) statistics for Experiment 1 using five Houston area observations.

Wind speed results (Figure 31) indicate a significant and consistent diurnal bias with a slow wind speed bias during the late morning and early afternoon hours and a high wind speed bias during the nighttime hours. The slow bias typically starts at 1400 UTC and ranges in value from 1 to 2 ms^{-1} through much of August. The slow bias becomes more significant, with values reaching 4 ms^{-1}, after 30 August through the remainder of the forecast period. Nighttime high wind speed biases tend to be on the low side (1-2 ms^{-1}), but they also increase somewhat during September. A detailed examination of the diurnal wind speed bias is presented with Experiment 3 results.

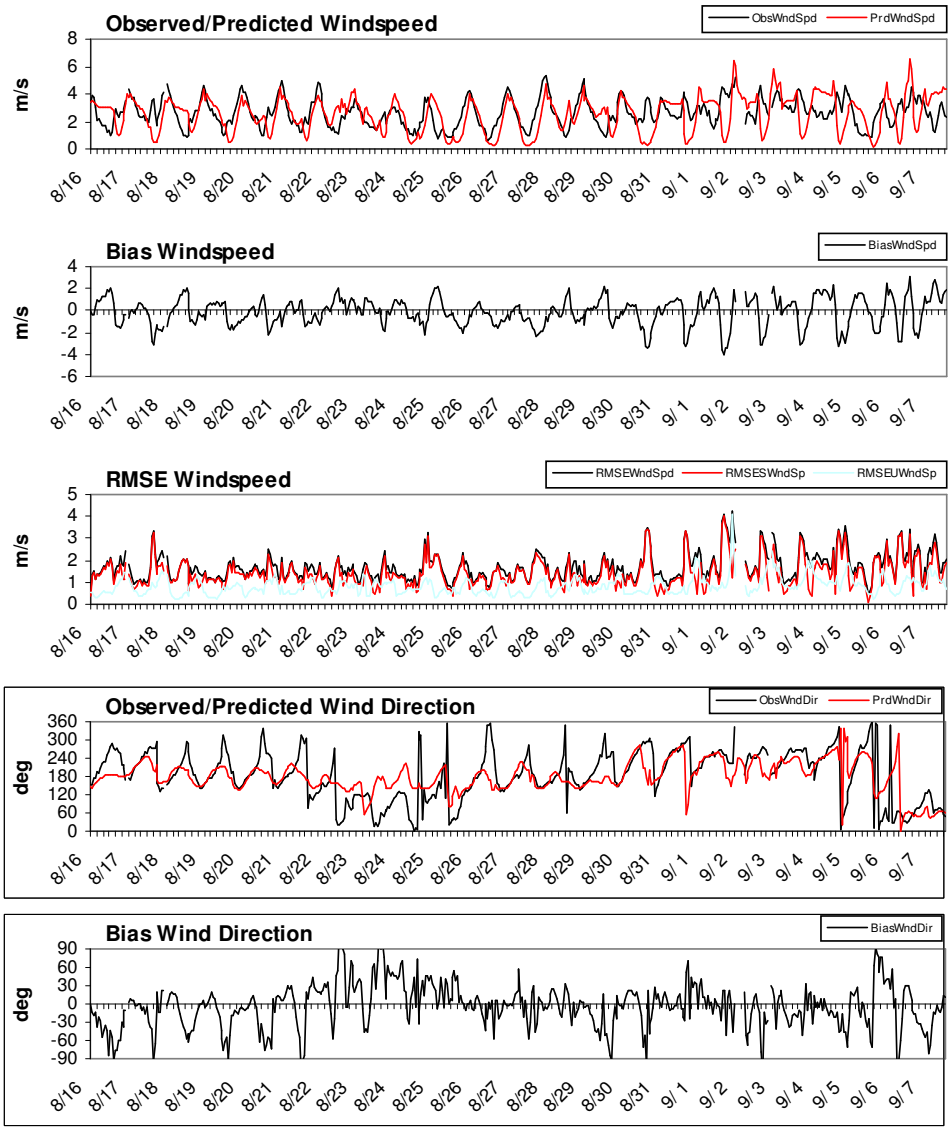

Figure 31: METSTAT hourly wind speed (ms^{-1}) and direction statistics for Experiment 1 using 30 Houston area observations.

Experiment 1 temperature and wind statistical validation results for the Beaumont area are summarized in Figure 32 and Figure 33 (moisture observations were not collected in the Beaumont area). Results are, overall, similar to those from the Houston analysis. Warm daytime temperature biases occurred during the 22-24 August convective period. The diurnal wind speed bias of slow daytime and high nighttime biases is also apparent.

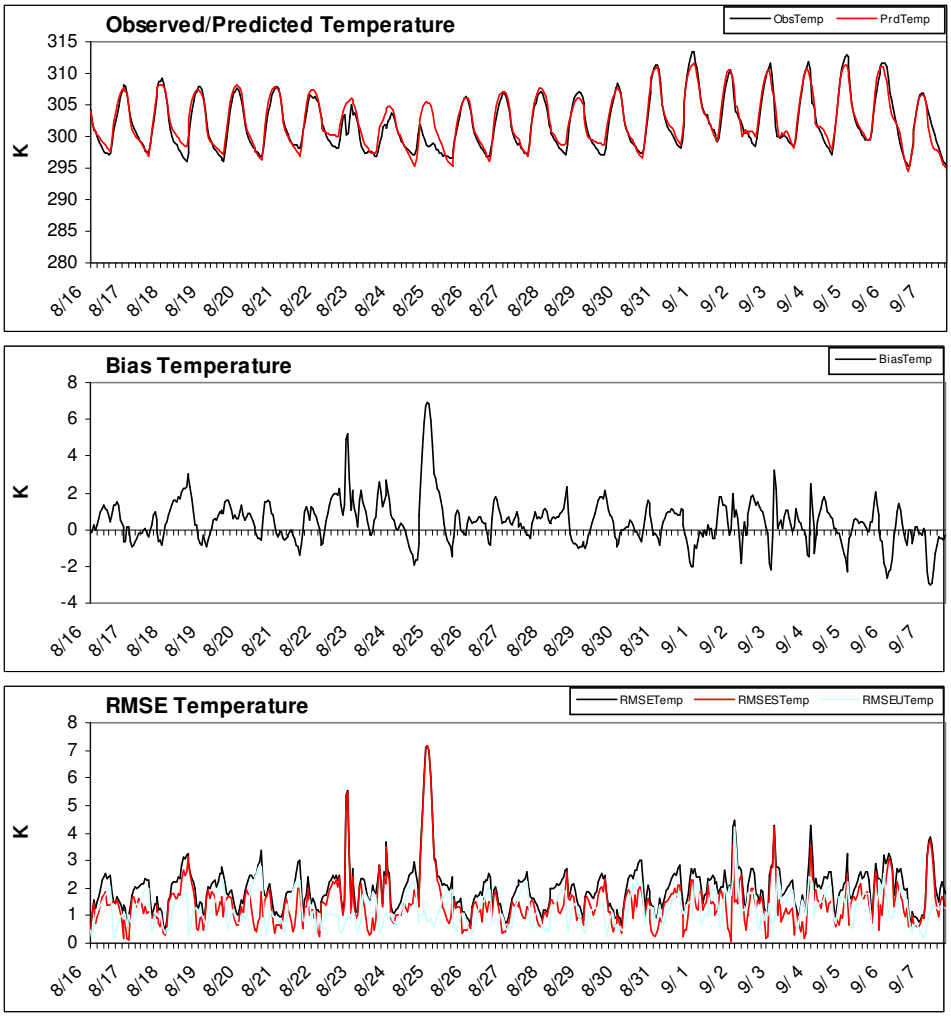

Figure 32: METSTAT hourly temperature (K) statistics for Experiment 1 using 10 Beaumont area observations.

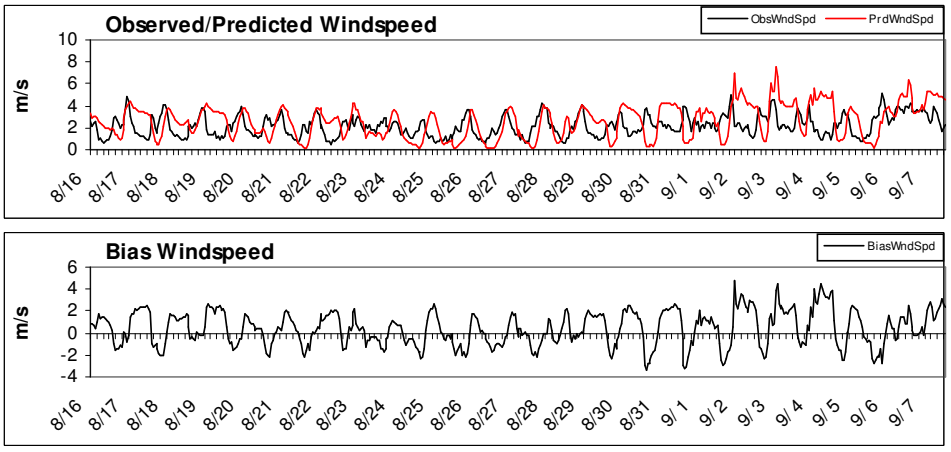

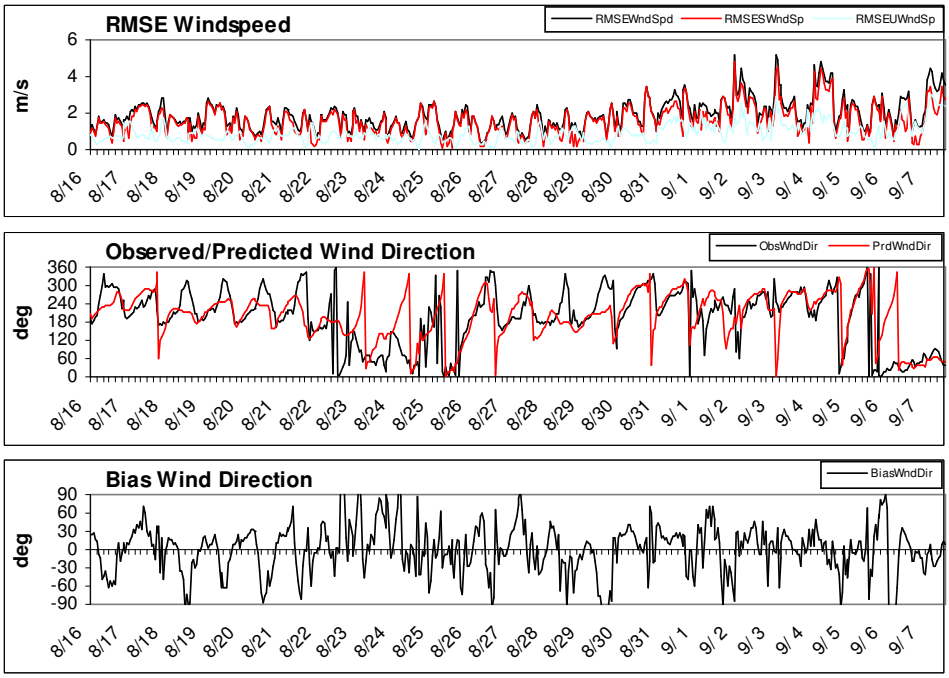

Figure 33: METSTAT hourly wind speed (ms^{-1}) and direction statistics for Experiment 1 using 10 Beaumont area observations.

5.1.2 *Dry dew point bias*

A more detailed examination of the significant dew point drop in the Houston vicinity observed in the MM5 simulation during the afternoon of 20 August is presented. Although observed dew points did lower from about 23 to 16 ^{o}C, MM5 dew points dropped to as low as 6 ^{o}C. The Corpus Christi soundings at 1200 UTC on the 19th and 0000 UTC on the 20th indicate that boundary layer moisture was quite shallow, being confined below 925mb with drier conditions aloft. Inspection of the EDAS moisture data at 850mb showed a specific humidity minimum of 4 $g\text{-}kg^{-1}$ positioned immediately east of Galveston Bay. The MM5 simulation showed a deep mixed boundary layer of up to 3000m at this time. This suggested that the MM5 model mixed the dry air aloft down to the surface, and cross-section analyses of mixing ratio also corroborate this hypothesis. Other studies have indicated that the MRF PBL scheme used in this experiment tends to over-forecast the PBL depth, and our results also suggest the same issue. It is our belief that this is the cause for the significant under-forecast of dew point on 20 August, and this likely contributed to the overall smaller dry bias observed through much of the MM5 simulation.

5.1.3 *Discussion*

Nielsen-Gammon (2001) defined two meteorological regimes during their period of interest: Regime 1) large-scale onshore flow from 25 to 29 August and Regime 2) large-scale offshore flow from 30 August through 1

September. For our extended period of interest, the same two regimes are present with regime 1 onshore flow lasting from 16 August through 29 August and regime 2 offshore flow observed through 7 September. Within the regime 1 timeframe, there was a dry period from 16 through 20 August with warmer daytime temperatures followed by a more convectively active period from 21 to 24 August that lowered maximum temperatures. During the latter portions of the regime 2 timeframe, the offshore flow shifted from westerly to north-northeasterly which caused daytime temperatures to fall after a several day warm period associated with the dry westerly flow.

The primary difference between the first ATMET MM5 forecast and the predictions completed by Nielsen-Gammon was the implementation of the NOAH LSM now available in MM5. A comparison of results illustrates some differences that are the likely attributed to using the new LSM. Nielsen-Gammon (2002c) reported that simulated maximum temperatures were too warm and minimum temperatures were very accurate. With the exception of the convective period (23-25 August), our experiment 1 results indicated slightly cooler temperatures with a cool morning bias and only a small warm afternoon bias. Figure 34 shows daily METSTAT temperature statistics for experiment 1 and is comparable to that presented by Nielsen-Gammon (2002c, see Fig. 6b). Consistent with the hourly statistics, Nielsen-Gammon results show mostly warm temperature biases through the period while our Experiment 1 exhibits both cool and small warm biases (i.e. overall slightly cooler forecasts than Nielsen-Gammon). Even with slightly different bias characteristics, the gross error temperature differences are comparable in the two studies. Also similar to Nielsen-Gammon, the index-of-agreement results are quite good with the exception of the active convective period from 22-24 August.

In order to obtain his particular performance for temperature, Nielsen-Gammon performed artificial modifications of soil moisture at various times during his runs. Note that our runs did not use these types of modifications, lending evidence that the LSM in MM5 is performing better than the older, simple soil schemes.

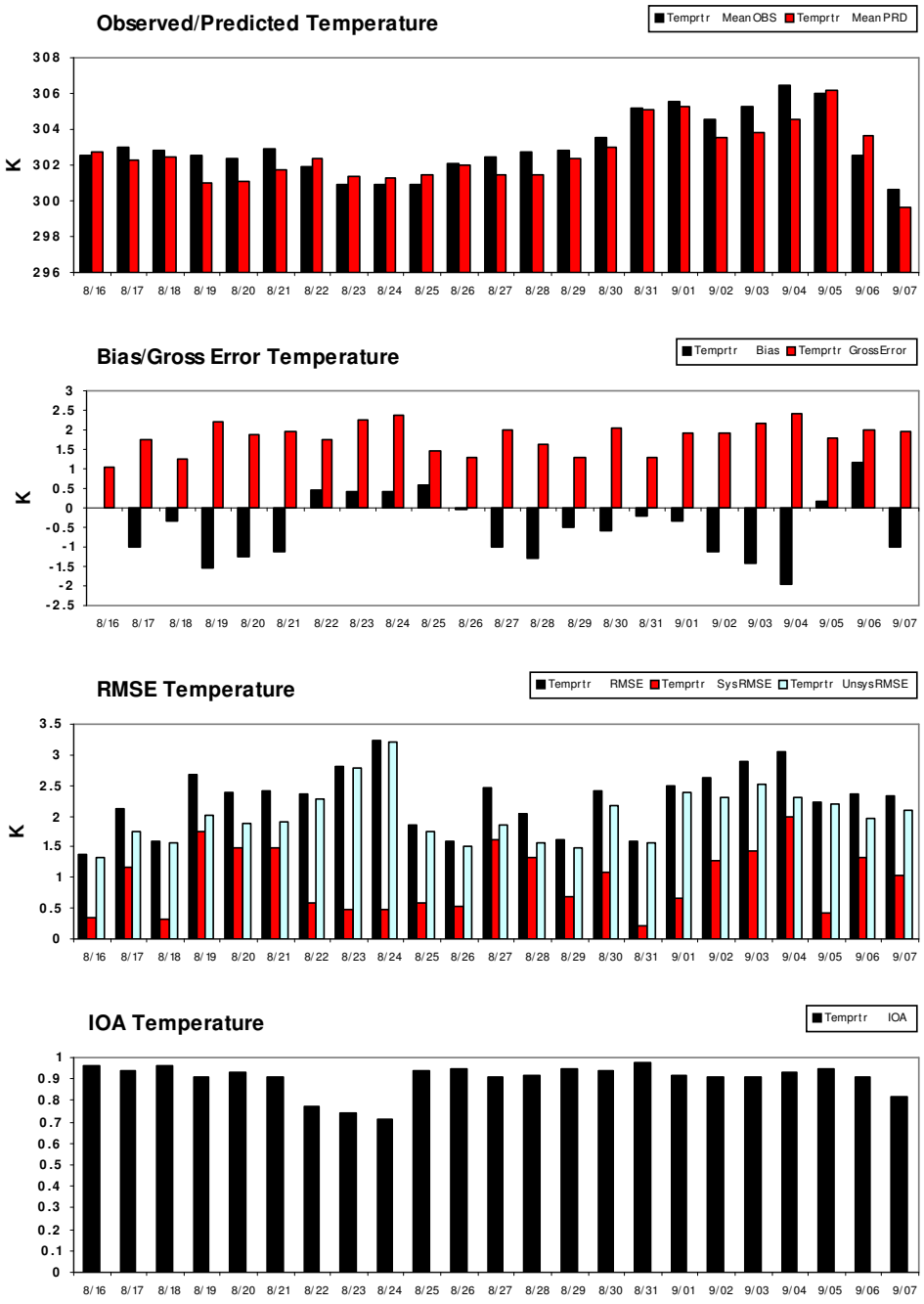

Figure 34: METSTAT daily temperature (K) statistics for Experiment 1 using 30 Houston area observations.

Results are quite similar for the wind speed predictions. Nielsen-Gammon noted differences between regimes 1 and 2, but a slow wind speed bias was noted during many daytime periods and a high wind speed bias was observed during most nighttime hours, similar to our results. Figure 35 illustrates daily METSTAT wind speed statistics for Experiment 1 and is comparable to that presented by Nielsen-Gammon (2002c, see Fig. 6a). Daily wind speed bias results are small through the entire period, but this

is primarily due to the offsetting nature of the high nighttime bias and the low daytime bias. A closer examination of the slow daytime wind speed bias is presented in conjunction with Experiment 3.

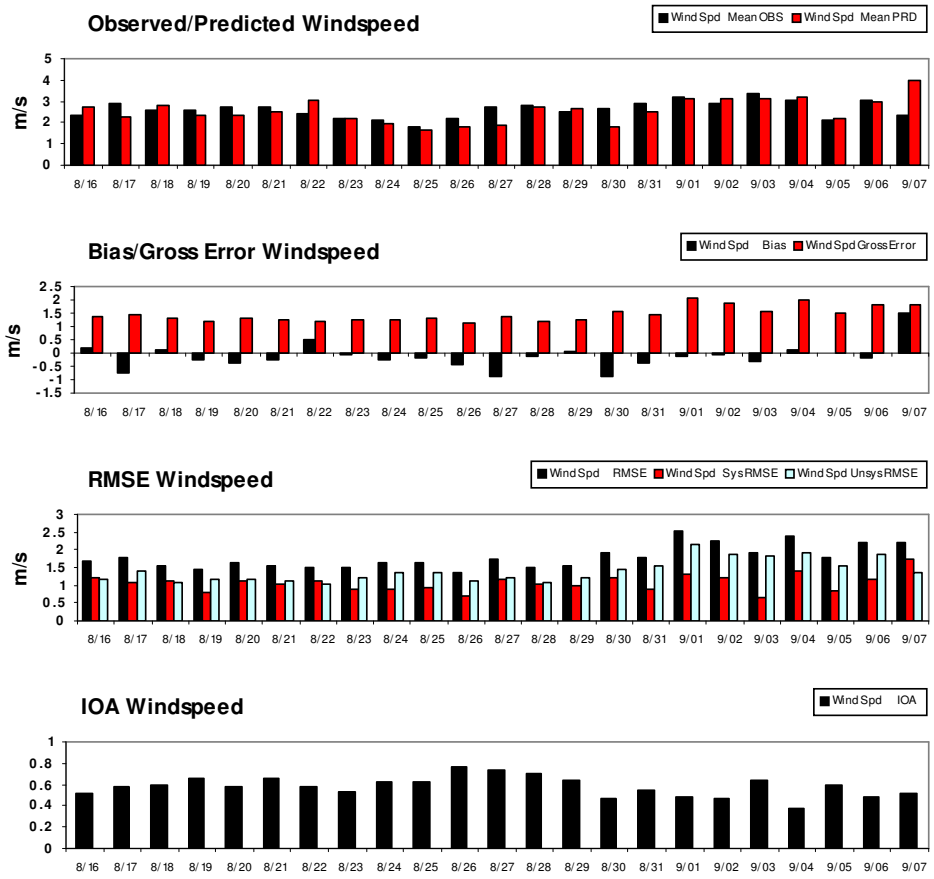

Figure 35: METSTAT daily wind speed statistics (ms^{-1}) for Experiment 1 using 30 Houston area observations.

Model forecast precipitation for all experiments is available on-line at http://bridge.atmet.org/tceq/forecast.shtml. Observations indicated an initial dry period through about 21 August which the model handled correctly. Persistent on-shore (regime 1) flow aided in developing periods of convective precipitation from 22 through 25 August. The model did produce precipitation late on the 22nd and early on the 23rd, but too far inland. In general, the model did not capture the change to more convective activity. Another dry period followed from the 26th to 30th and the model was dry as well. Some isolated convection was observed during regime 2 from the 31st through the 3rd, and in general, the model did better at producing isolated precipitation during this period of regime 2. Conditions were dry through the remainder of the period in both the observations and the model forecasts.

5.2 Experiment 2 – Observation nudging sensitivity

Nielsen-Gammon (2002b) results suggested an improvement in model forecast quality, especially during the high ozone event of 25 August, through the use of observation nudging to Houston area wind profilers and lidar deployed during the period of interest. Experiment 2 uses all the same physics as Experiment 1 with the addition of observation nudging to five Houston area wind profilers and one lidar.

5.2.1 *Observation nudging methodology*

There are 3 sources of profiler/lidar observation data available - 1) the White profiler data set, 2) the Angevine profiler data set, and 3) an MM5 observation-nudging file created by Nielsen-Gammon that includes a merged data set of profiler and lidar observations for the time period from 25 August through 1 September. Nielsen-Gammon (2002c) invested a fair amount of time merging the data sets into a single MM5 observation-nudging file, and we desired to utilize that file for that period of time. The extended time period of this study necessitated that we consistently merge the profiler data from prior to 25 August and after 1 September with the Nielsen-Gammon data.

Each data source, unfortunately, indicated different geographical locations for the profiler sites. The locations in the White files were clearly spurious for at least one of the profiler sites, and several files contained different locations for the same profiler site. Based on personal communication with Nielsen-Gammon, we elected to use the Nielsen-Gammon locations, and not the Angevine positions, uniformly for all data sources. The next step was to identify specific stations within the Nielsen-Gammon MM5 file because this file contained only grid dependent (i,j) locations and did not contain station identifiers. The Nielsen-Gammon (i,j) locations were converted to latitude/longitude positions and then were compared to the Angevine latitude/longitude locations. The correspondence was close and, hence, we could identify specific stations in the Nielsen-Gammon data set.

The ATMET MM5 observation nudging file was then created as follows: the profiler and lidar site locations from the Nielsen-Gammon data set were used at all available times. The Nielsen-Gammon data set was used verbatim for the period from 25 August through 1 September. This required modifying the ATMET vertical grid to match the Nielsen-Gammon vertical grid. Since MM5 uses a downward vertical grid index system that starts at the top of the model domain, we were able to add an additional model level near the surface (~10m AGL), that was not used by Nielsen-Gammon, to mimic the lowest level used in Experiment 1. This additional low level was found to improve the simulation and model validation when compared to shelter-height observations. This did not affect the use of the Nielsen-Gammon data. The resulting vertical grid

contained 44 levels (Table 6). One modification to the Nielsen-Gammon data was required. The Nielsen-Gammon file contained (i,j) locations positioned within MM5 grid 4. Since the ATMET run used 2-way grid nesting, these (i,j) locations had to be converted to MM5 grid 1. For the time periods prior to and after the Nielsen-Gammon data set, the White profiler data was converted to the MM5 format and merged chronologically with the Nielsen-Gammon data set to create the final MM5 observation-nudging file.

Table 6: Experiment 2 MM5 vertical sigma levels.

1.000	0.998	0.996	0.990	0.980	0.970	0.960	0.950
0.940	0.930	0.920	0.910	0.895	0.880	0.865	0.850
0.825	0.800	0.775	0.750	0.720	0.690	0.660	0.630
0.600	0.570	0.540	0.510	0.475	0.440	0.405	0.370
0.330	0.290	0.250	0.210	0.175	0.145	0.115	0.090
0.065	0.045	0.025	0.010	0.000			

There are four parameters that control the observational nudging characteristics in MM5: 1) time interval, 2) vertical radius of influence, 3) horizontal radius of influence, and 4) nudging strength. Experiment 2 nudging weights are summarized in Table 7. We used the same vertical radius of influence (0.001) as Nielsen-Gammon (2002b), and the same nudging time interval (120 minutes) adopted by Nielsen-Gammon in later runs (2002c). Nielsen-Gammon used a horizontal radius of influence of 150 km to allow the profiler data to influence the model solution over most of the coastal plain. We felt, given the relatively close proximity of the profiler data, that a smaller horizontal radius of influence of 40 km was more appropriate. Nielsen-Gammon reported that using a nudging time-scale weight of 0.0001 s^{-1} was too weak, which was subsequently increased to 0.0004 s^{-1}. We elected to use a time-scale of one hour (0.000278 s^{-1}) that is the frequency of available profiler data.

Table 7: Observation nudging coefficients (grid 4 wind only).

Nudging coefficient (s^{-1})	2.78e-4
Time window (min)	120
Horizontal radius of influence (km)	40
Vertical radius of influence (sigma levels)	0.001

5.2.2 *Summary of differences between Experiments 1 and 2*

In addition to observation nudging and changes to the vertical grid structure, one other notable difference was employed for Experiment 2. A higher resolution 30-sec USGS data set was used to construct

land/soil/water characteristics (e.g. topography) for grid 4. Figure 36 illustrates grid 4 dominant land use category and shows the improvements of using the higher resolution USGS data (compare to Figure 26).

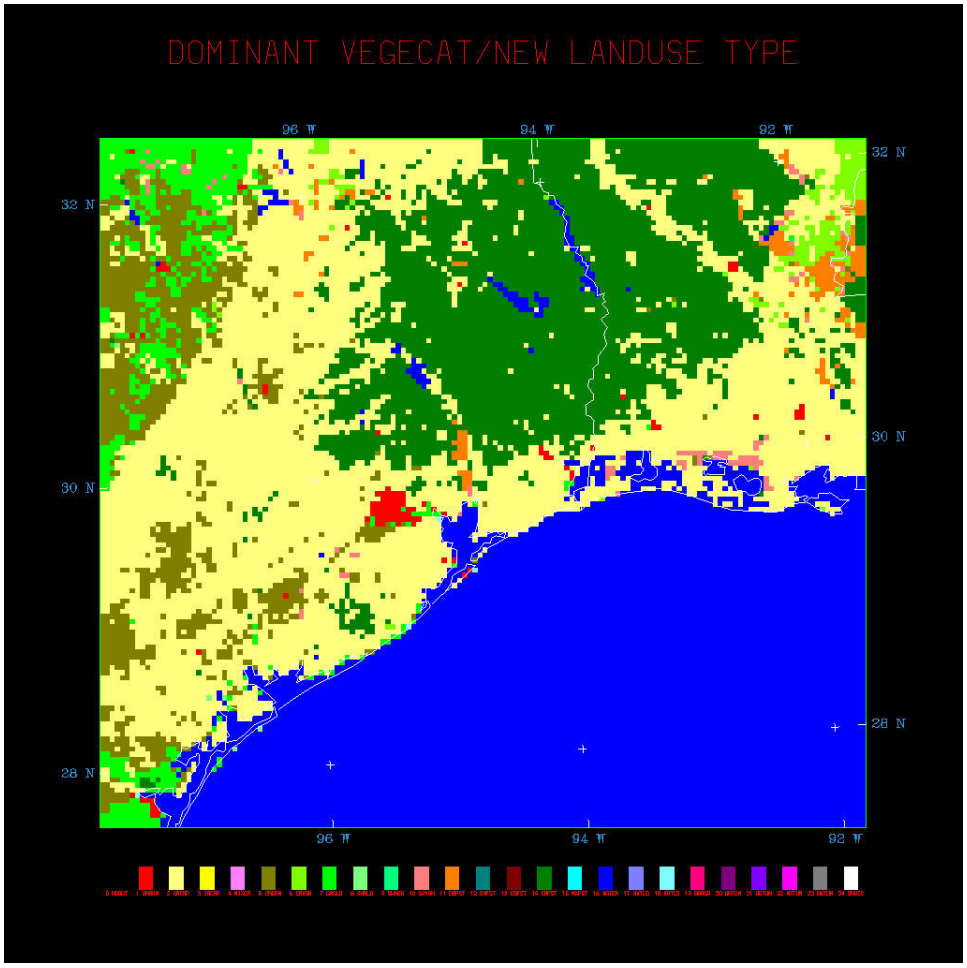

Figure 36: Grid 4 dominant land use category derived from 30-sec USGS data.

5.2.3 *Results*

Experiment 2 statistical validation results are summarized in Figure 37 and Figure 38. The results, in general, suggest that observation nudging provided only minor, insignificant differences to the model forecast. The overall biases of cool morning/warm afternoon temperature, dry dew point, and slow daytime wind speed remain essentially unchanged through the forecast period. More detailed comparison of the two forecasts can be viewed online at http://bridge.atmet.org/tceq/stats.shtml. A closer examination of the August 25 high ozone day is discussed below.

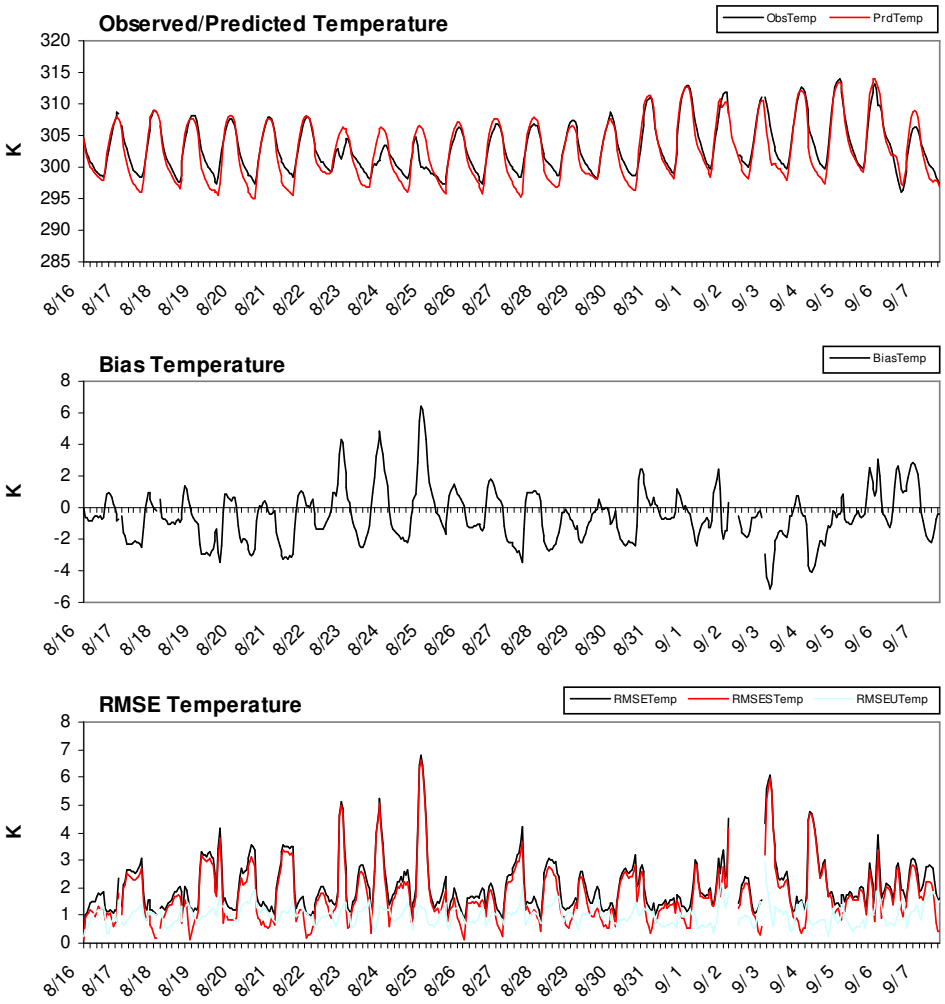

Figure 37: METSTAT hourly temperature (K) statistics for Experiment 2 using 30 Houston area observations.

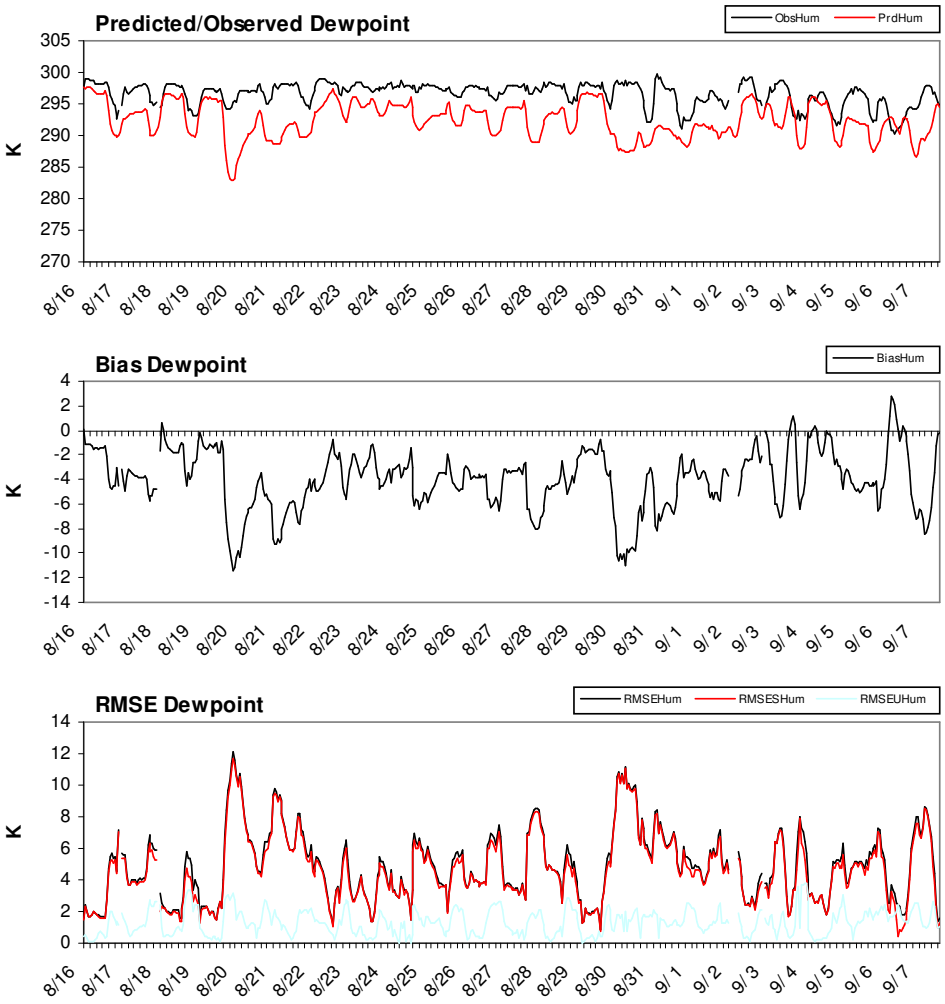

Figure 38: METSTAT hourly dew point (K) statistics for Experiment 2 using five Houston area observations.

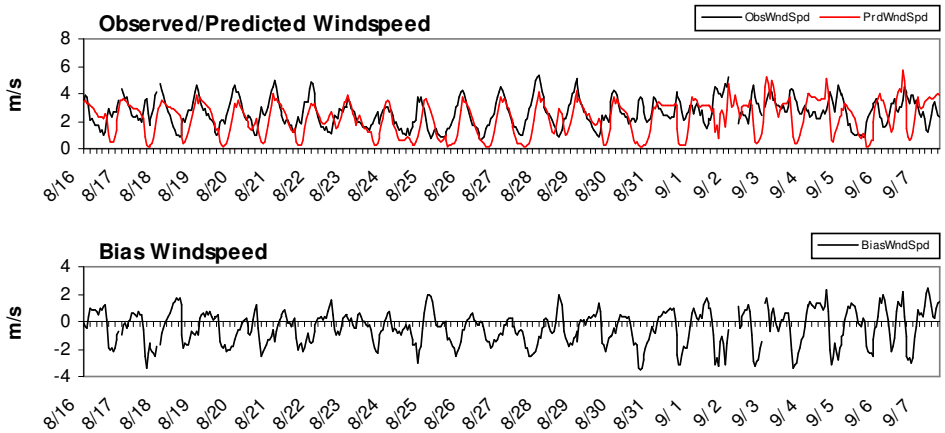

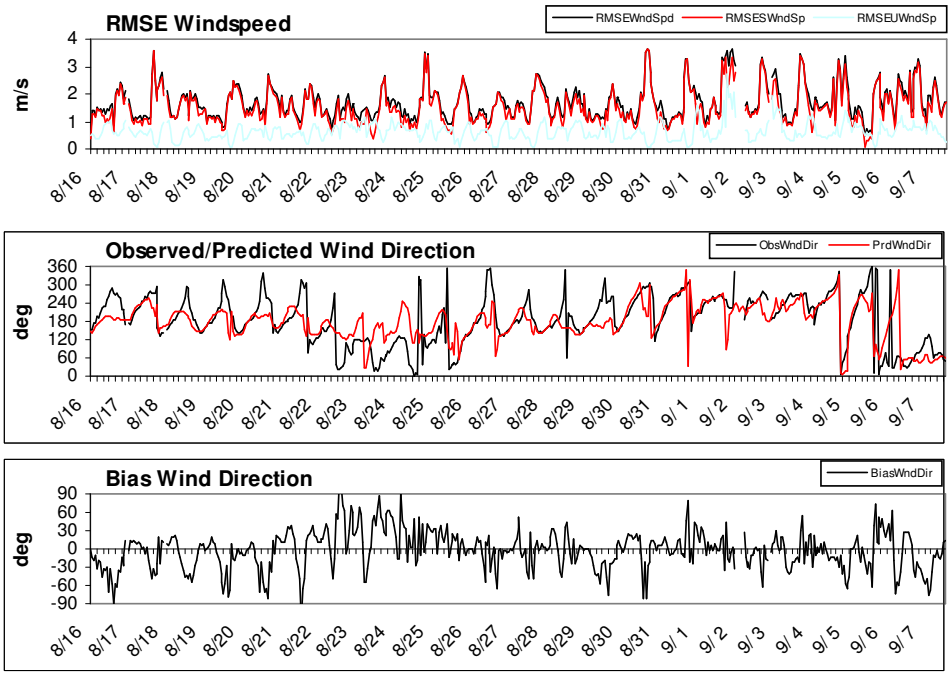

Figure 39: METSTAT hourly wind speed (ms^{-1}) and direction statistics for Experiment 2 using 30 Houston area observations.

Experiment 2 temperature and wind statistical validation results for the Beaumont area are summarized in Figure 40 and Figure 41. No significant differences are noted between experiments 1 and 2, as expected, since the observational nudging was confined to the Houston area.

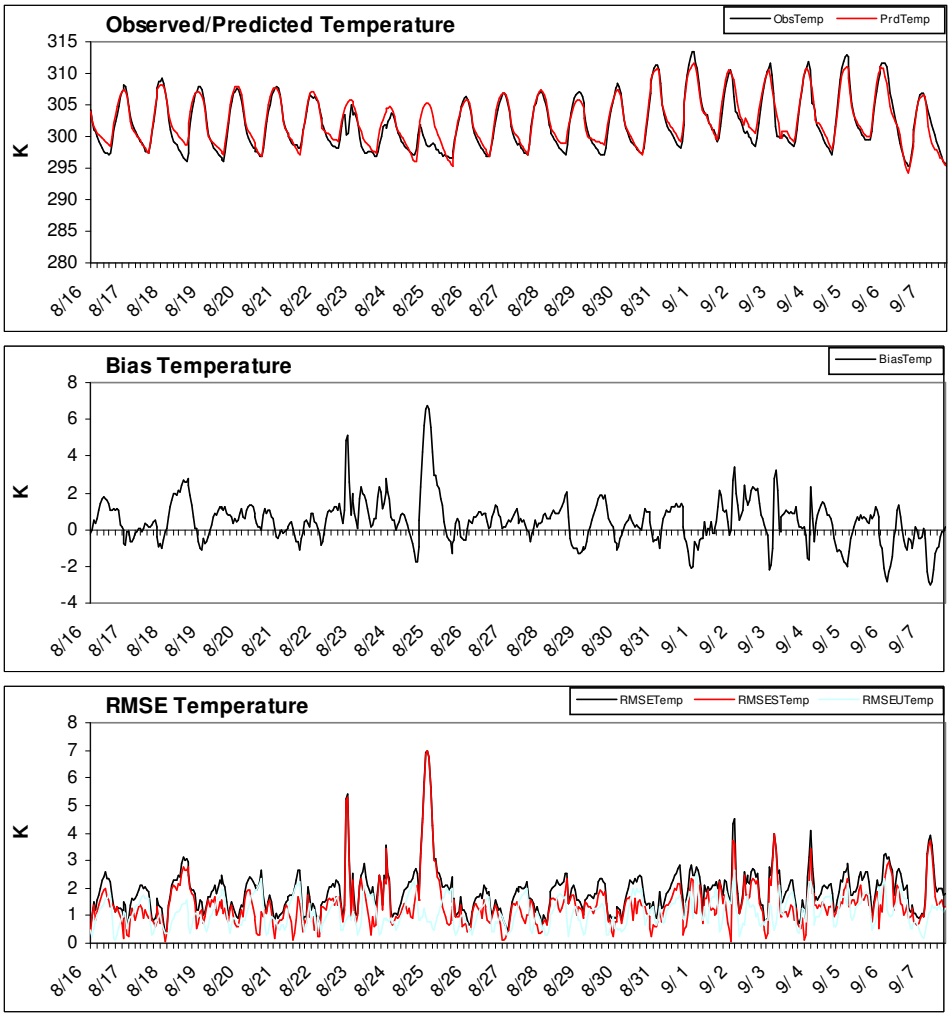

Figure 40: METSTAT hourly temperature (K) statistics for Experiment 2 using 10 Beaumont area observations.

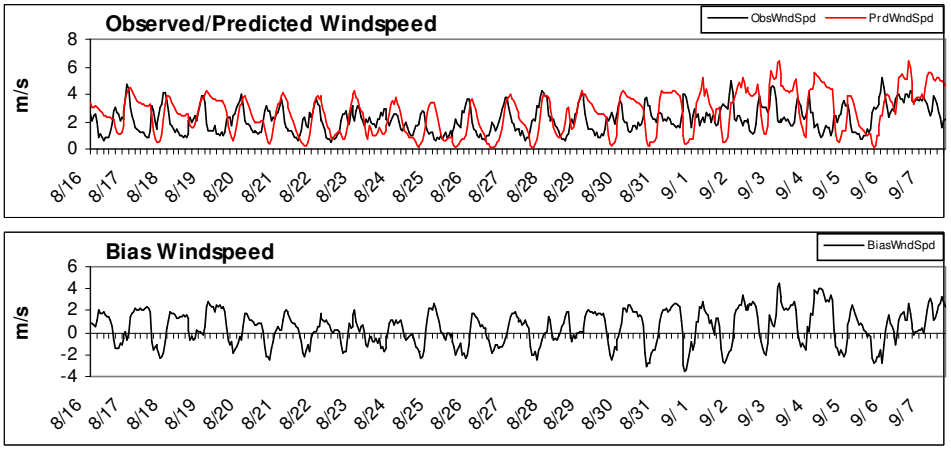

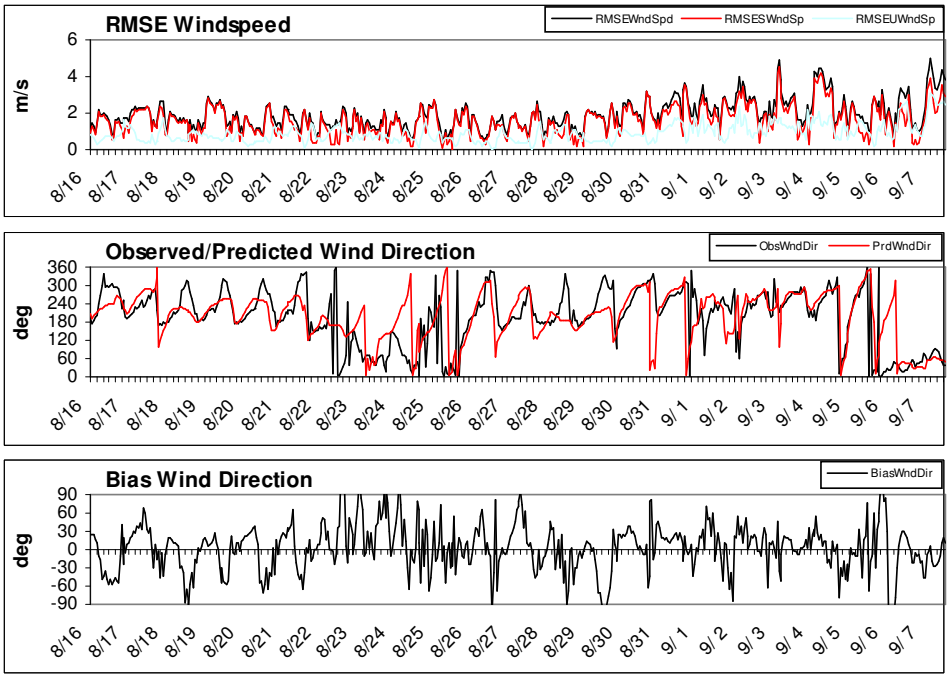

Figure 41: METSTAT hourly wind speed (ms^{-1}) and direction statistics for Experiment 2 using 10 Beaumont area observations.

5.2.4 *Additional nudging parameter sensitivity runs*

A doubling of the nudging weight to 0.000556 s-1, which corresponds to a 30 minute time-scale, was tested to investigate the sensitivity of the nudging weight parameter. A history restart of the model at 0000 UTC 25 August, the time that lidar data became available, was performed using the stronger weight. Results from this run show only small differences when compared to the previous simulation, suggesting that the weaker weight is sufficiently strong. A second, similar experiment was conducted that used the stronger nudging weight combined with the larger 150 km horizontal radius of influence. Once again, results show only small differences, suggesting that the smaller horizontal radius of influence is acceptable.

5.2.5 *Discussion*

The overall Experiment 2 results did not indicate that observation nudging provided any wholesale forecast improvements. But since the observation nudging is essentially confined to the Houston area, a more detailed examination of the forecasts in the metro area is warranted. Nielsen-Gammon (2002b) examined the two high ozone periods – 25-26 August and 29 August-1 September, and noted some localized improvements.

5.2.5.1 25 August rapid ozone formation event

Observed surface winds at 1600 UTC (Figure 42), as described by Nielsen-Gammon, were generally very light northeasterly around the Houston area. By 1800 UTC, the metro winds strengthen from the east, and a bay breeze initiates along the coastal boundary. The bay breeze moved westward from Galveston Bay just reaching eastern Houston by 2000 UTC and pushing through most of Houston by 2200 UTC (Nielsen-Gammon 2002b, see Fig. 30). High ozone was first observed just southwest of the Houston shipping channel, which then tracked westward and northwestward during the afternoon.

Nielsen-Gammon noted that the model forecasts also had light morning winds but tended to be out of the southwest, and the model had difficulties simulating the strengthening easterlies over land. Apparently, there was an improvement with the forecast using observation nudging, but the easterlies still developed later than observed, which would cause the high ozone region to be more concentrated and slower moving than observed.

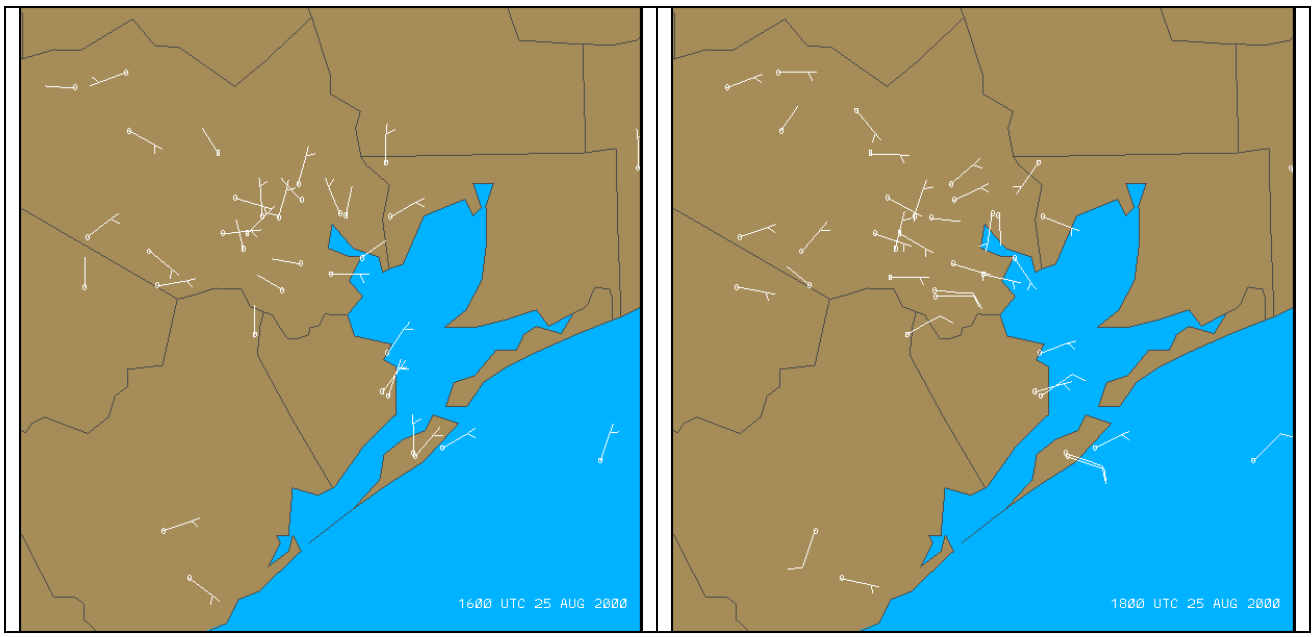

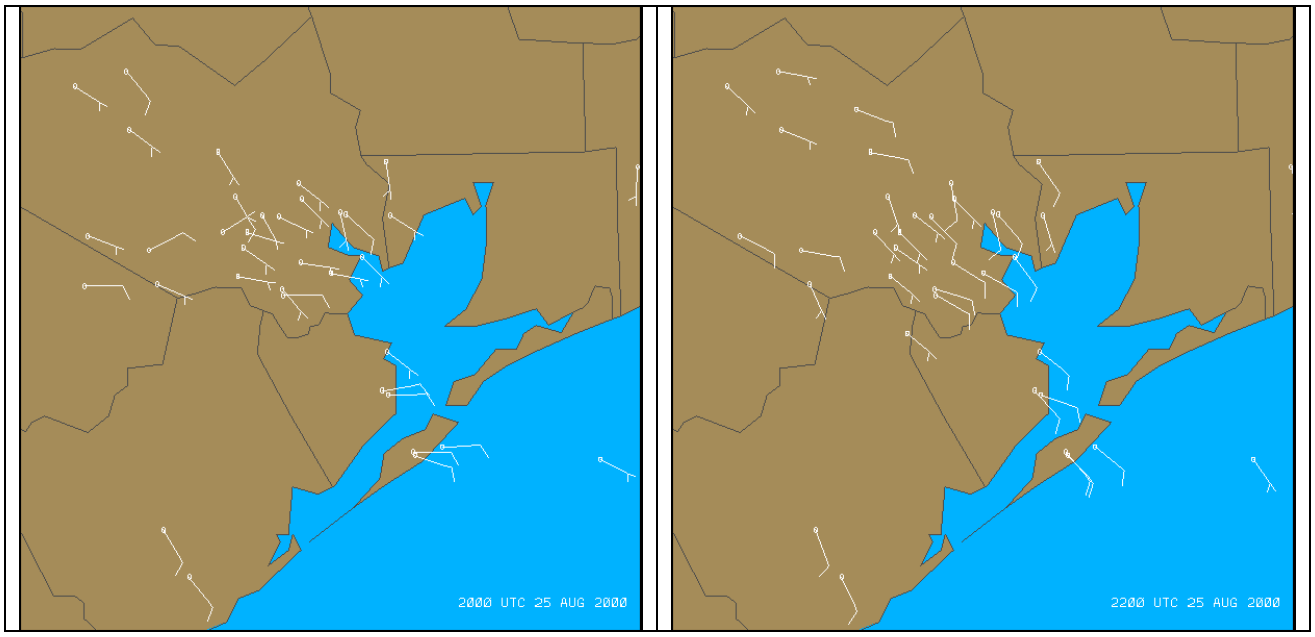

Figure 42: Surface wind observations (full barb = 10 knots) for 25 August at a) 1600 UTC, b) 1800 UTC, c) 2000 UTC, and d) 2200 UTC.

Figure 43 shows the evolution of low-level temperature and wind during the same time period for Experiment 2. At 1600 UTC, the land-based winds were essentially calm, although they have a northeast component as observed. The land-based winds increased speed slightly at 1800 UTC, although they appeared under-forecast compared to observations, but still retain an easterly component. The initiation of the bay breeze compared well with observations. The movement of the bay breeze front, reaching southeast Houston at 2000 UTC and moving through much of the metro area by 2200 UTC, also compared well with observations. This bay breeze progression suggested that the model would more correctly advect the ozone plume into Houston when compared to the Nielsen-Gammon simulations. A comparison of the flow fields between Experiments 1 and 2 showed very few differences (not shown) suggesting that the observation nudging did not play a significant role in the forecast improvement. Indeed, if the simulation is already close to observations, then the nudging would do little to alter the prediction. The more likely scenario is that the simulation improvement resulted from a better representation of the land-water interface provided by the NOAH LSM.

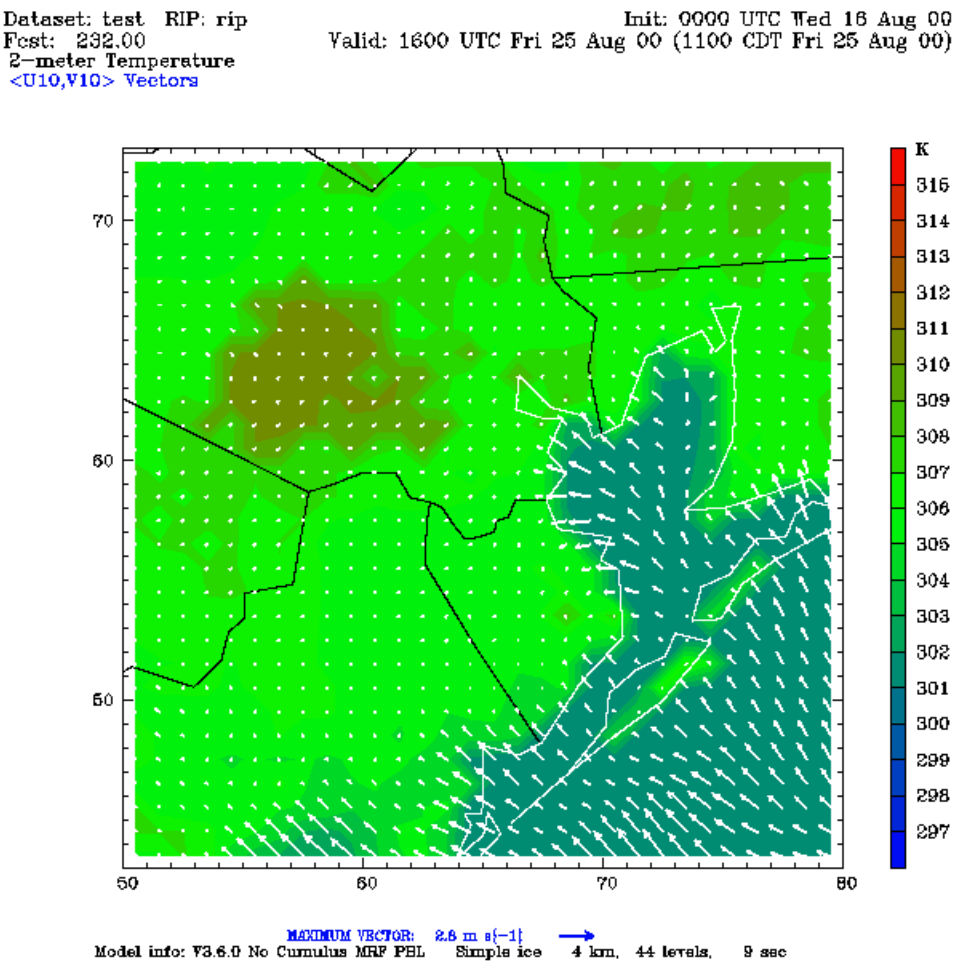
Dataset: test RIP: rip
Fcst: 232.00
2-meter Temperature
<U10,V10> Vectors
Init: 0000 UTC Wed 16 Aug 00
Valid: 1600 UTC Fri 25 Aug 00 (1100 CDT Fri 25 Aug 00)
K
316
314
313
312
311
310
309
308
307
306
305
304
303
302
301
300
299
298
297
70
60
50
50
60
70
80
MAXIMUM VECTOR: 2.6 m s(-1)
Model info: V3.6.0 No Cumulus MRF PBL Simple ice 4 km, 44 levels, 9 sec

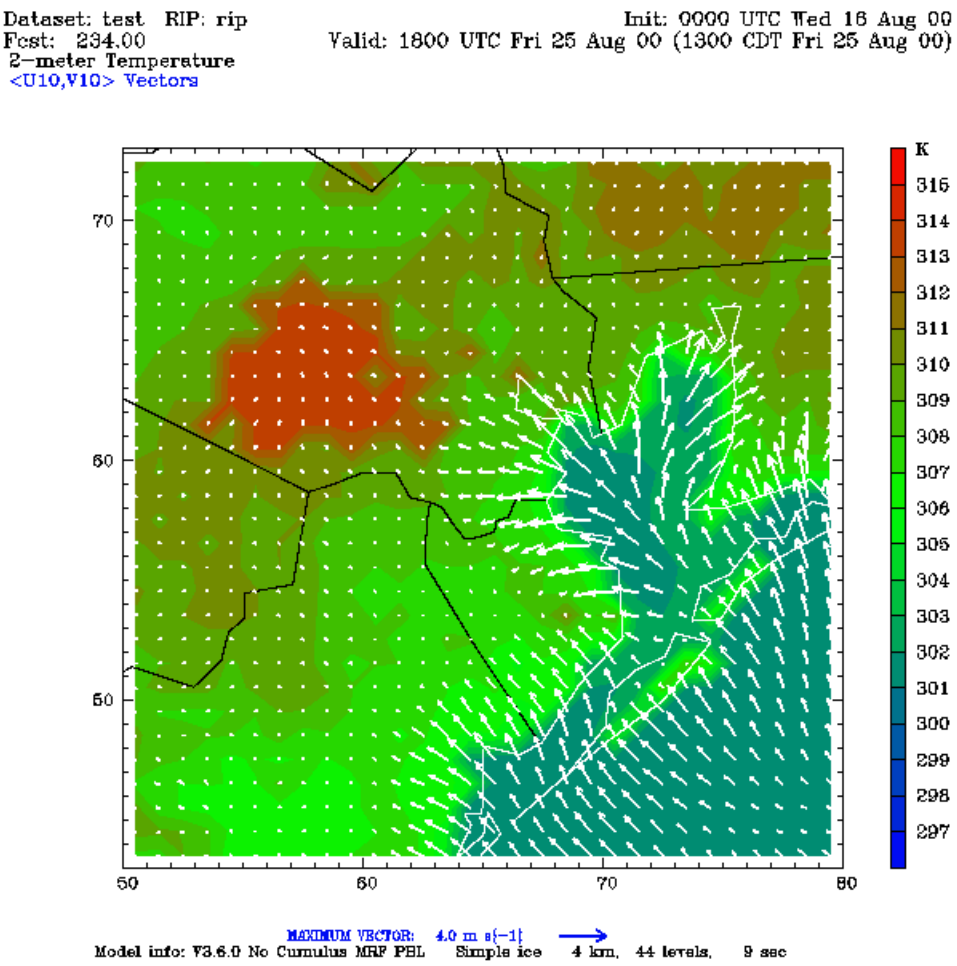
Dataset: test RIP: rip
Fcst: 234.00
2-meter Temperature
<U10,V10> Vectors
Init: 0000 UTC Wed 16 Aug 00
Valid: 1800 UTC Fri 25 Aug 00 (1300 CDT Fri 25 Aug 00)
K
316
314
313
312
311
310
309
308
307
306
305
304
303
302
301
300
299
298
297
70
60
50
50
60
70
80
MAXIMUM VECTOR: 4.0 m s(-1)
Model info: V3.6.0 No Cumulus MRF PBL Simple ice 4 km, 44 levels, 9 sec

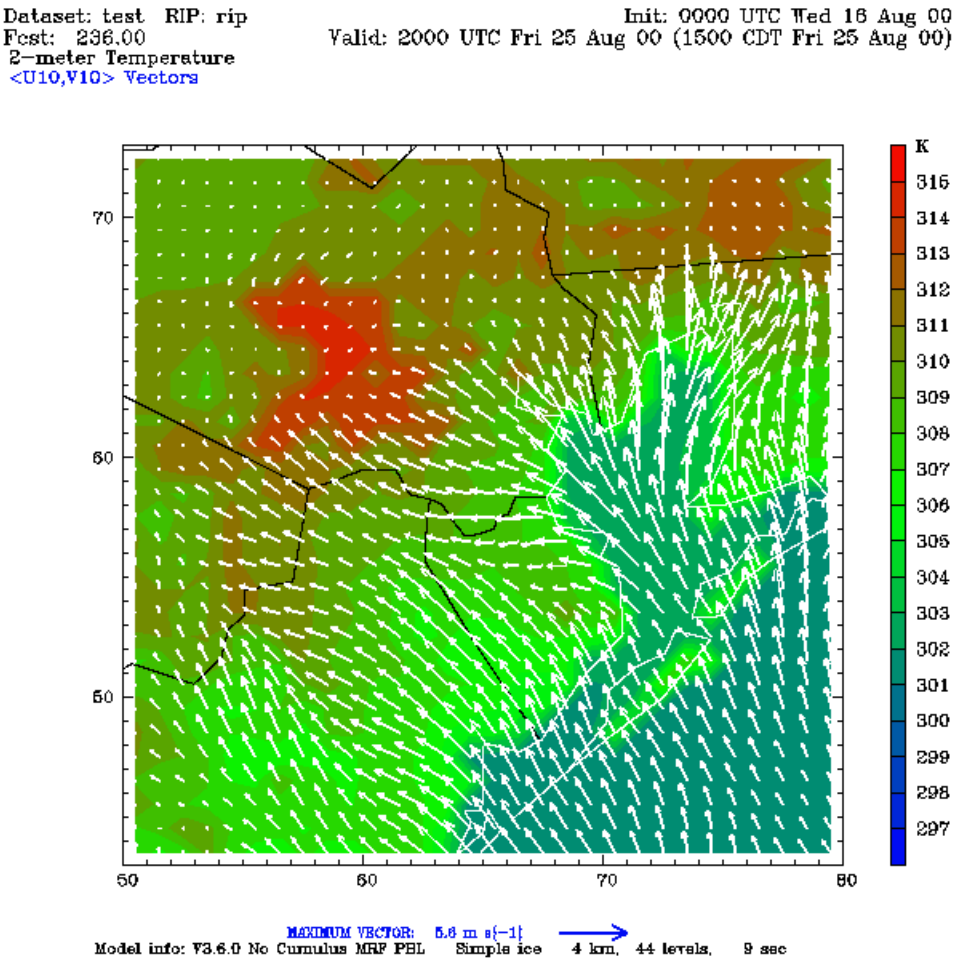
Dataset: test RIP: rip
Fcst: 236.00
2-meter Temperature
<U10,V10> Vectors
Init: 0000 UTC Wed 16 Aug 00
Valid: 2000 UTC Fri 25 Aug 00 (1500 CDT Fri 25 Aug 00)
K
316
314
313
312
311
310
309
308
307
306
305
304
303
302
301
300
299
298
297
70
60
50
50
60
70
80
MAXIMUM VECTOR: 5.6 m s(-1)
Model info: V3.6.0 No Cumulus MRF PBL Simple ice 4 km, 44 levels, 9 sec

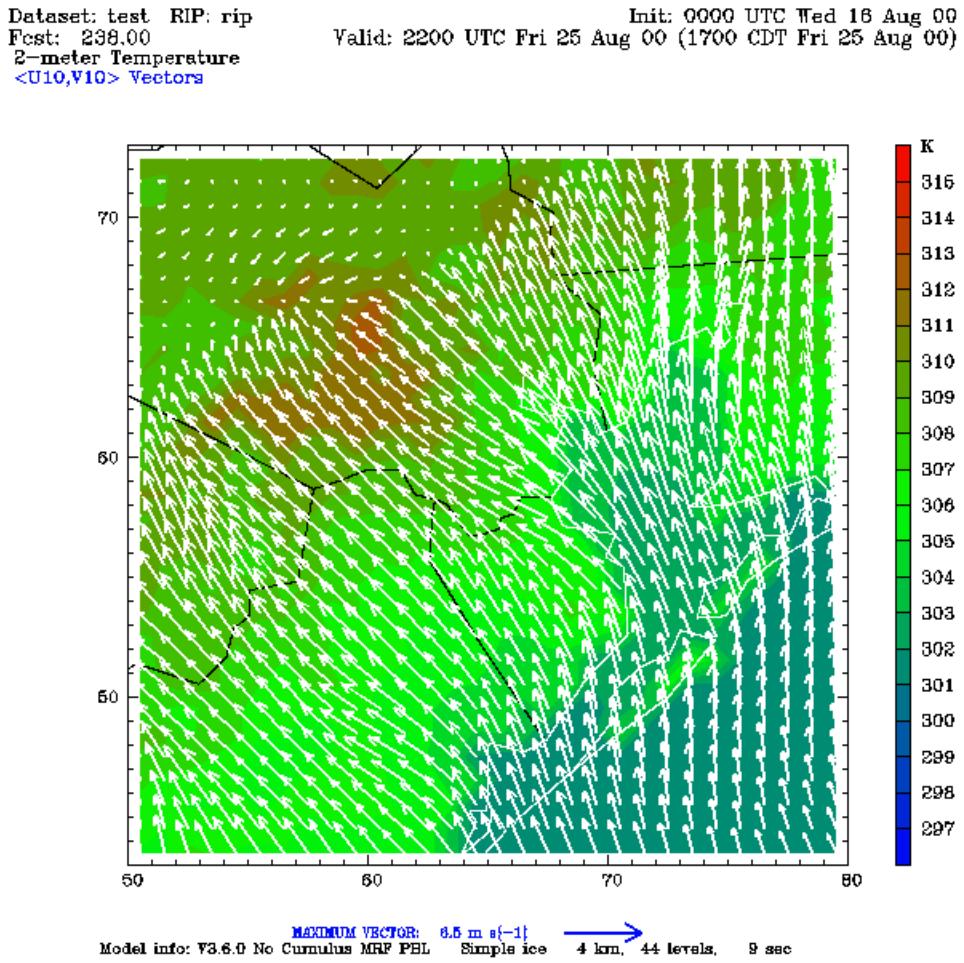

Figure 43: Experiment 2 predictions of low-level temperature (K) and wind (ms^{-1}) for 25 August at a) 1600 UTC, b) 1800 UTC, c) 2000 UTC, and d) 2200 UTC.

5.2.5.2 30 August rapid ozone formation event

A second rapid ozone formation event occurred on 30 August. In contrast to 25 August, the synoptic flow was primarily westerly (off-shore), the first day of regime 2 (Nielsen-Gammon 2002b). The winds were primarily west to northwest at 5 to 10 knots at 1600 UTC (Figure 44). Around mid-day (1800 UTC), winds remained weak out of the west-northwest with only a hint of a developing bay breeze. At 2000 UTC, most winds were weak and variable with still only a hint of a bay breeze. Two hours later (2200 UTC), winds remained light and variable over the metro area and a weak bay breeze appeared to have reached the southeast edge of Houston. Nielsen-Gammon (2002b) reported that high ozone was observed south of the Ship Channel in stagnant winds late in the day. Even higher ozone was reported behind the bay breeze that advanced into the stagnant air mass.

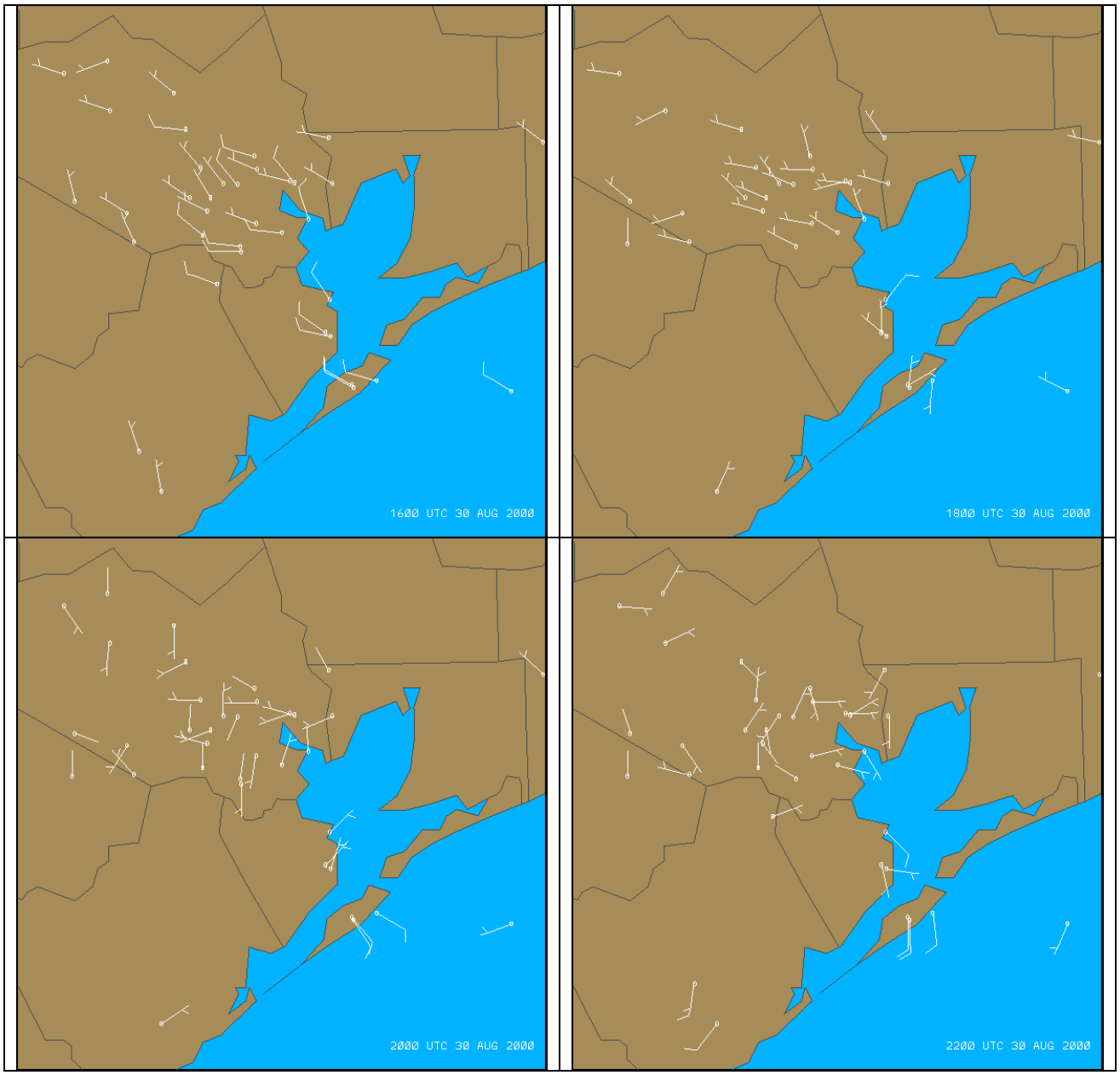

Figure 44: Surface wind observations (full barb = 10 knots) for 30 August at a) 1600 UTC, b) 1800 UTC, c) 2000 UTC, and d) 2200 UTC.

Figure 45 shows the evolution of low-level temperature and wind during the same time period for Experiment 2. Consistent with the statistical slow daytime wind speed bias, model forecast winds over land were essentially calm. Over water, predicted winds have a westerly component, but they appeared to have too much of a southerly component compared to observations. At 1800 UTC, winds remain essentially calm over land, while a developing bay breeze was just starting to come on-shore which compared well with shore line observations. Only minimal penetration of the bay breeze was forecasted at 2000 UTC, also consistent with

observations. Two hours later, a well defined, although weak, bay breeze had propagated to southeast Houston. Forecast wind speeds over land were under-forecast through the period, which was analyzed in more detail in the subsequent experiment. The evolution of the bay breeze appears consistent with observations suggesting that the model possibly could successfully emulate the observed development of high ozone behind the bay breeze.

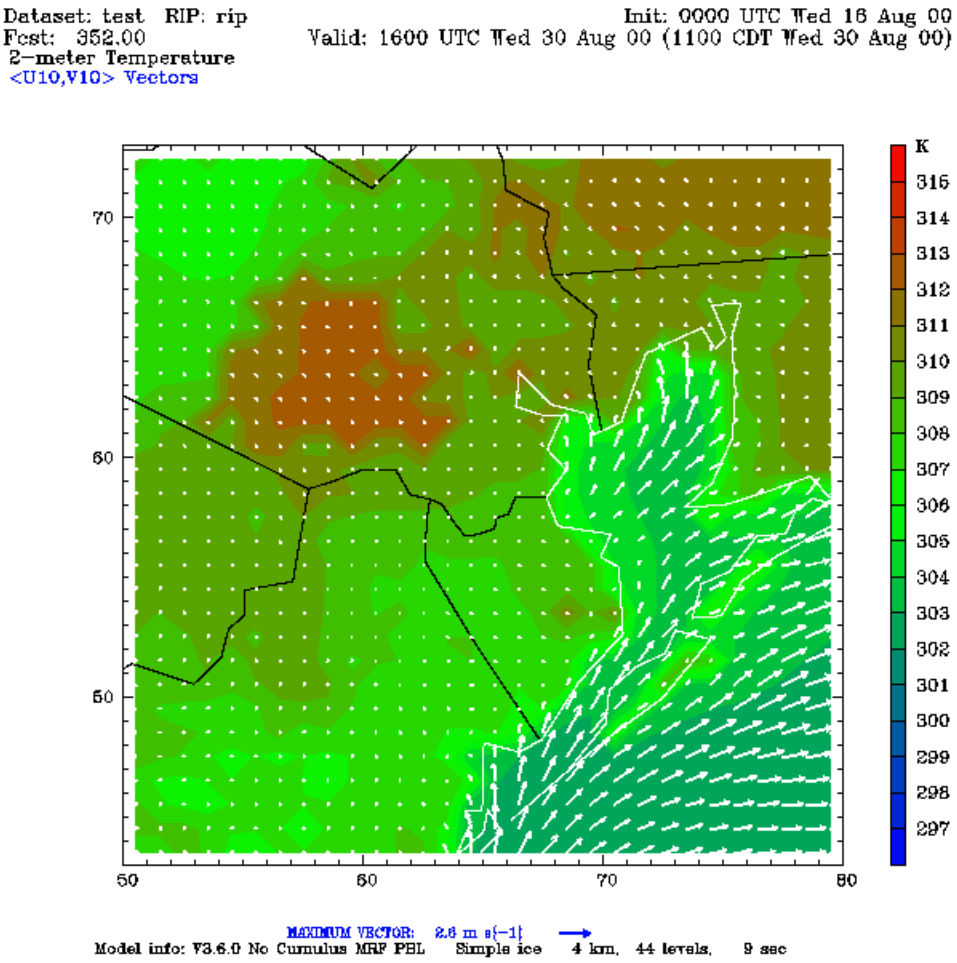
Dataset: test RIP: rip
Fcst: 352.00
2-meter Temperature
<U10,V10> Vectors
Init: 0000 UTC Wed 16 Aug 00
Valid: 1600 UTC Wed 30 Aug 00 (1100 CDT Wed 30 Aug 00)
K
316
314
313
312
311
310
309
308
307
306
305
304
303
302
301
300
299
298
297
70
60
50
50
60
70
80
MAXIMUM VECTOR: 2.6 m s(-1)
Model info: V3.6.0 No Cumulus MRF PBL Simple ice 4 km, 44 levels, 9 sec

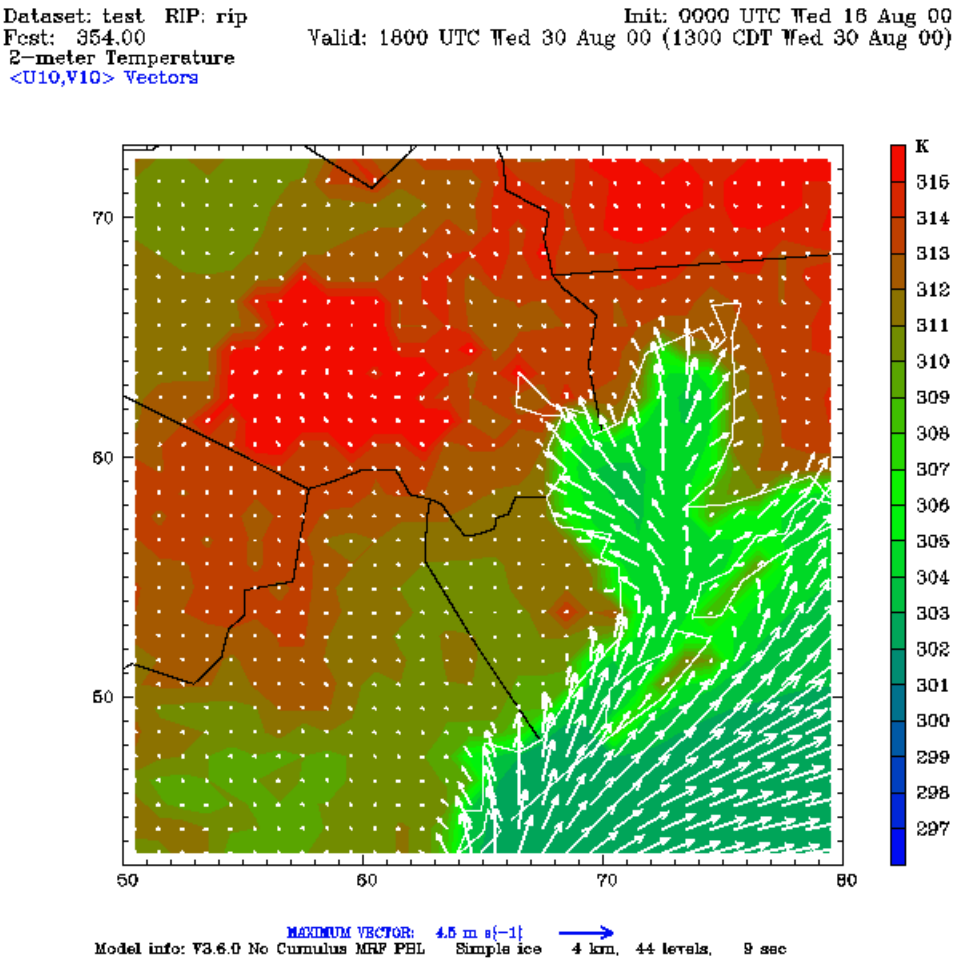
Dataset: test RIP: rip
Fcst: 354.00
2-meter Temperature
<U10,V10> Vectors
Init: 0000 UTC Wed 16 Aug 00
Valid: 1800 UTC Wed 30 Aug 00 (1300 CDT Wed 30 Aug 00)
K
316
314
313
312
311
310
309
308
307
306
305
304
303
302
301
300
299
298
297
70
60
50
50
60
70
80
MAXIMUM VECTOR: 4.5 m s(-1)
Model info: V3.6.0 No Cumulus MRF PBL Simple ice 4 km, 44 levels, 9 sec

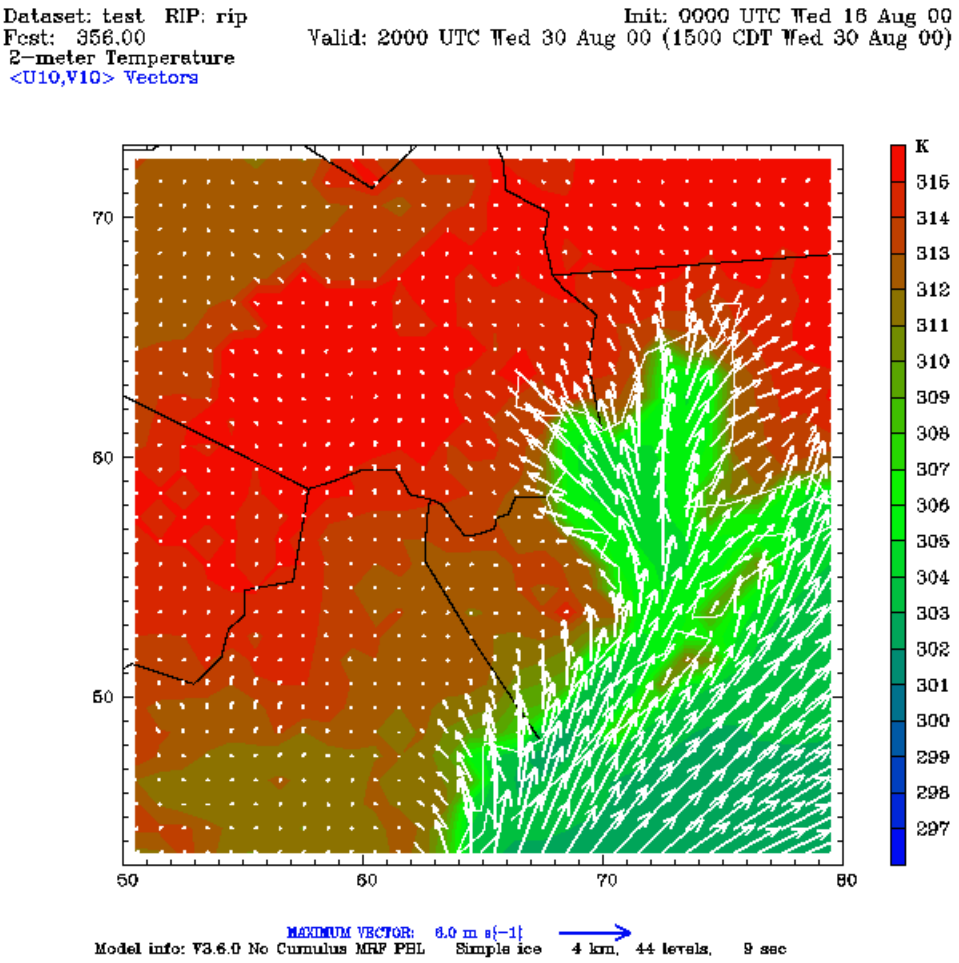
Dataset: test RIP: rip
Fcst: 356.00
2-meter Temperature
<U10,V10> Vectors
Init: 0000 UTC Wed 16 Aug 00
Valid: 2000 UTC Wed 30 Aug 00 (1500 CDT Wed 30 Aug 00)
K
316
314
313
312
311
310
309
308
307
306
305
304
303
302
301
300
299
298
297
70
60
50
50
60
70
80
MAXIMUM VECTOR: 6.0 m s(-1)
Model info: V3.6.0 No Cumulus MRF PBL Simple ice 4 km, 44 levels, 9 sec

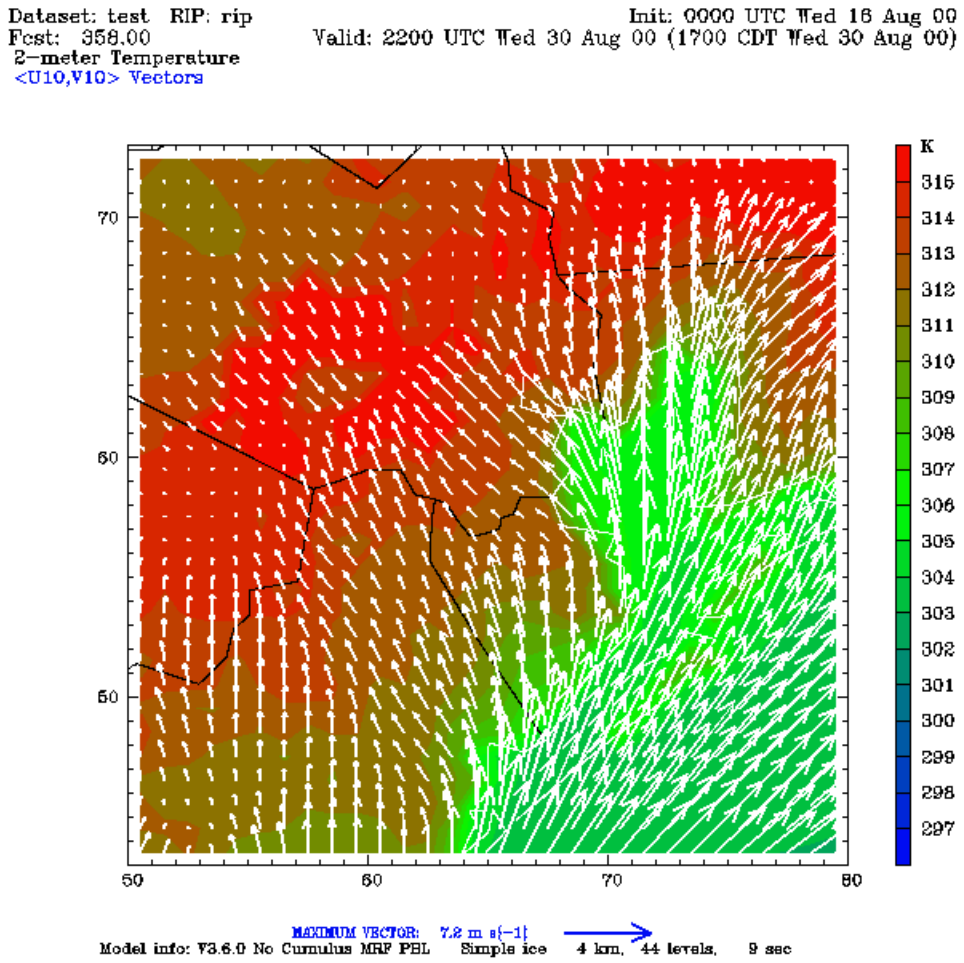

Figure 45: Experiment 2 predictions of low-level temperature (K) and wind (ms^{-1}) for 30 August at a) 1600 UTC, b) 1800 UTC, c) 2000 UTC, and d) 2200 UTC.

5.3 Experiment 3 – Surface momentum flux sensitivity

5.3.1 *Daytime slow wind speed bias in Experiment 1*

Results from Experiment 1 indicated that MM5 simulated wind speeds tended to be slow during the daylight hours. This was especially apparent on August 17 and then from August 30 forward. Curiously, the wind speed started to slow each day around 1400 UTC, at a time when the observed winds showed increasing speed. Cross-sectional analysis of the MM5 simulation revealed that while winds were weak up to 1km, vertical mixing of the boundary layer should still increase the shelter height wind speed. The analysis, however, showed the low-level wind speed to diminish to less than 1 ms^{-1}.

5.3.1.1 Roughness sensitivity

A series of short sensitivity runs were performed to analyze the effects of the MM5 roughness length on the low-level wind speeds. Three sensitivity simulations were completed: 1) the roughness length was reduced by two-thirds for the four land use categories that are most prevalent in southeast Texas, excluding the urban category, 2) the roughness length was reduced by two-thirds for all land use categories, and 3) the roughness length was reduced to 0.1 mm, which is the same value used over water. Comparison of simulated wind speeds with observations (Figure 46) does show a marginal improvement in daytime wind speed bias for the first two sensitivity experiments, but the daytime decrease in wind speed is still apparent. The third sensitivity experiment, while exhibiting a high-speed bias, shows a more realistic diurnal pattern of wind speed with wind speeds increasing during the daylight hours.

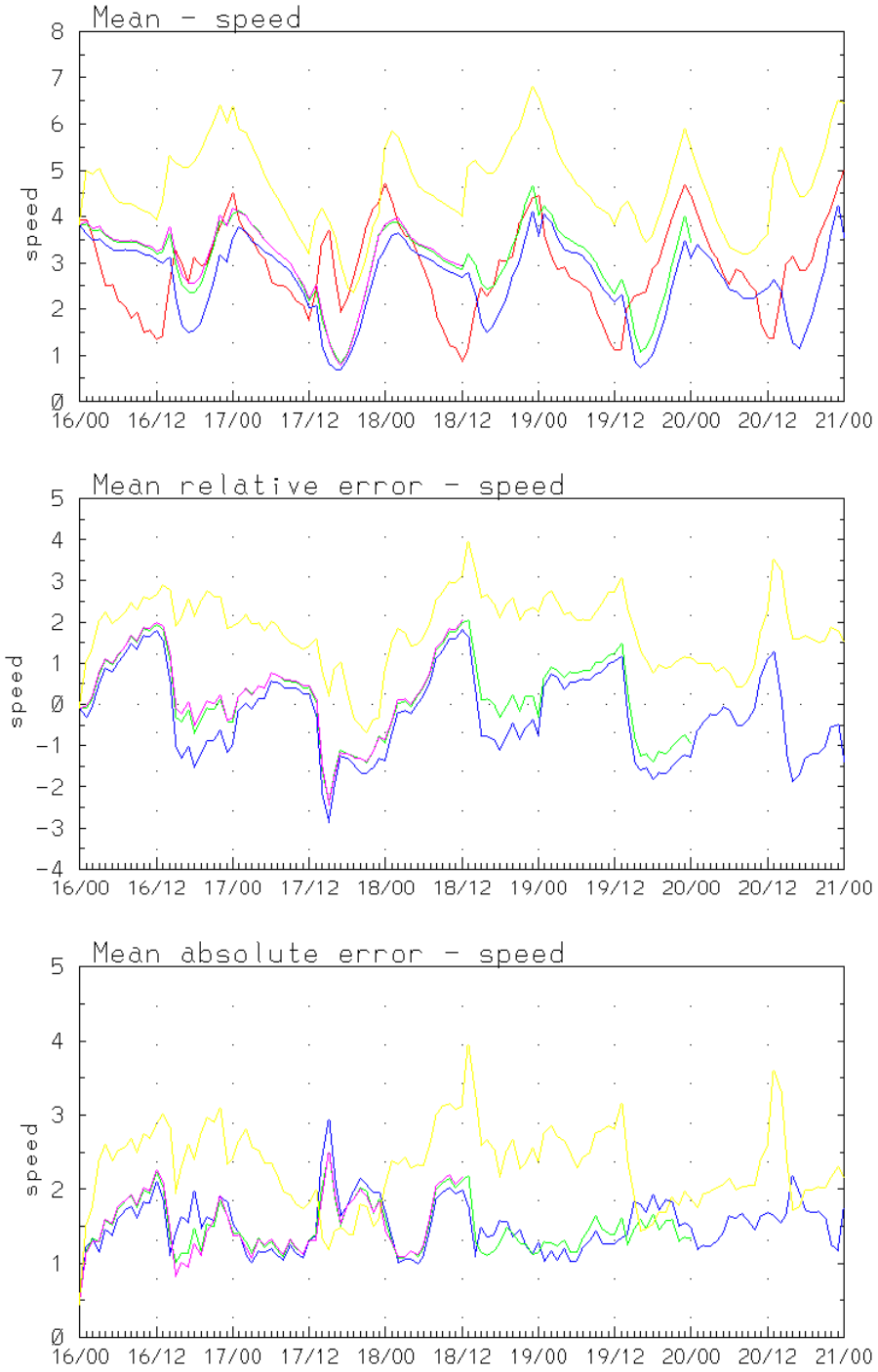

Figure 46: Hourly wind speed (ms^{-1}) statistics using all available domain 4 observations (red) for Experiment 1 (blue), four category roughness reduction (green), all category roughness reduction (purple), and all roughnesses set to 0.1 mm (yellow).

5.3.1.2 U* sensitivity

Discussions with Jimy Dudhia (NCAR/MMM) indicated that, in the MRF boundary layer scheme, there is a contribution from a "convective velocity" added to the total wind speed that is used in the U* computation when the boundary layer is unstable. This contribution effectively raises the momentum flux transfer into the ground, and could result in lower near-surface wind speed forecasts. A short sensitivity run using the Experiment 1 setup was performed in which this convective velocity contribution was removed. A comparison of simulated wind speeds with observations shows higher daytime wind speeds and suggests an overall improvement in the daytime wind forecasts.

5.3.2 *Model Modifications*

The promising results from the short Experiment 1 sensitivity run prompted us to perform a full-length run with the convective velocity contribution removed. Specifically, in the MM5 MRF PBL scheme (mrfpbl.F), the convective velocity contribution is called VCONV and is derived as a function of model forecast instability in the lowest model layer. This term was commented out in the code resulting in no convective velocity contribution to the wind speed that is used in the U* computation.

5.3.3 *Results*

METSTAT hourly statistics from Experiment 3 are illustrated in Figures 47-49. As expected the largest differences are the significant improvements in wind speed. The slow daytime wind speed bias has been cut by at least half, to mostly less than 1 ms^{-1}, through the entire forecast period. The greatest improvement is noted during regime 2, after August 30, when there was a more significant slow speed bias in Experiment 2. During this period, the surface temperatures were warmer resulting in greater boundary layer instability, which likely created a greater convective velocity contribution (VCONV), and hence the larger slow wind speed bias. Nighttime wind speed results, as expected, are essentially unchanged from the previous experiments. Somewhat surprisingly, little differences are observed in the temperature and dew point statistics. One might expect to see more change as the stronger daytime wind might affect the boundary layer characteristics.

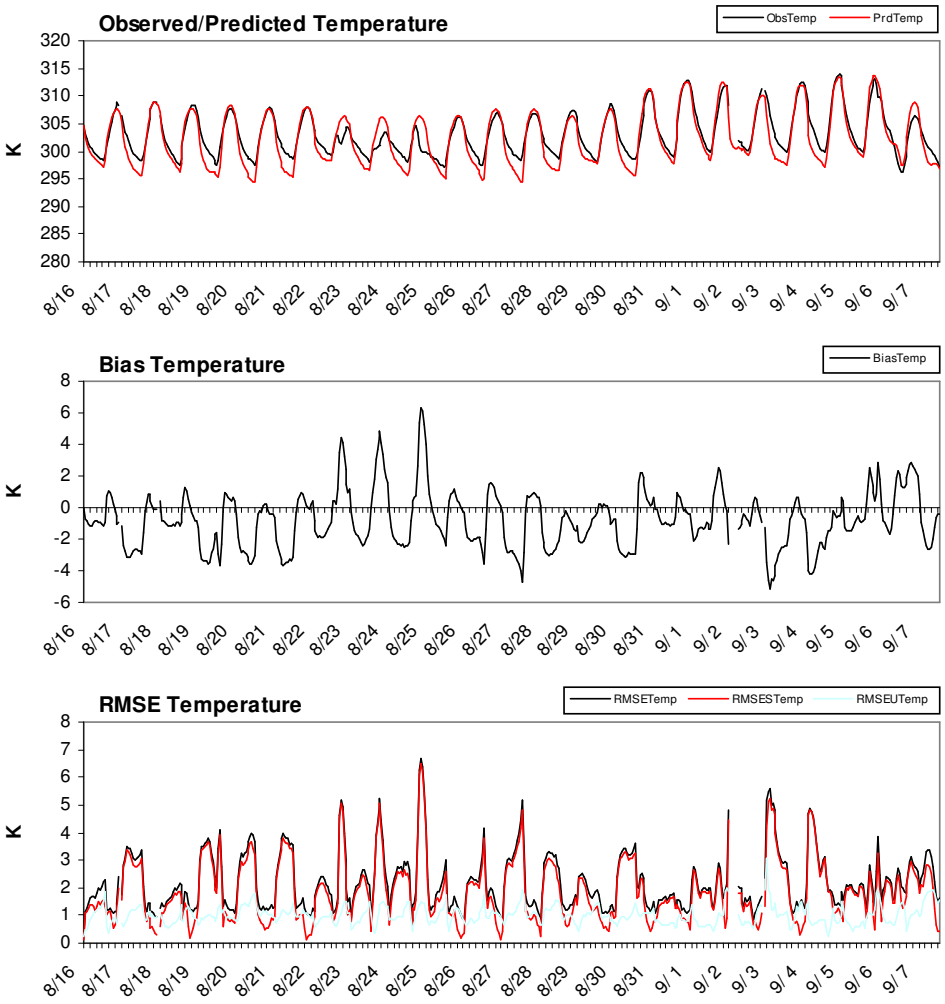

Figure 47: METSTAT hourly temperature (K) statistics for Experiment 3 using 30 Houston area observations.

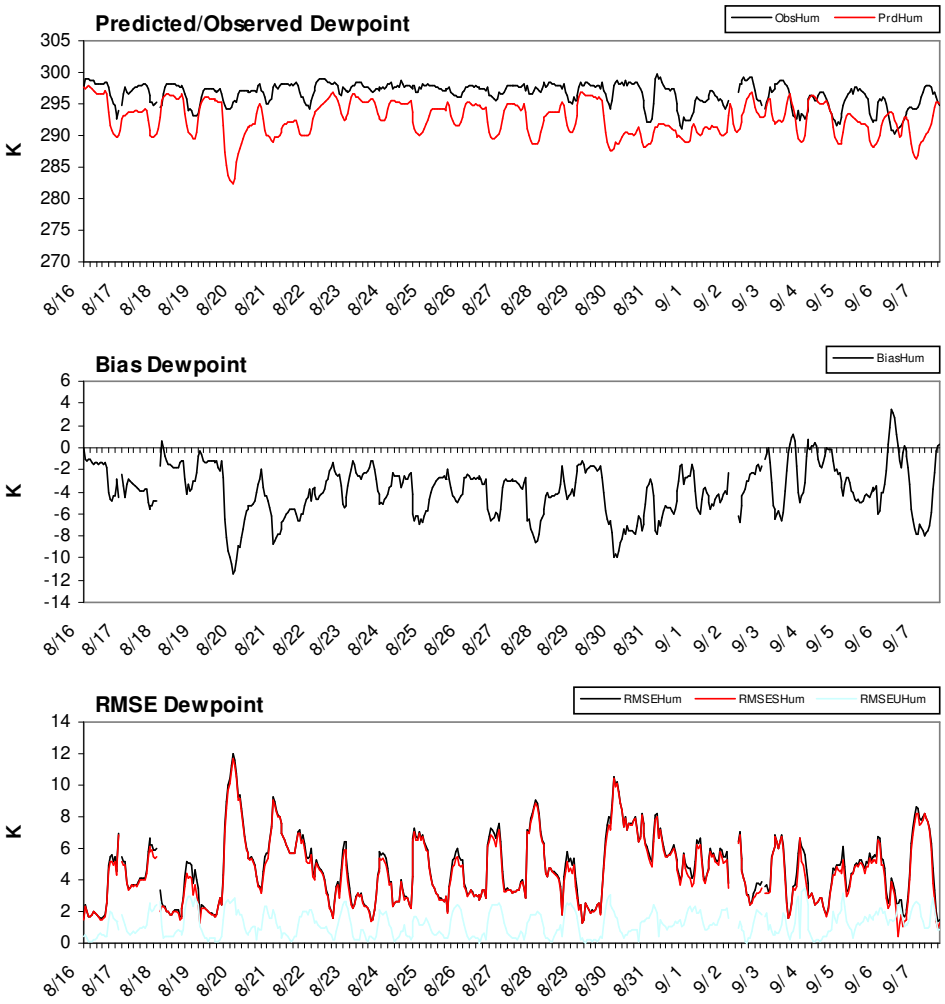

Figure 48: METSTAT hourly dew point statistics (K) for Experiment 3 using five Houston area observations.

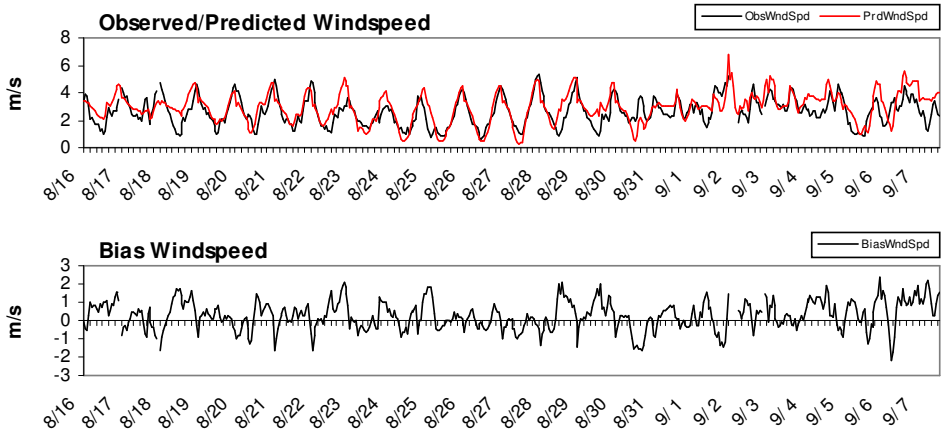

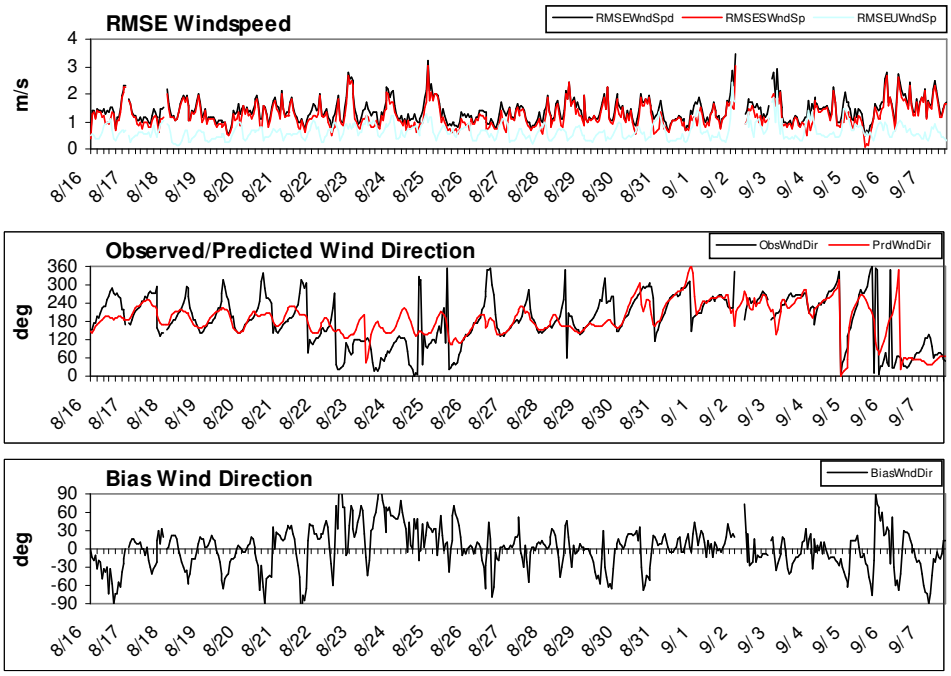

Figure 49: METSTAT hourly wind speed (ms^{-1}) and direction statistics for Experiment 3 using 30 Houston area observations.

Experiment 3 temperature and wind statistical validation results for the Beaumont area are summarized in Figure 50 and Figure 51. Significant temperature differences between Experiment 3 and the earlier experiments are not apparent. Similar to the Houston analysis, the slow daytime wind speed bias has been mostly eliminated, while the high nighttime bias is still apparent.

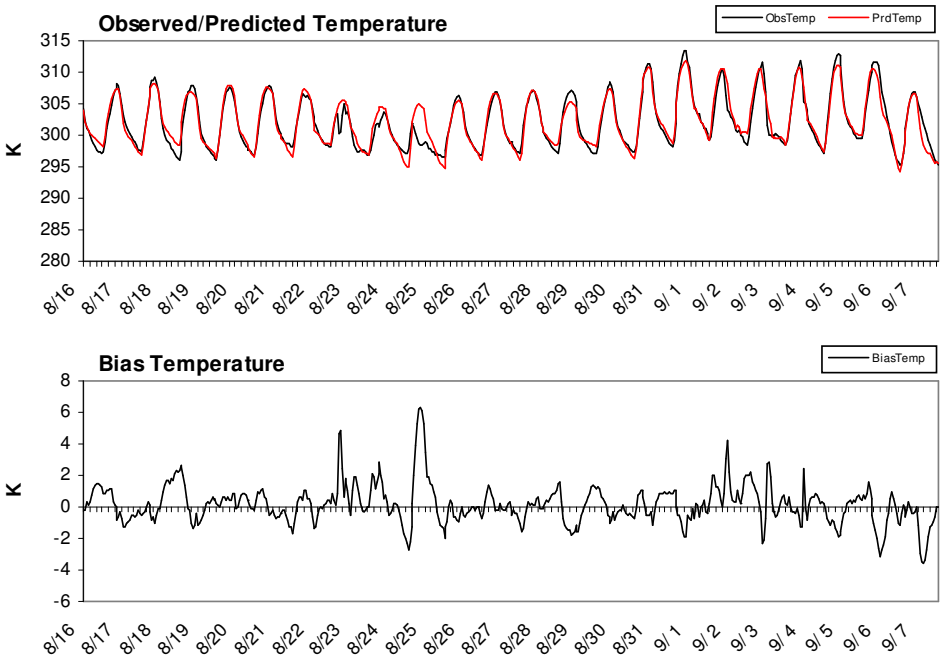

Figure 50: METSTAT hourly temperature (K) statistics for Experiment 3 using 10 Beaumont area observations.

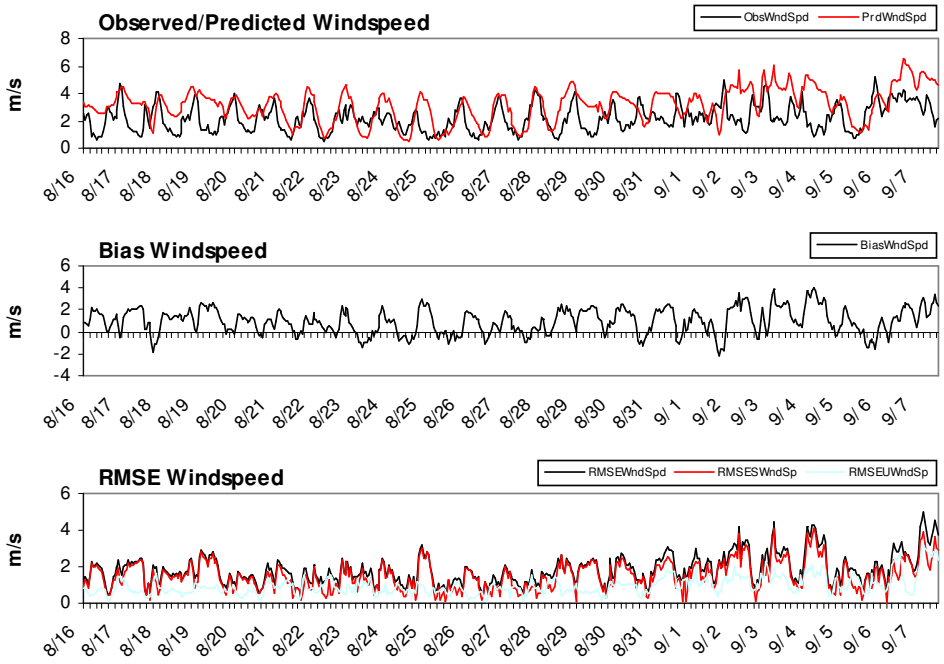

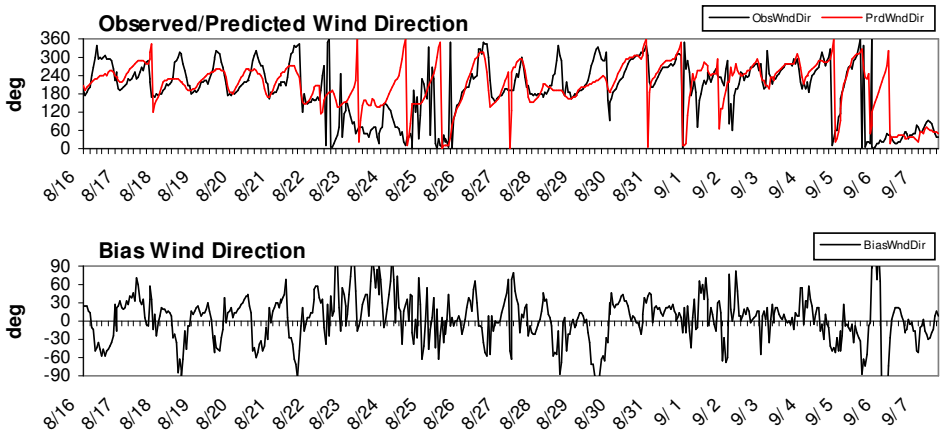

Figure 51: METSTAT hourly wind speed (ms^{-1}) and direction statistics for Experiment 3 using 10 Beaumont area observations.

5.3.4 *Discussion*

5.3.4.1 25 and 30 August rapid ozone formation events

A closer view of the 25 August high ozone day shows more interesting results. Figure 52 illustrates the evolution of the low-level temperature and wind predictions. Unlike Experiment 2, the land-based winds at 1600 UTC are somewhat stronger with an east to southeast direction component. These stronger winds appear to speed the progression of the bay breeze front inland and through the Houston metro area, which compares more favorably to observations. This is in sharp contrast to the previous experiments and to the Nielsen-Gammon simulations that showed a too slow progression of the bay breeze front.

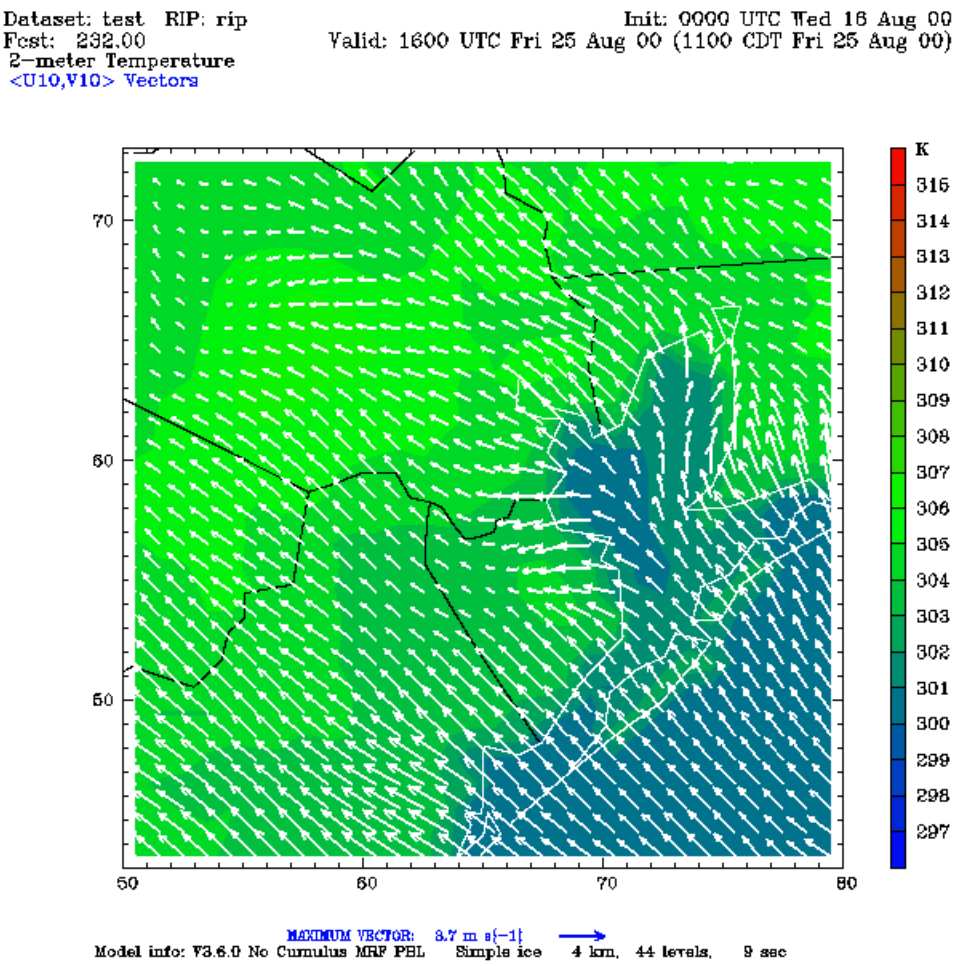
Dataset: test RIP: rip
Fcst: 232.00
2-meter Temperature
<U10,V10> Vectors
Init: 0000 UTC Wed 16 Aug 00
Valid: 1600 UTC Fri 25 Aug 00 (1100 CDT Fri 25 Aug 00)
K
316
314
313
312
311
310
309
308
307
306
305
304
303
302
301
300
299
298
297
70
60
50
50
60
70
80
MAXIMUM VECTOR: 8.7 m s{-1}
Model info: V3.6.0 No Cumulus MRF PBL Simple ice 4 km, 44 levels, 9 sec

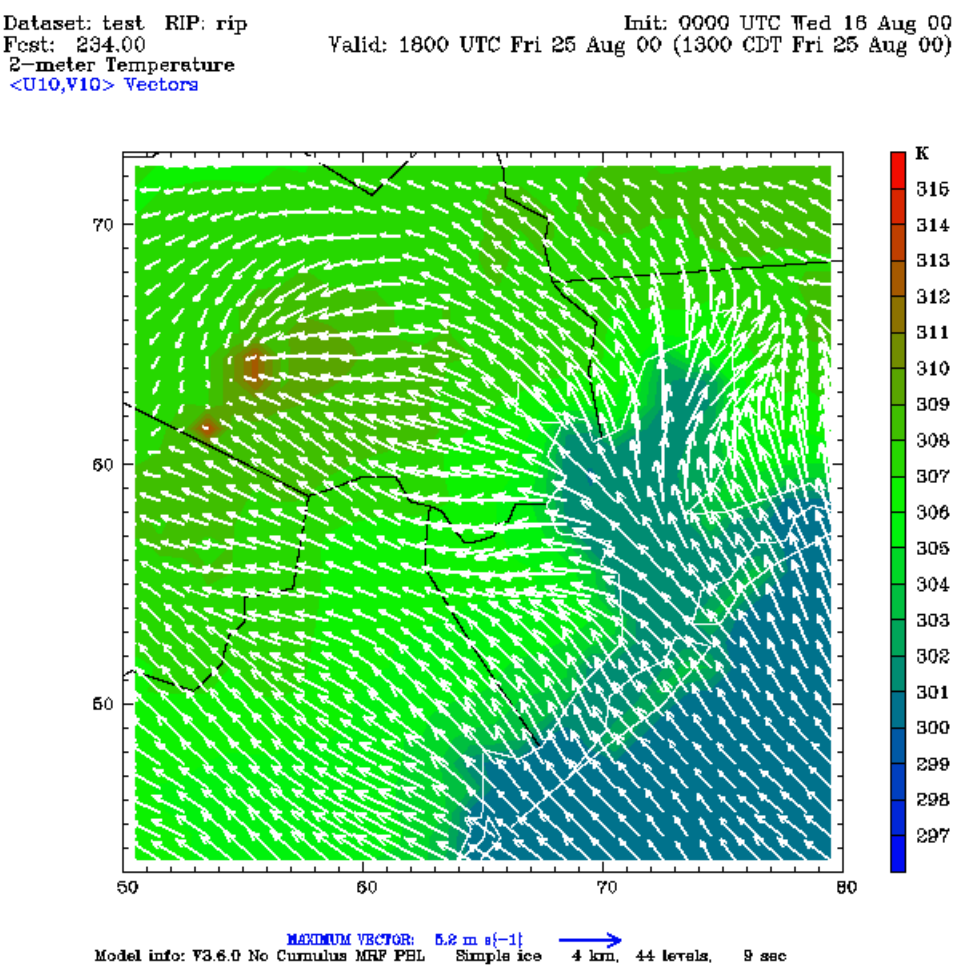
Dataset: test RIP: rip
Fcst: 234.00
2-meter Temperature
<U10,V10> Vectors
Init: 0000 UTC Wed 16 Aug 00
Valid: 1800 UTC Fri 25 Aug 00 (1300 CDT Fri 25 Aug 00)
K
316
314
313
312
311
310
309
308
307
306
305
304
303
302
301
300
299
298
297
70
60
50
50
60
70
80
MAXIMUM VECTOR: 5.2 m s(-1)
Model info: V3.6.0 No Cumulus MRF PBL Simple ice 4 km, 44 levels, 9 sec

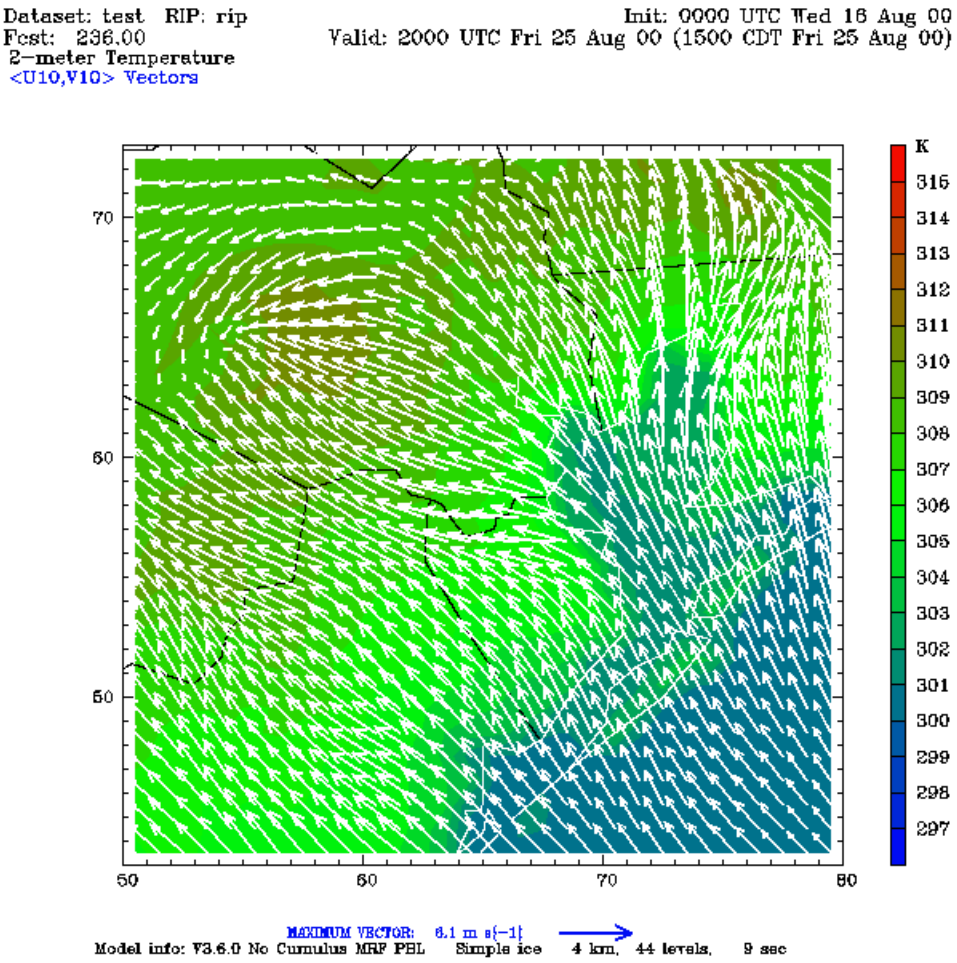
Dataset: test RIP: rip
Fcst: 236.00
2-meter Temperature
<U10,V10> Vectors
Init: 0000 UTC Wed 16 Aug 00
Valid: 2000 UTC Fri 25 Aug 00 (1500 CDT Fri 25 Aug 00)
K
316
314
313
312
311
310
309
308
307
306
305
304
303
302
301
300
299
298
297
70
60
50
50
60
70
80
MAXIMUM VECTOR: 6.1 m s(-1)
Model info: V3.6.0 No Cumulus MRF PBL Simple ice 4 km, 44 levels, 9 sec

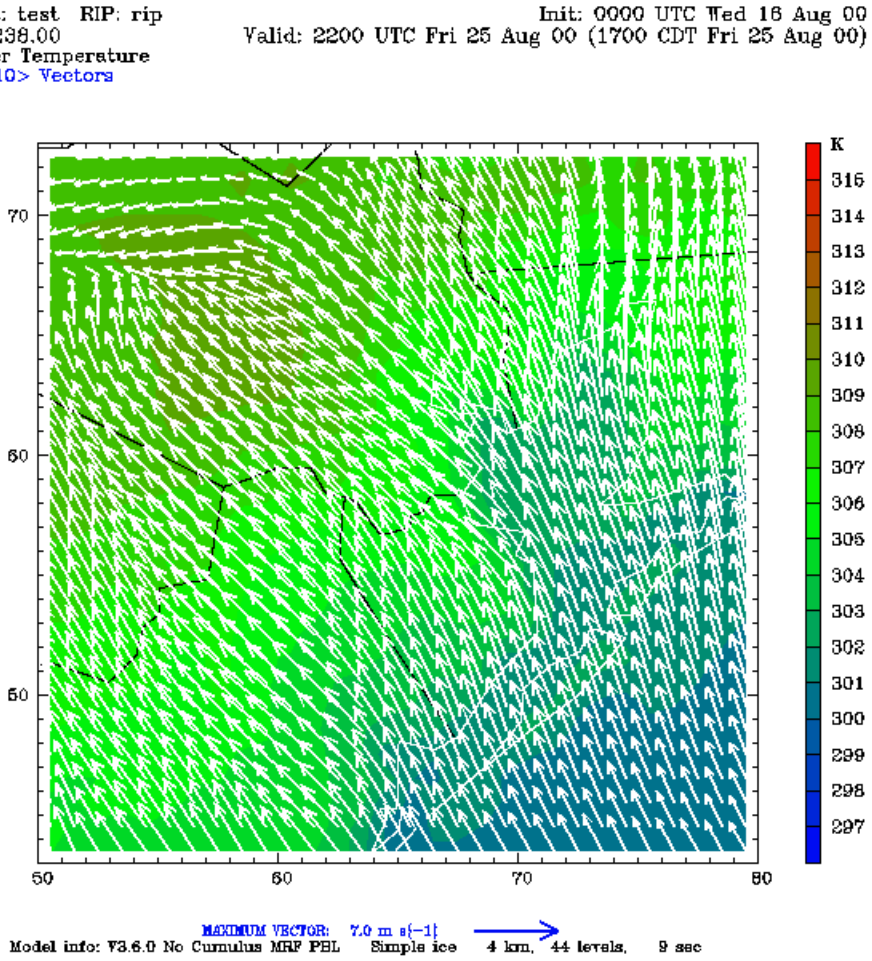

Figure 52: Experiment 3 predictions of low-level temperature (K) and wind (ms^{-1}) for 25 August at a) 1600 UTC, b) 1800 UTC, c) 2000 UTC, and d) 2200 UTC.

Similar results are indicated from Experiment 3 for 30 August as well (Figure 53). Land-based wind speeds are stronger as observed with a greater westerly component, but in general still contain too much of a southerly component especially south of Houston. As with 25 August, the progression of the bay breeze front is accelerated when compared to experiment, somewhat surprisingly given the stronger land-based winds opposing the bay breeze progression. Unlike 25 August, this speedier progression is quicker than observed, although the eventual penetration of the front is similar in distance with slightly stronger winds predicted behind the front.

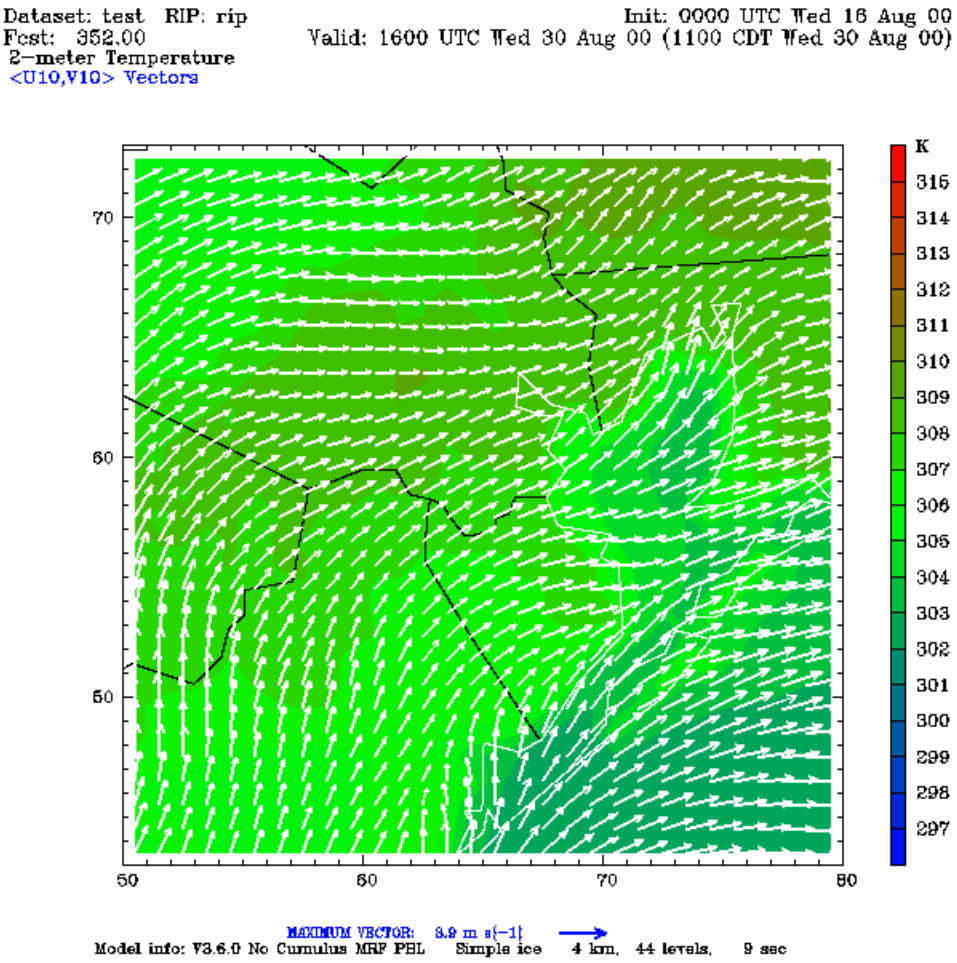
Dataset: test RIP: rip
Fcst: 352.00
2-meter Temperature
<U10,V10> Vectors
Init: 0000 UTC Wed 16 Aug 00
Valid: 1600 UTC Wed 30 Aug 00 (1100 CDT Wed 30 Aug 00)
K
316
314
313
312
311
310
309
308
307
306
305
304
303
302
301
300
299
298
297
70
60
50
50
60
70
80
MAXIMUM VECTOR: 8.9 m s(-1)
Model info: V3.6.0 No Cumulus MRF PBL Simple ice 4 km, 44 levels, 9 sec

Dataset: test RIP: rip
Fcst: 354.00
2-meter Temperature
<U10,V10> Vectors

Init: 0000 UTC Wed 16 Aug 00
Valid: 1800 UTC Wed 30 Aug 00 (1300 CDT Wed 30 Aug 00)

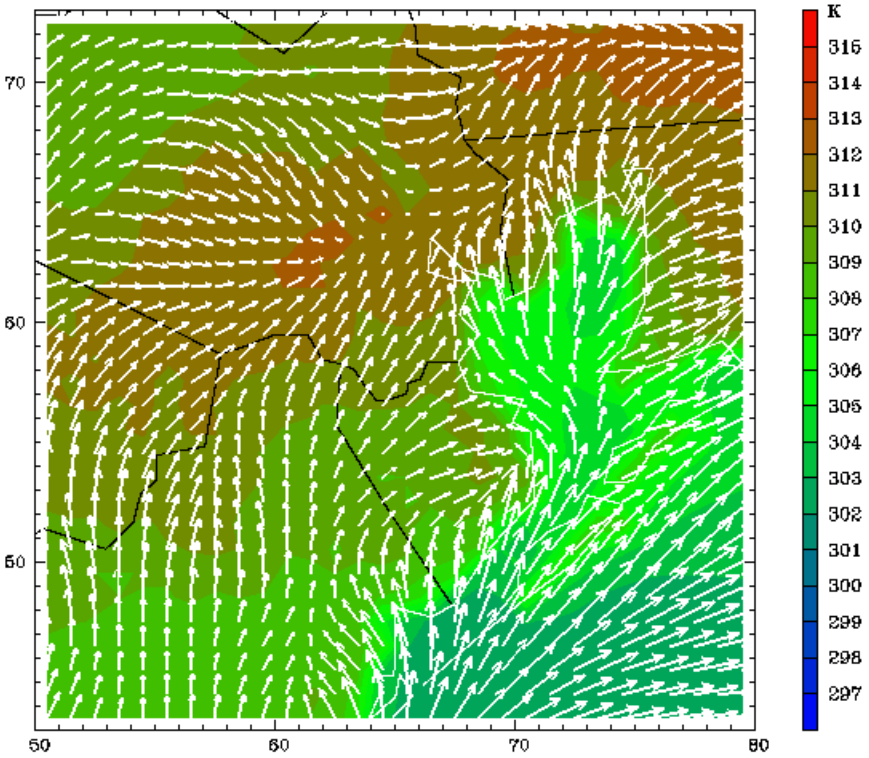

MAXIMUM VECTOR: 4.9 m s(-1)

Model info: V3.6.0 No Cumulus MRF PBL Simple ice 4 km, 44 levels, 9 sec

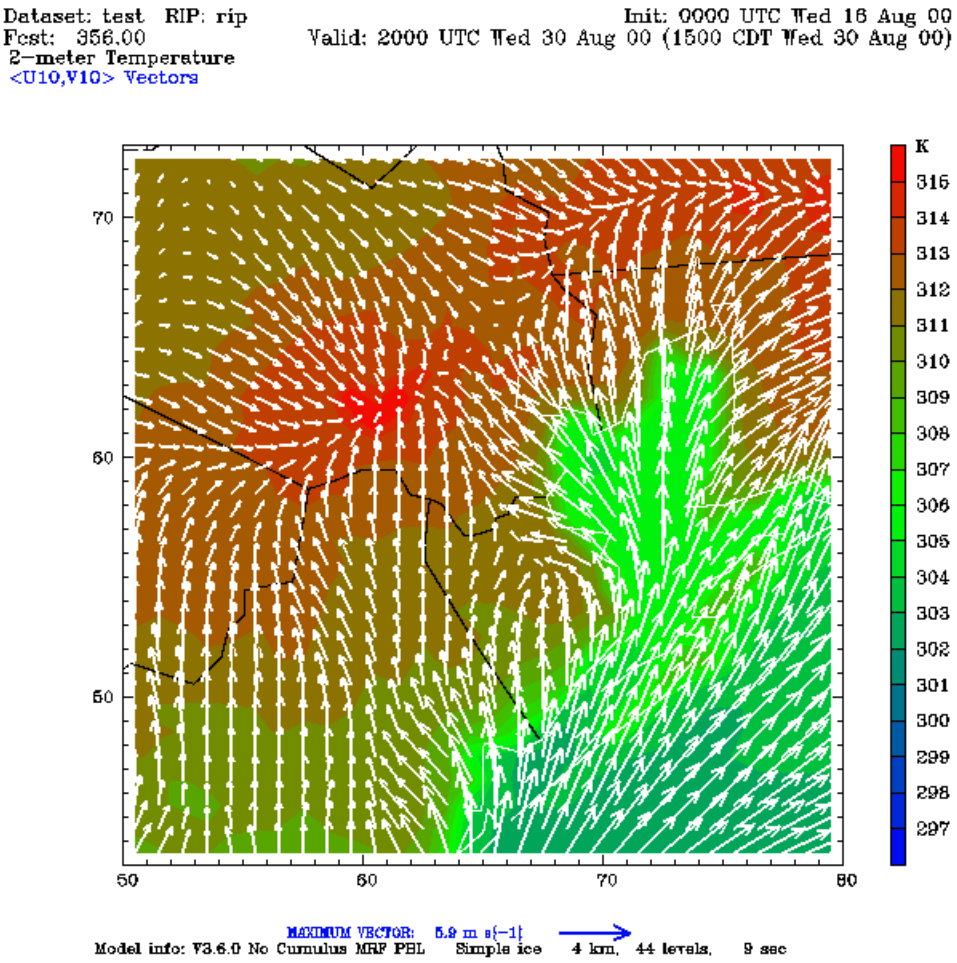
Dataset: test RIP: rip
Fcst: 356.00
2-meter Temperature
<U10,V10> Vectors
Init: 0000 UTC Wed 16 Aug 00
Valid: 2000 UTC Wed 30 Aug 00 (1500 CDT Wed 30 Aug 00)
K
316
314
313
312
311
310
309
308
307
306
305
304
303
302
301
300
299
298
297
70
60
50
50
60
70
80
MAXIMUM VECTOR: 5.9 m s(-1)
Model info: V3.6.0 No Cumulus MRF PBL Simple ice 4 km, 44 levels, 9 sec

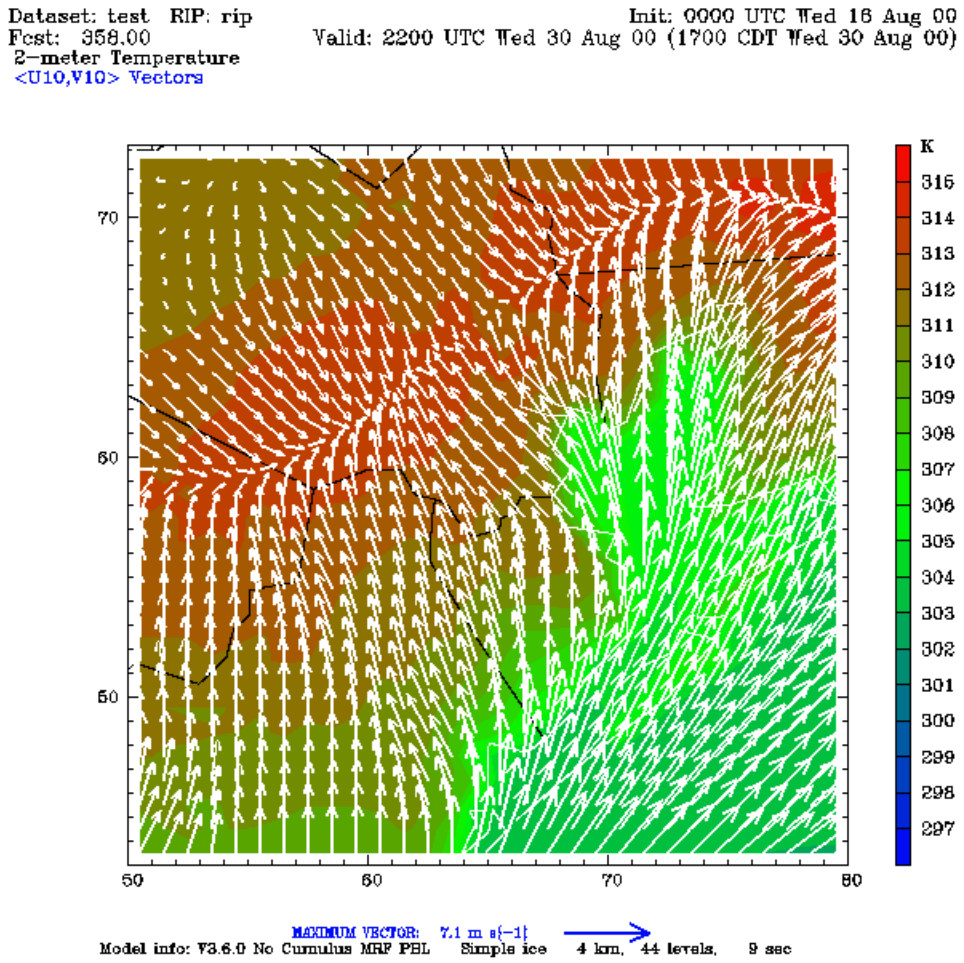

Figure 53: Experiment 3 predictions of low-level temperature (K) and wind (ms-1) for 30 August at a) 1600 UTC, b) 1800 UTC, c) 2000 UTC, and d) 2200 UTC.

5.3.4.2 PBL height comparisons

Correctly diagnosing the depth of the PBL is an important aspect of properly defining pollutant concentrations. Nielsen-Gammon (2002b, see Figures 3, 7, and 12) presented composite PBL depth observations for three locations: LaMarque located southeast of Houston, downtown Houston, and Wharton power plant located northwest of Houston. It was noted that at Wharton, positioned away from the water, there was little sea breeze effect on the observed PBL depth, and hence, there was little variation of observed PBL depth between regimes 1 and 2. Houston and LaMarque did show varying effects due to differing sea breeze characteristics between regimes 1 and 2, and separate composite observations were generated for the two regimes. Observed PBL depths were generally shallower during regime 1 than for regime 2 at Houston and LaMarque. An increase in PBL depth was noted as one traversed from southeast to northwest away from the water.

Figure 54 illustrates forecast PBL height from Experiment 3 for 25 August. Times were selected (1700, 2000, 2300 UTC) to compare with Nielsen-Gammon (2002b) results shown at these times. Nielsen-Gammon (2002b) reported that, in general, model forecast PBL heights tended to be too deep during the early part of an episode and too shallow during the latter stages of an episode and our results are consistent with that assessment. The overall pattern of increasing PBL height from southeast to northwest is captured, but note forecast PBL depths around 1200 m at 1700 UTC while composite observations are from 500 to 1000 m. Forecast PBL depths compare rather favorably with composite observations at 2300 UTC with 2500 m predicted near LaMarque suggesting that predicted depths increase too rapidly and then actual depths catch up to the predictions later in the day. A dramatic erosion of the forecast PBL occurs after 2300 UTC as sunset approaches, and this erosion is far quicker than observed.

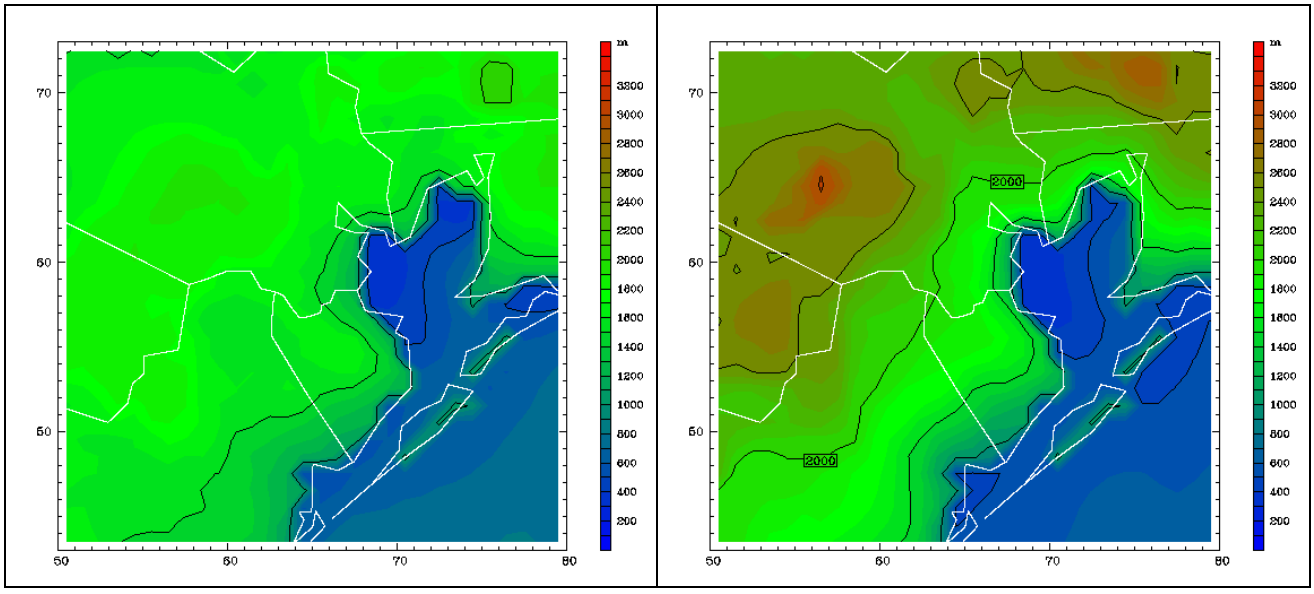

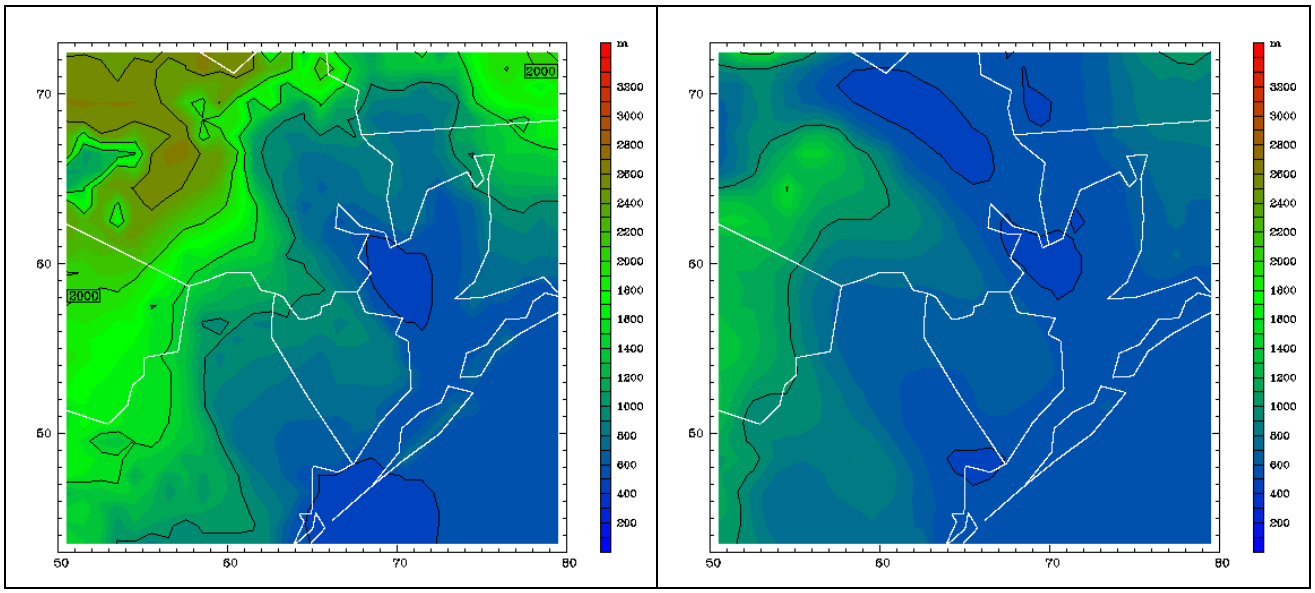

Figure 54: Experiment 3 MM5 predicted planetary boundary layer height (m) for a) 1700 UTC 25 August, b) 2000 UTC 25 August, c) 2300 UTC 25 August, and d) 0000 UTC 26 August. Contour interval = 500 m.

Observations of PBL depth derived from airborne lidar are displayed in Figure 55 for 29 and 31 August. Note the much deeper PBL observed on 31 August, a regime 2 day. Figure 56 and Figure 57 illustrate predicted PBL heights for similar time periods. Again, the overall patterns and trends are captured with progressively deeper heights from southeast to northwest and much greater depths during regime 2. Forecast PBL depths again compare favorably with observations around 2300 UTC. But then the wholesale collapse of the PBL after 2300 UTC is largely overdone.

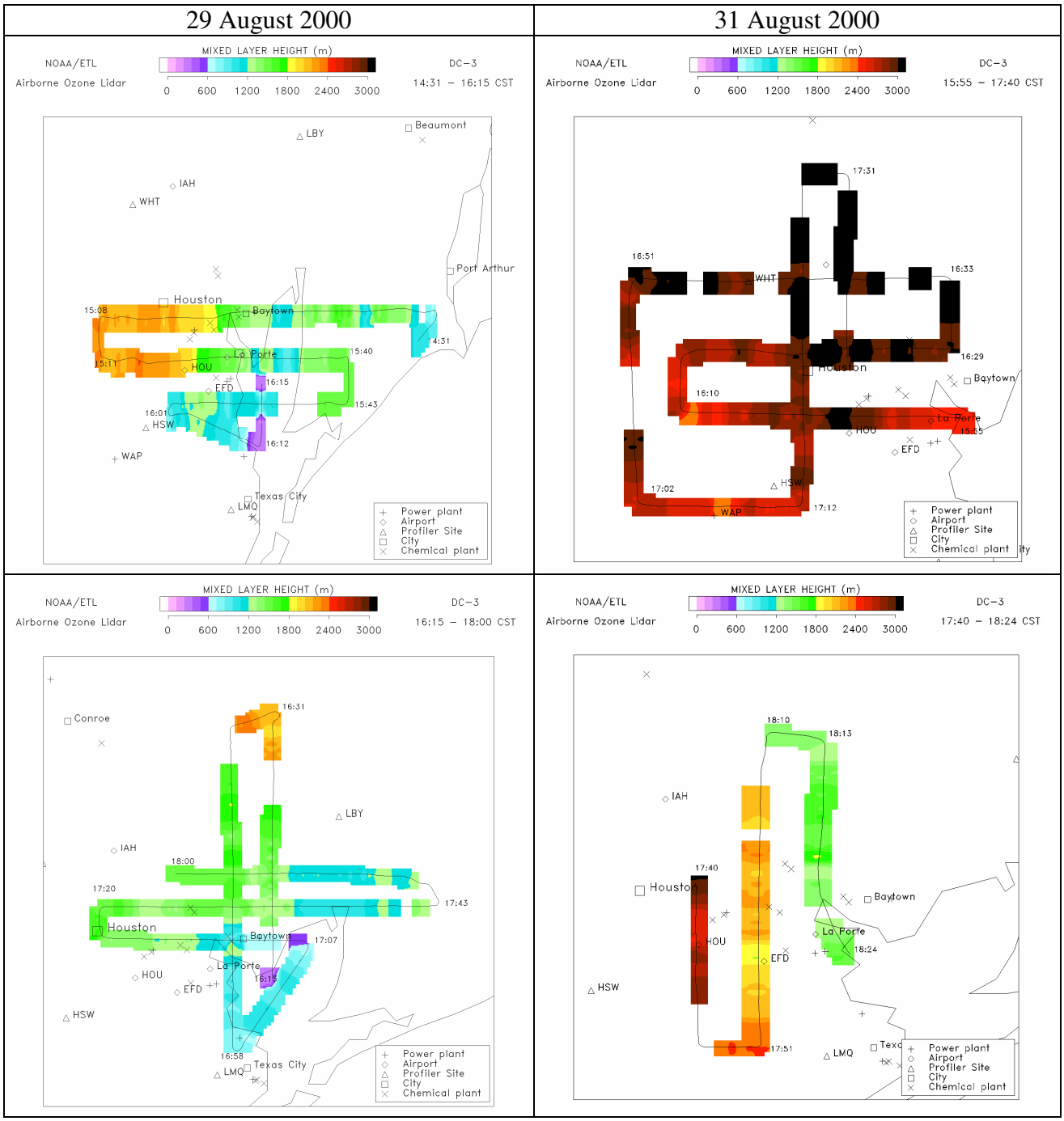

Figure 55: Planview plots of mixing depth derived from airborne lidar data for 29 and 31 August, for 2 different flight segments on each day. All images are excerpted from Senff et al. (2002).

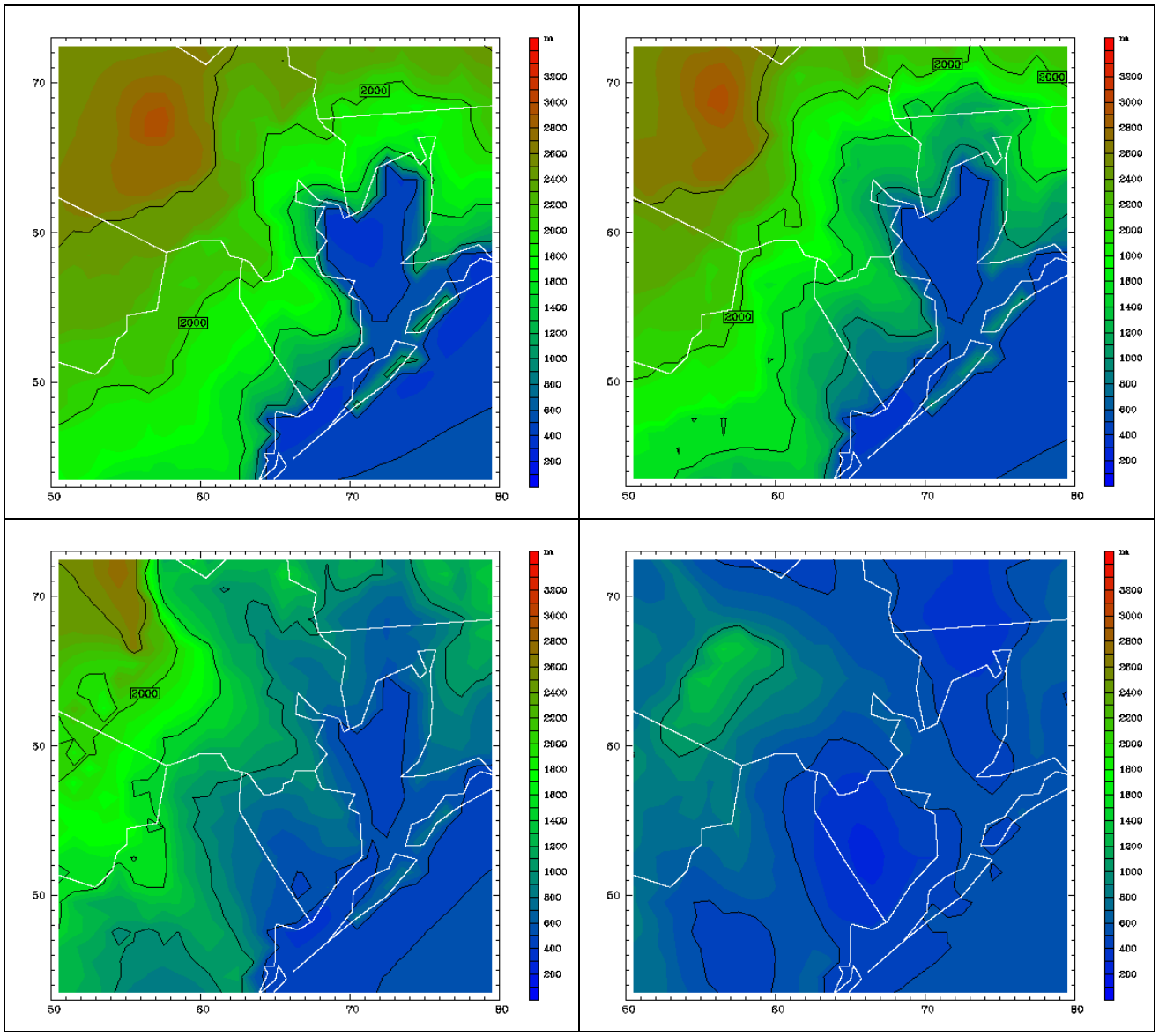

Figure 56: Experiment 3 MM5 predicted planetary boundary layer height (m) for a) 2100 UTC 29 August, b) 2200 UTC 29 August, c) 2300 UTC 29 August, and d) 0000 UTC 30 August. Contour interval = 500 m.

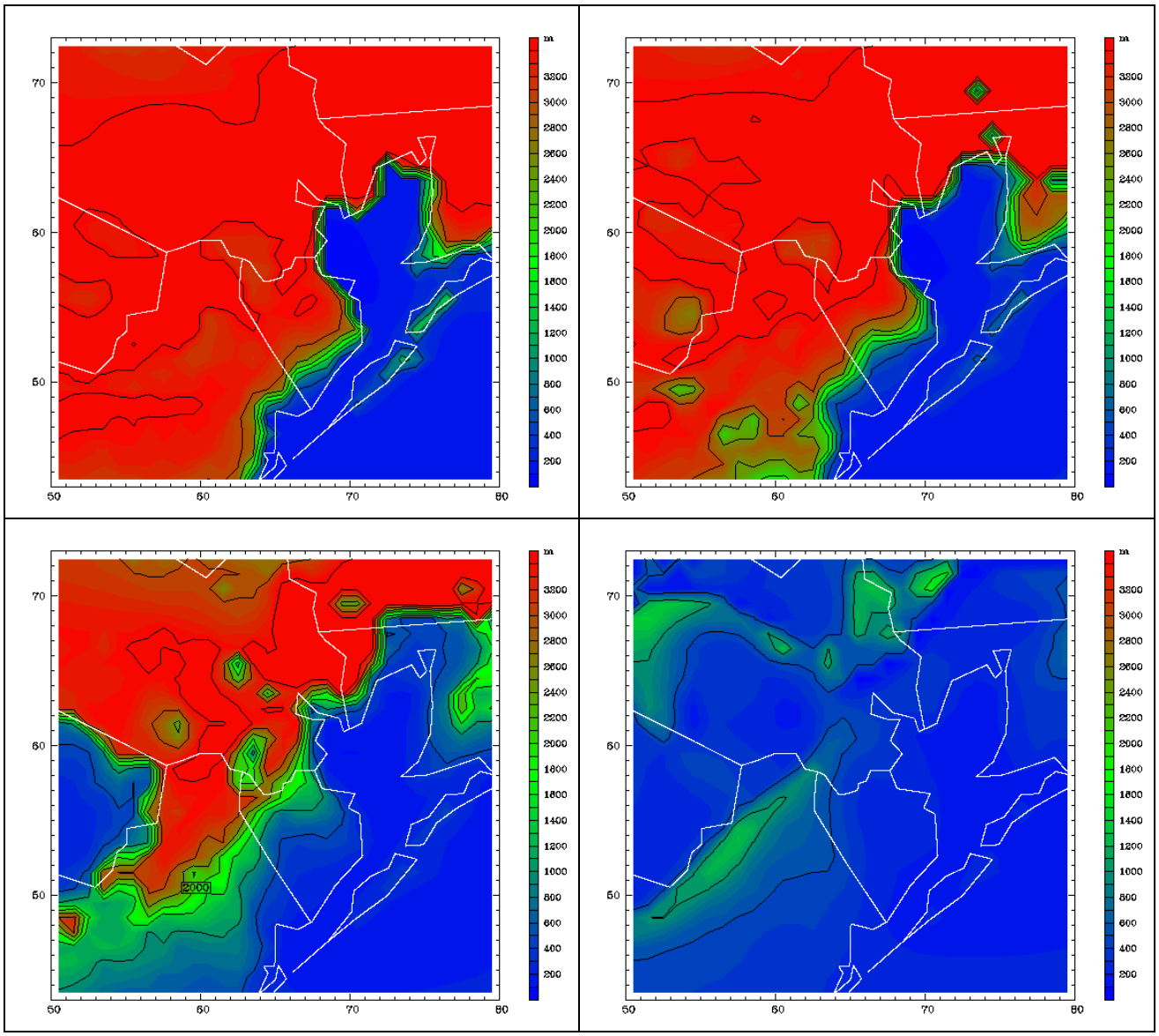

Figure 57: Experiment 3 MM5 predicted planetary boundary layer height (m) for a) 2100 UTC 31 August, b) 2200 UTC 31 August, c) 2300 UTC 31 August, and d) 0000 UTC 1 September. Contour interval = 500 m.

5.4 Additional investigations

5.4.1 *MRF scheme and PBL depth*

ATMET has performed numerous sensitivity simulations with MM5 for both the 1993 and 2000 episodes for the Houston-Galveston region. A major component of these simulations was testing of the various PBL schemes that are implemented in MM5. The results of these simulations consistently showed that, of all the PBL schemes in MM5, the MRF scheme usually provided the best results.

However, as many other MM5 users have noted also, the MRF scheme consistently overestimates the height of the PBL, which is crucial for good air quality simulations. All experiments conducted here have shown this tendency to overestimate the depth of the boundary layer especially during the afternoon hours. This played a role in the large low bias of dew point temperature on several days as described above.

The MM5 MRF PBL scheme is designed after a procedure described by Hong and Pan (1996), which followed very closely on earlier work of Troen and Mahrt (1986). Hong and Pan first implemented this scheme in the NCEP MRF model, which is the main global forecast model run at NCEP to produce the AVN forecasts (the name of the model and forecasts have recently been changed to the GFS, Global Forecasting System). It was developed with the MRF model in mind, relatively coarse horizontal and vertical resolution with a requirement that very little computer resources be used. The scheme was later implemented in MM5 by Dudhia and Hong.

There are several aspects to the scheme (stable vs. unstable boundary layers, diffusion above and below the boundary layer height). We focused on the regime of that seems to cause the most problems, diffusion within the unstable boundary layer.

We have reviewed the formulation of the MRF scheme and have identified several features in the implementation that could lead to this overprediction. The MRF scheme is based on the use of a profile function for the vertical exchange coefficient. Sub-grid diffusion schemes based on the O'Brien profile function date back to at least the early 1970's. While termed a "non-local" scheme by Hong and Pan, this scheme still produces an eddy exchange coefficient where the mixing is done locally (i.e., from layer to layer). The computation of the eddy viscosity coefficients is done taking into account "non-local" effects (e.g., the O'Brien profile function). However, the usual use of the term "non-local diffusion" in the literature refers to a scheme that can mix characteristics of the atmosphere beyond the adjoining layer.

The MRF scheme requires the computation of a PBL height. Similar schemes have prognosed the height; the MRF scheme uses a diagnosis on each timestep. This diagnosis is based on the definition of a bulk Richardson number:

$$Ri = \frac{\frac{g}{\theta_v}\frac{\partial \theta_v}{\partial z}}{\left(\frac{\partial V}{\partial z}\right)^2}$$

where g is gravity, V is the wind speed, and θ_v is virtual potential temperature.

Two assumptions are then made by Troen and Mahrt:

- The Richardson number will be assumed to apply over the depth of the boundary layer.
- A critical Richardson number can be defined and used over this depth to compute the boundary layer height.

Typically, the bulk Richardson number is used to determine if the vertical wind shear is adequate to overcome the level of stability and make a layer prone to turbulence. Usually, this has been applied to relatively shallow layers (e.g., of order 100 m), not to entire boundary layer depths that can reach several kilometers. When applied to shallow layers, the theoretical value of the critical Richardson number is usually taken to be 0.25. If the value is more than this, the flow is likely to be laminar; when the value is less, turbulence is likely. Various researchers have used a larger number for the critical Richardson due to discretization and numerical arguments.

If we make the assumptions of Troen and Mahrt, replace ∂z with the symbol h for PBL height, and discretize over the entire PBL depth, we arrive at the expression used for PBL height used in the MRF scheme:

$$h = Ri_{cr} \frac{\theta_{va} \left| V(h) \right|^2}{g \left(\theta_v(h) - \theta_s \right)}$$

where $V(h)$ and $\theta(h)$ are the wind speed and virtual potential temperature at height h, θ_{va} is the virtual potential temperature at the first model level above the ground, and θ_s is a representative air temperature near the surface. θ_s is further defined as:

$$\theta_s = \theta_{va} + \theta_T$$

where θ_T is defined as a "scaled virtual temperature excess near the surface". This term is based on surface layer sensible heat flux and was considered necessary because the scheme was intended for vertical resolutions near the ground that were on the order of 30-50 m, typical of those used in global models. Further, it was limited to a maximum of 3K, since it could become very large if wind speeds were small.

Examination of the PBL computation suggests two immediate possibilities for testing to reduce the PBL heights. First, the PBL depth is directly correlated to the critical bulk Richardson number (Ri_{cr}). The MM5 code uses a Ri_{cr} value of 0.5. Since this number is somewhat arbitrary, lower values could be tested. The second possibility for sensitivity testing is the

scaled virtual temperature excess that is designed to account for a near-surface temperature that is warmer than the lowest-level model temperature. Given that current mesoscale model implementations typically utilize higher grid resolution near the ground than used in global models (e.g., our experiments used a lowest level under 10m), the scaled virtual temperature excess term may be too large for these applications.

Several short diagnostic simulations were run to determine the characteristics of the PBL height and eddy viscosity coefficients that were produced by the MRF scheme. We found that in the early afternoon, the temperature excess was typically 1-2K, with the eddy viscosity coefficients reaching as large as 1000-1500 m^2/s. A short sensitivity simulation was completed with the scaled virtual temperature excess contribution removed. Results indicate that boundary layer depths were reduced by as much as 1000 m during the afternoon hours.

With these brief sensitivity runs, it seems there is promise to be able to reduce the daytime PBL heights from the MRF scheme to more accurate values. The magnitude of the eddy viscosity coefficients should also be investigated, since the values produced are much larger than is typical.

We also recommend investigating replacements for the MRF profile-based scheme. While these schemes can provide an adequate result in a "classic" PBL (surface-based, well-mixed from the ground to a strong capping inversion), profile schemes are unable to correctly simulate features that deviate from this classic case. This is important for the Texas Gulf Coast region because of the sea breeze development. As the cooler marine air moves ashore into a deep well-mixed PBL, an internal boundary layer is developed. A profile scheme will diagnose a particular boundary layer height. Under this level, significant vertical sub-grid mixing can occur; over this level, very little mixing is done. If the scheme diagnoses the PBL height at the level of the internal, marine air boundary layer, then vertical mixing will be shut down in the remainder of the mixed layer that lies atop the marine air. If the PBL height is diagnosed at the top of the existing deep mixed layer, then the internal boundary layer will be quickly mixed out. In either case, the physical process is not represented correctly.

In theory, a TKE-based scheme (such as Mellor-Yamada) can more correctly simulate these types of "non-classic" situations. But as mentioned above, the current implementations of TKE schemes in MM5 usually provide worse results than the MRF scheme. However, most other models (RAMS, COAMPS, ARPS, etc.) use TKE schemes almost exclusively. In our experience with RAMS, there has been little bias in the PBL depth (for example, see 1993 and 2000 episode RAMS reports for TNRCC). We recommend a review of the MM5 TKE schemes, comparison with other models' schemes, and possible modification of the MM5 schemes to allow them to work for more general situations.

6 Summary

This project contained a number of different aspects regarding the use of MM5 for simulations of the 16 August – 7 September 2000 TexAQS period. We will briefly summarize these aspects below.

- As a follow-on to MM5 sensitivity experiments we performed for the COAST 1993 episode for Houston/Galveston (ATMET, 2002a), we repeated several of these sensitivities for the 2000 episode. These are detailed in the Interim Report (ATMET, 2003). With the version of MM5 we used at that time (v3.5), we recommended the use of the OSU LSM or the RRTM radiation scheme, which reduced a nighttime warm bias. Subsequently, v3.6 was able to use the NOAH LSM with the RRTM radiation with only a small bias.
- We performed several idealized tests of the MM5 non-hydrostatic scheme. The scheme performed reasonably well, but the model as a whole exhibited some difficulties which may have been caused by boundary conditions or other aspects. These tests are detailed in the Interim Report (ATMET, 2003).
- A series of full episode runs was performed for 16 August – 7 September. These experiments utilized the MM5 mesoscale model setup with four domains ranging in grid spacing from 108 km down to 4 km on grid 4 centered over the Houston-Galveston area. The configuration, domain and physics, was based on Nielsen-Gammon's previous work. Three main differences between our runs and his were:
    - The use of 2-way nesting rather than 1-way.
    - A slightly different vertical grid structure (the first layer was 10 m rather than 20 m)
    - The use of the NOAH LSM rather than the simpler soil model.

  Corrections needed to made to the MM5 initialization code to be able to correctly initialize the LSM from the EDAS data.
- A control experiment (Exp.1) showed a diurnal temperature with cool biases during the early morning and slightly warm biases during the afternoon. More significant warm biases were indicated during convective periods that the model did not capture. Overall, the magnitude of the errors was about the same as Nielsen-Gammon without the need to artificially modify soil moisture. The major reason for this was likely the inclusion of the new NOAH LSM.
- Experiment 2 tested the sensitivity to observational nudging to the profile and lidar data similar to the runs performed by Nielsen-Gammon. The results showed very little improvement due to the

fact that our control simulation was already closer to the observations that his.

- Both experiment 1 and 2 showed a significant diurnal wind speed bias with slow daytime biases and high nighttime biases. Sensitivity runs suggested that there was too much downward momentum flux during the day. We isolated an aspect of the surface layer scheme where a "convective contribution" to the total wind speed is used in the U* computation when the boundary layer is unstable. Removal of this convective contribution eliminated much of the slow daytime wind speed bias.
- Experiment 3 was a full episode run that removed this convective velocity. Results showed that this was the best performing run meteorologically.
- A high daytime PBL height bias was consistently present, a well-known "feature" of the MRF PBL scheme. This manifested itself in several ways, one being a significant dry dewpoint bias for nearly all times, especially during the afternoon. This was at least partially attributed to the MRF PBL scheme over-estimating the PBL depth during the afternoon hours.
- A review of the MRF scheme formulation suggested two potential improvements to the MRF PBL scheme: 1) reduce the critical bulk Richardson number used by the scheme and 2) reduce or eliminate the scaled virtual temperature excess that is designed to account for a near-surface temperature that is warmer than the lowest-level model temperature.
- We recommend a review of the MM5 TKE schemes with a comparison to other mesoscale model schemes, and possible modification of the MM5 schemes to allow them to work for more general situations.

7 References

ATMET, 2002a: High resolution (1.33 km) MM5 modeling of the September 1993 COAST episode: Sensitivity to model configuration and performance optimization. Final report to Texas Natural Resource Conservation Commission, 15 February 2002, 63 pp.

ATMET, 2002b: RAMS Simulations for TexAQS 2000 Episode. Final report to Texas Natural Resource Conservation Commission, 31 August 2002, 65 pp.

ATMET, 2003: MM5 Simulations for TexAQS 2000 Episode. Interim report to HARC, January 2003, 65 pp.

Chen, F. and J. Dudhia, 2001a: Coupling an advanced land-surface/hydrology model with the Penn State-NCAR MM5 modeling system. Part I: Model implementation and sensitivity. *Mon. Wea. Rev*., **129**, 569-585.

Chen, F. and J. Dudhia, 2001b: Coupling an advanced land-surface/hydrology model with the Penn State-NCAR MM5 modeling system. Part II: Preliminary model validation. *Mon. Wea. Rev*., **129**, 587-604.

Hong, S-Y and H-L Pan, 1996: Nonlocal boundary layer vertical diffusion in a medium-range forecast model. *Mon. Wea. Rev*., **124**, 2322-2339.

Nielsen-Gammon, John W., 2001: Initial modeling of the August 2000 Houston Galveston ozone episode. Report to the Technical Analysis Division, Texas Natural Resource Conservation Commission, December 19, 2001, 71 pp.

Nielsen-Gammon, John W., 2002a: Evaluation and comparison of preliminary meteorological modeling for the August 2000 Houston-Galveston ozone episode. Report to the Technical Analysis Division, Texas Natural Resource Conservation Commission, February 5, 2002, 83 pp.

Nielsen-Gammon, John W., 2002b: Meteorological modeling for the August 2000 Houston-Galveston ozone episode: PBL characteristics, nudging procedure, and performance evaluation. Report to the Technical Analysis Division, Texas Natural Resource Conservation Commission, February 28, 2002, 109 pp.

Nielsen-Gammon, John W., 2002c: Meteorological modeling for the August 2000 Houston-Galveston ozone episode: METSTAT statistical evaluation and model runs from March-June 2002. Report to the Technical Analysis Division, Texas Natural Resource Conservation Commission, June 21, 2002, 23 pp.

Nielsen-Gammon, John W., 2002d: Meteorological modeling for the August 2000 Houston-Galveston ozone episode: Improved data assimilation and statistical evaluation. Report to the Technical Analysis Division, Texas Natural Resource Conservation Commission, August 29, 2002, 30 pp.

Senff, C., R. Banta, L. Darby, W. Angevine, A. White, C. Berkowitz , C. Doran, 2002: Spatial and Temporal Variations in Mixing Height in Houston. Final report for TNRCC project F-20. 58 pp.

Troen, I., and L. Mahrt, 1986: A simple model of the atmospheric boundary layer: Sensitivity to surface evaporation. *Bound.-Layer Meteor.*, **37**, 129-148.